LEBANESE AMERICAN UNIVERSITY

Targeting Solid Tumor Cells with Novel Photosensitive Ruthenium-Based Metal-Organic Compounds

By

Stephanie Roy Farhat

A thesis
Submitted in partial fulfillment of the requirements
for the degree of Master of Science in Molecular Biology

School of Arts and Sciences
April 2016

LAU
الجامعة اللبنانية الأميركية
Lebanese American University

Lebanese American University
School of Arts and Sciences: Byblos Campus

THESIS APPROVAL FORM

Student Name: Stephanie Farhat I.D. #: 201003282

Thesis Title : Targeting solid tumor cells with novel photosensitive Ruthenium-based metal-organic compounds

Program: Master in Molecular Biology

Department: Natural Sciences

School: Arts and Sciences

The undersigned certify that they have examined the final electronic copy of this thesis and approved it in Partial Fulfillment of the requirements for the degree of:

Masters in the major of Molecular Biology

Thesis Advisor's Name HIRVAT E [redacted] 4/ 2016

Committee Member's Name [redacted] 2-04-2016

Committee Member's Name [redacted] 2/04/2016

LAU
الجامعة اللبنانية الأميركية
Lebanese American University

THESIS COPYRIGHT RELEASE FORM

LEBANESE AMERICAN UNIVERSITY NON-EXCLUSIVE DISTRIBUTION LICENSE

By signing and submitting this license, you (the author(s) or copyright owner) grants to Lebanese American University (LAU) the non-exclusive right to reproduce, translate (as defined below), and/or distribute your submission (including the abstract) worldwide in print and electronic format and in any medium, including but not limited to audio or video. You agree that LAU may, without changing the content, translate the submission to any medium or format for the purpose of preservation. You also agree that LAU may keep more than one copy of this submission for purposes of security, backup and preservation. You represent that the submission is your original work, and that you have the right to grant the rights contained in this license. You also represent that your submission does not, to the best of your knowledge, infringe upon anyone's copyright. If the submission contains material for which you do not hold copyright, you represent that you have obtained the unrestricted permission of the copyright owner to grant LAU the rights required by this license, and that such third-party owned material is clearly identified and acknowledged within the text or content of the submission. IF THE SUBMISSION IS BASED UPON WORK THAT HAS BEEN SPONSORED OR SUPPORTED BY AN AGENCY OR ORGANIZATION OTHER THAN LAU, YOU REPRESENT THAT YOU HAVE FULFILLED ANY RIGHT OF REVIEW OR OTHER OBLIGATIONS REQUIRED BY SUCH CONTRACT OR AGREEMENT. LAU will clearly identify your name(s) as the author(s) or owner(s) of the submission, and will not make any alteration, other than as allowed by this license, to your submission.

Name: [redacted]

Signatu

Date:

LAU
الجامعة اللبنانية الأميركية
Lebanese American University

PLAGIARISM POLICY COMPLIANCE STATEMENT

I certify that:

- I have read and understood LAU's Plagiarism Policy.
- I understand that failure to comply with this Policy can lead to academic and disciplinary actions against me.
- This work is substantially my own, and to the extent that any part of this work is not my own I have indicated that by acknowledging its sources.

Name: [redacted]

Signatu

Date: 19 April 2016

ACKNOWLEDGEMENT

This project would not have been possible without the support of many people.

First, I would like to thank my advisor, Dr. Mirvat El-Sibai, for accepting me in her research team and for teaching me everything that I know. Thank you for making me the researcher that I am today. All the scientific knowledge and lab skills that I acquired the last couple of years are because of you. You made me leap a large step towards achieving my career goals, and therefore, I owe my future success to you.

Also, I would like to thank our collaborators Dr. Ralph Abi-Habib, Dr. Rony Khnayzer, and Dr. Hassib Audi for their precious advices, constant follow-ups, and for the materials that provided the possibility of working on this project. Thank you for helping guide me through the meanders of this project.

In addition, thanks to my committee members, Dr. Ralph Abi-Habib and Dr. Rony Khnayzer for their precious time and efforts.

Furthermore, I would like to thank all of my colleagues in the MS program.

And finally, thanks to my parents, family and friends, who supported me in every step in my professional journey so far.

Targeting Solid Tumor Cells with Novel Photosensitive Ruthenium-Based Metal-Organic Compounds

Stephanie Roy Farhat

ABSTRACT

Cancer incidence has been increasing worldwide in the last few decades. Solid tumors are hard to treat, primarily due to drug resistance as well as to the struggle in delivering the drugs specifically to the tumor. Various therapeutic approaches for treating solid tumors have been exploited. A very promising approach has been the use of Ruthenium-based complexes conjugated to different ligands that are characterized by having a photochemical potential rendering them only active after exposure to light, which can be ultimately specifically delivered to the site of tumor. This study aims to find the most efficient Ru-based compounds on a set of 6 cell lines from different solid tumors. Different ruthenium precursors (bis-bidentate), final complexes (tris-bidentate) and free phenanthroline- or bipyridine-derived ligands were tested. The bis-bidentate complexes tested were four: **Ru-I**: [Ru(II)(1,10-phenanthroline)$_2$Cl$_2$]; **Ru-II**: [Ru(II)(4,7-diphenyl-1,10-phenanthroline)$_2$Cl$_2$]; **Ru-III**: [Ru(II)(4,7-diphenyl-1,10-phenanthroline-disulfonate)$_2$Na$_2$]$^{2+}$ and **Ru-IV**: [Ru(II)(2,2'-bipyridine)$_2$Cl$_2$], along with their corresponding free ligands **L-I**, **L-II**, **L-III** and **L-IV**, respectively. **Ru-II** showed significant potency on most of the cell lines tested (5 out of 6), as well as **Ru-I** on two of them while the others were inert. As for the free ligands, **L-II** presented major cytotoxic effect on five out of six cell lines, **L-I** on two cell lines, **L-IV** on one cell line only. The addition of diphenyl groups to the phenanthroline of **L-I** rendered its structure bulkier and more hydrophobic (**L-II**), and showed an increase in its potent activity, same result when it was bound to the metal. Therefore, a structure activity relationship was established between precursors and their free ligands. However, when adding sulfonate groups to the diphenylphenanthroline structures, the cytotoxic effect is inhibited in the free ligand and its precursor, **L-III** and **Ru-III** respectively, thus suggesting a possible DNA intercalation mechanism of these compounds. On the other hand, neither bipyridine nor its corresponding precursor **L-IV** and **Ru-IV,** bipyridine and its corresponding precursor respectively, shown no cytotoxic activity. In addition, four final compounds were synthesized to study the photochemical potential of our metal-based complexes. There structure bear combinations of **L-II** and **L-III** yielding the tris-bidentate compounds, **Ru-II$_3$**, **Ru-II$_2$-III**, **Ru-II-III$_2$** and **Ru-III$_3$**, having different net charges

ranging between +2 and -4, and their effect was studied in the dark and after exposure to blue light. Activity was detected only in **Ru-II$_3$** against all the tested cell lines in the dark, **Ru-II$_2$-III** in three cell lines while the others showed no effect. When exposed to blue light against the astrocytoma cell line all four compounds showed high levels of potency, including **Ru-II-III$_2$** and **Ru-III$_3$** that were biologically inert in the dark. It is hypothesized that these final compounds' cytotoxic action is due to the generation of Reactive Oxygen Species (ROS), causing DNA damage, oxidation of amino acids and enzyme co-factors, as well as lipid peroxidation, thus leading to cell death. The ultimate goal is to base future selective anticancer treatments using Ru-based compounds. The mechanisms by which Ru-based compounds work is still being explored, and other ligands and combination of ligands are also being tested to find the most selective, and potent complex.

Keywords: Solid Tumors, Ruthenium, Metal-based complexes, Photochemistry.

Table of Contents

List of Tables

List of Figures/Charts

List of Abbreviations

PDT: Photodynamic therapy

L-I: 1,10-Phenanthroline

L-II: 4,7-Diphenyl-1,10-phenanthroline

L-III: 4,7-Diphenyl-1,10-phenanthroline disulfonic acid

L-IV: 2,2-Bipyridine

Ru-C: $RuCl_2(DMSO)4$

Ru-I: $[Ru(II)(1,10\text{-phenanthroline})_2Cl_2]$

Ru-II: $[Ru(II)(4,7\text{-diphenyl-}1,10\text{-phenanthroline})_2Cl_2]$

Ru-III: $[Ru(II)(4,7\text{-diphenyl-}1,10\text{-phenanthroline-disulfonate})_2Na_2]^{2-}$

Ru-IV:$[Ru(II)(2,2'\text{-bipyridine})_2Cl_2]$

$Ru\text{-}II_3$: $[Ru(II)(4,7\text{-diphenyl-}1,10\text{-phenanthroline})_3]^{2+}$

$Ru\text{-}II_2\text{-}III$: $[Ru(II)(4,7\text{-diphenyl-}1,10\text{-phenanthroline})_2(4,7\text{-diphenyl-}1,10\text{-phenanthroline-disulfonate})]$

$Ru\text{-}II\text{-}III_2$: $[Ru(II)(4,7\text{-diphenyl-}1,10\text{-phenanthroline})(4,7\text{-diphenyl-}1,10\text{-phenanthroline-disulfonate})_2]^{2-}$

$Ru\text{-}III_3$: $[Ru(II)(4,7\text{-diphenyl-}1,10\text{-phenanthroline-disulfonate})_3]^{4-}$

CHAPTER ONE

Introduction

1.1 Solid Tumor Epidemiology

Statistics measuring cancer mortalities worldwide existed since the emergence of this disease. In 2005 for example, around 7.5 million people died of cancer out of 60 million deaths worldwide (Gavhan et al., 2011). This study predicted the number of deaths related to cancer to be 9 million in 2015. The number of deaths related to cancer has been increasing over the past decades reaching 8 million in 2012 (World cancer report, 2014). An estimated 14.1 million cancer cases were diagnosed around the world in 2012, with the incidence in men (7.4 million cases) being slightly higher than the incidence in women (6.7 million cases). Statistical projections suggest that this number will reach 24 million by 2035 (Ferlay et al., 2015). 13% of the cancer cases in 2012 were diagnosed as lung cancer, making it the most common cancer worldwide. Breast cancer was the second most dominant cancer worldwide with 1.7 million new cases in 2012 (in women only). And the third most common cancer with 1.4 million new cases diagnosed was colorectal cancer (Ferlay et al., 2012).

In general, most cancers develop in older people; around 80% of cancers worldwide are diagnosed in people of 55 years of age or older (World cancer report, 2014). In addition, certain lifestyle aspects can increase the incidence of developing cancer. These include smoking, unhealthy diets, and lack of physical activity. People who smoke, eat an unhealthy diet, or are physically inactive also have a higher risk of cancer (Kunnumakkara et al., 2008). Probabilities of developing cancer are estimated based on family history, genetic susceptibility, and whether the country is a developed or a third world country (Parkin et al., 2011). For the majority of cancer types, the risk is higher when the family history has a high incidence of this disease. However, many familial cancers do not arise exclusively from the genetic makeup of the individual, but from interplay between genetic variations, lifestyle, and environmental risk factors (Parkin et al., 2011).

1.2 Cancer Overview

Cancer consists of a family of diseases that share the characteristic of having uncontrollably proliferative cells which accumulate several mutations in their genetic material. Many factors, external and internal, are causative agents of cancer. External factors include chemicals, radiation, tobacco, and some infectious organisms including viruses. As for the internal factors, they include hormones, immune conditions, genetically inherited mutations, or mutations that occur from cell cycle division and metabolism (Parsa, 2012).

1.2.1 The Progression of Cancer as a Disease

The transition of cancer cells from a primary tumor to a potential metastasis site depends on a series of biological steps. Tumor development is a complex multi-step process, with cells evolving progressively from being totally normal, to becoming highly malignant (Nimmerjahn et al., 2005). The stages that tissues within a tumor pass through in the process of tumor development cause it to be heterogenic because within the same tissue, some cells may be in a certain stage, while others are in different stages.

1.2.1.1 Different Stages of Cancer Growth

Hyperplastic growths are characterized by an excessive number of cells (Skarin, 2003). Metaplasia refers to the process where a type of a normal layer is replaced by another type, such as a squamous epithelium replacing a mucus-secreting epithelium or vice-versa (Skarin, 2003). Both hyperplasia and metaplasia are considered minimal deviations from normal tissues. Dysplastic tissues bear more cytological abnormalities. The changes in these tissues include a variable nuclear size and shape. These changes, along with increased mitotic activity, alter the tissues architecture (Skarin, 2003). That's the reason why dysplasia is considered a transitional state between completely benign and premalignant growths. The next stage of tumor development is the appearance of macroscopic masses of cells such as polyps and warts termed adenomas (Skarin, 2003). These tissues do not invade the basement membrane separating them from the underlying stroma because they reach a certain size and stop growing. As the cells advance in abnormality stages, they undergo several mutations including over expression of some membrane proteases and increased mobility (Weinberg, 2013).

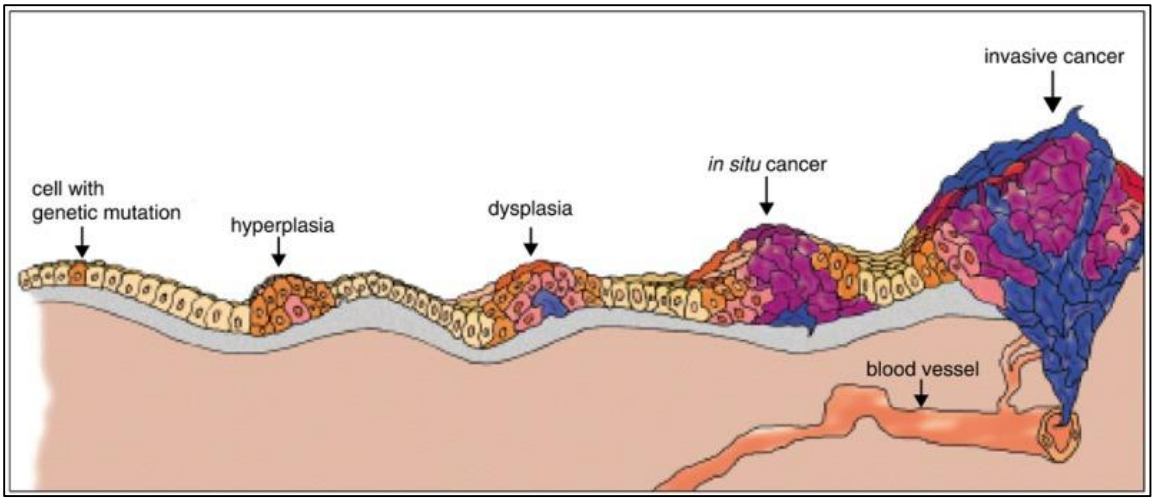

Figure 1: Overview of cancer metastasis. (McKinnell, 2007)

1.2.1.2 The "Seed and Soil" Theory

Once the tumor accumulates enough mutations to evade the underlying basal membrane and undergo metastasis, it becomes malignant (McKinnell et al., 1998). The process of metastasis is extremely complex. The cancer cells should be able to invade close-by tissues, migrate through the blood and lymph vessels to distant sites as well as having the capacity to leave the vessels and invade basal membranes (Weinberg, 2013). As per Doctor Stephen Paget, a surgeon from the late 19th century, cancer metastasis can be explained through the "seed and soil" theory. The cancer cell is the seed, and the environment where it has an affinity to grow is the soil. Metastasis occurs solely when the seed and soil are compatible (Ribatti, 2011). Not any cancer cell can metastasize to any tissue. Some cancers are known to metastasize to certain tissues more than others. Breast cancer, for example, mostly metastasizes to lung and bone. In contrast, very low metastasis events are observed from breast cancer in the spleen and heart (Weigelt et al., 2005). This is because the "soil" is not very compatible for cancer cells originating from breast tissues in some organs, while it is more compatible in others (Ribatti, 2011).

1.2.1.3 Cancer Metastasis

Cancer metastasis is the spread of the cancer cells to organs that are usually distant from the site where the tumor was formed. Metastasis is believed to be the cause of death of most cancer patients (Connolly et al., 2003). The process of metastasis is composed of sequential events that have to be completed so that the tumor cell can successfully

metastasize. Metastasis adds even more complexity to this multiplex disease. The most important and essential events allowing metastasis to occur are changes in cell-cell and cell-matrix adhesion (Martin TA et al., 2009). It all starts with the formation of a genetically heterogeneous primary tumor which becomes a localized invasion when the tumor evades the underlying basal membrane. The tumor cell dissociates from the primary tumor mass due to the loss of cell-cell adhesion capacity. The cancer cells then enter into the closest blood vessels and then interact with the platelets, lymphocytes, and other blood components through a process called intravasation. Even if the primary tumor was removed, some metastatic cells are able to disseminate to subsequently form micrometastasis. To do so, these cells must be transported through circulation to different parts of the body. Some of the cells arrest in the capillaries and microvessels of many organs. Extravasation of cancer cells then takes place initiating the formation of a micrometastasis. Some of the cells, mainly the ones that acquired enough mutations, will gain the ability to colonize and form a macroscopic metastasis. To do that, the tumor must induce angiogenesis to assure a potential source of oxygen and nutrients. This large mass of cells will undergo a new secondary wave of metastatic dissemination, forming new micrometastasis which in turn form multiple macroscopic metastasis. This is thought to be the mechanism by which most cancers are able to relapse after treatment or removal of the primary tumor (Weinberg, 2013).

1.3 Tumor Physiology

Solid tumors are lumps of genetically, morphologically, and functionally abnormal cells. The unique physiology of solid tumors comes mainly from the vasculature that is composed of two types of vessels: the existing vessel that used to nourish the normal tissue before tumor cells took over, and the microvessels arising from neovascularization caused by proangiogenic factors produced by cancer cells (Brown et al., 1998). Although having the same structures as blood vessels found in other body parts, tumor blood vessels are irregular in shape, have arterio-venous shunts, blind ends, and they lack smooth muscle, making them much leakier than other vessels (Ribatti 2011).

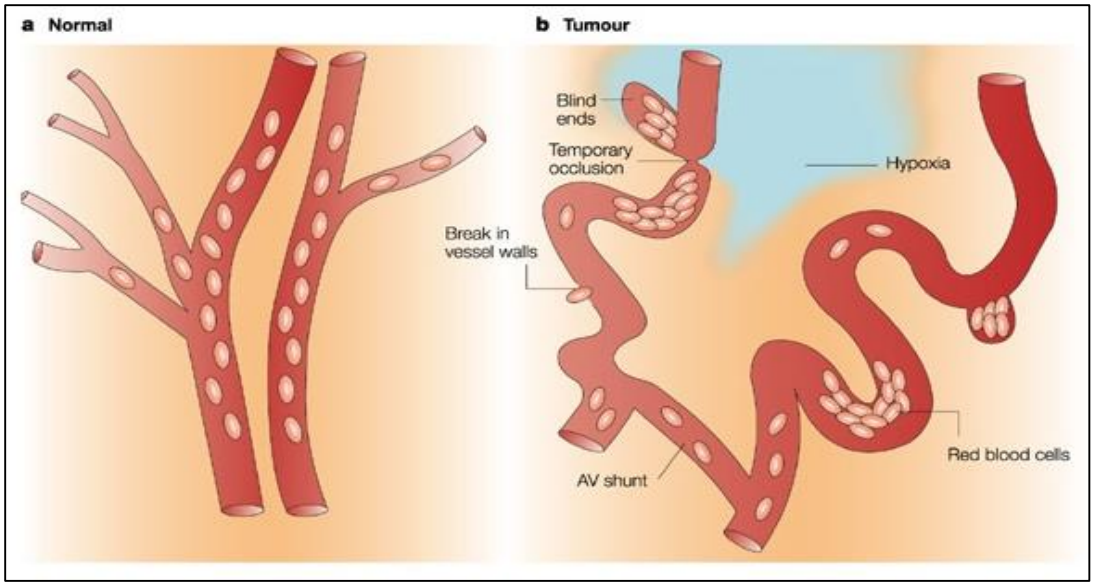

Figure 2: Normal vasculature VS vasculature of a tumor cell. (Brown et al., 2004)

1.4 Types of Cancers Arising from Solid Tumors and Respective Cell Lines

1.4.1 Lung Cancer

Lung cancer is a cancer that usually forms in the tissues lining the air passages. Two main types of lung cancers are small cell lung cancer (SCLC) and non-small cell lung cancer (NSCLC). These two types are distinguished based on the morphologies of the cells observed under the microscope. Lung cancer constitutes a major worldwide health problem since it causes around 18% of deaths worldwide (Hoffman PC et al., 2000). Around 220,000 cases of lung cancer were expected in 2015, constituting about 13% of all diagnosed cancers (Cancer.org). The most important risk factor for lung cancer is cigarette smoking mainly, but other environmental factors such as pollution, as well as professions where exposure to different chemicals occurs (deGroot et al., 2012). The risk of developing lung cancer increases also with family history and among individuals with a medical history of tuberculosis (Cancer.org). Symptoms of lung cancer are respiratory such as coughing up blood and shortness of breath, systemic such as weakness and fever, and symptoms caused by the tumor pressing on adjacent tissues such as chest pain, bone pain, and difficulty of swallowing (Horn et al., 2015). Many panel cancer cell lines are used in

the lab. A549 cells are adenocarcinoma human alveolar basal epithelia cells. These cell lines were first developed by the culturing of a cancerous lung tissue transferred from an elderly Caucasian male (Giard et al., 1973). The primary function of these cells are diffusion and osmosis across alveoli. In vitro, these cells form a monolayer and grow adherent to the flask (Giard et al., 1973). High levels of unsaturated fats are found in A549 cell lines; these are crucial to maintain the membrane phospholipids. (Giard et al., 1973).

1.4.2 Breast Cancer

Breast cancer is the most common type of cancer in women worldwide (McGuire et al., 2015). The variability of breast cancer incidence around the world is huge; its incidence is the lowest in less-developed countries, and it increases in the most developed countries (Stewart et al., 2003). The risk factors of breast cancers are numerous: breast cancer incidence increases in females and in elderly people (Yager et al., 2006). In addition to genetic factors, lack of breastfeeding appears to induce higher levels of certain hormones, increasing the incidence of breast cancer in women (Santoro et al., 2009). Plus, recently, light pollution has been indicated an important risk factor for the development of breast cancer (Portnov et al., 2013). Symptoms of breast cancer are visually noticeable. They include a lump with a different texture than the rest of the breast tissue, thickening of a breast, a rash around a nipple, discharge from nipples, and sometimes a change in shape or position of a nipple is detected (Watson, 2008). Breast cancer is known to metastasize occasionally and spread beyond the breast. Most common sites of metastasis include lung, liver, bone, and mostly brain (LaCroix, 2006). Different panels of breast cancer cell lines including MCF-7 and MDA-MB231 are used in the labs. MCF-7 is a breast cancer cell line isolated from an elderly Caucasian women. It is named after the institute where the cell line was first established: Michigan Cancer Foundation-7 (Soule et al., 1973). MCF-7 are primary invasive breast ductal carcinoma, bearing estrogen receptors and highly tumorigenic (Levenson et al., 2007; Ross et al., 2001). In addition to MCF-7, two other breast cancer cell lines account for over 60% of research done on breast cancers: these are T-47D and MDA-MB-231 (LaCroix, 2004).

1.4.3 Colorectal Cancer

Colorectal cancer is diagnosed in 1 million cancer patient each ear, and is responsible of about 750,000 deaths since 2010 (Cunningham et al., 2010). Its incidence is higher in developed countries than in developing countries: Colorectal cancer incidence is 10-fold higher in Europe and Australia than in Africa and South-Central Asia (Ferlay et al., 2010). The incidence of colorectal cancer increases with patients suffering from inflammatory bowel disease, and with the cancer being diagnosed in the family, especially in first-degree relatives (Jawad et al., 2011; Cunningham et al., 2010). The symptoms of colorectal cancer largely depend on the precise location of the tumor. However, most common signs include nausea, vomiting, constipation, blood in stool and rectal bleeding, especially in individuals above 50 years old (Alpers et al., 2008; Astin et al., 2011). Caco-2 is an example of a continuous heterogeneous human epithelial colorectal adenocarcinoma cells (Fogh et al., 1975). In vitro, these cells form a monolayer that allows the passage of electrolytes and small molecules (Hidalgo et al., 1989). And when cultured under specific conditions, these cells differentiate and polarize such as their morphology and function becomes similar to that of the enterocytes of the small intestine, expressing tight junctions, microvilli and numerous enzyme transporters (Pinto, 1983; Hidalgo et al., 1989). Comparing results of experiments done on Caco-2 cell lines between labs is difficult due to the heterogeneity of these cells (Sambuy et al., 2005).

1.4.4 Melanoma

Skin cancer is a common type of cancer that resulted in around 80,000 death a year since 2010 (Lozano, 2012). It is more common in Australia and New Zealand, reaching around 4-fold higher incidence than in the United States (Jones et al., 1999). Although the incidence of skin cancer has been increasing over the past few years, the survival rate of melanoma patients is relatively high (Skin cancer facts, 2016). It mainly depends on the stage that the cancer reaches when they start treatment (Skin cancer facts, 2016). The incidence of skin cancer increases with HPV infections (mainly increasing the risk of squamous cell carcinoma), Marjolin's ulcers (chronic non-healing wounds), and most importantly, the exposure to ionizing radiation, UV radiation, and environmental

carcinogens (Saladi et al., 2005; Amdt, 2010). Skin cancer types include basal-cell carcinoma, squamous-cell carcinoma, melanoma, and Merkel cell carcinomas. The most common symptoms is formation of skin ulcers (What You Need To Know About Melanoma And Other Skin Cancers, 2010; Bickie et al., 2004). Different cell lines are derived from a range of skin cancer types. These include, but are not limited to 721 melanoma cell line, FM3 melanoma cell line, and B16 melanoma cell lines. B16 cell lines are extracted from mice and are highly variable, even within the same lab; they can change in the metastatic potential and tumorigenic dose (Overwijk et al., 2001).

1.4.5 Astrocytoma

Astrocytoma is a type of brain cancer that originates in a particular kind of start-shaped glial cells called astrocytes. Cancers that originate in the brain constitute around 1.4% of all cancers and are responsible for 2.3% of deaths related to cancer. Brain cancer usually interferes with the normal brain functions and affects areas of the brain that have critical role in the function of the brain (El-Zein et al., 2002). The incidence of astrocytoma increases with ionizing radiation. In addition to environmental factors, genetic risk factors also increase the risk of astrocytoma; these include mutations passed from a generation to another. These mutations are known to cause abnormal cell growth and proliferation leading to the development of a tumor (Stupp et al., 2007). The symptoms of astrocytoma are due to the pressure growing inside the skull. Other symptoms include drowsiness, eye swelling. The symptoms of astrocytoma depend on the part of the brain where the tumor grows. This can sometimes be determined by the nature of the seizures that a cancer patient suffers from (Smith et al., 2001). Experiments are done on different cell lines to try to get a better knowledge of astrocytoma. SF268 cell lines are an example. They were first harvested from the right parietal lobe of a 24 year old brain cancer patient. They are highly anaplastic and relatively hard to grow (Westphal et al., 1985).

1.5 Main Approaches in Treating Solid Tumors

1.5.1 Surgery

Surgery is the first cancer treatment developed and the most frequently used to inhibit small tumors from developing into larger ones. It involves resecting primary tumors aiming

to reducing metastatic relapse risks. The earlier the tumor is detected, the higher chances to remove the tumor without extending the surgical margins (Weinberg, 2013). However, during the excision process, a part of the tumor's surrounding is also removed because most malignant solid tumors spread through the lymphatic system, hence most regional lymph nodes are eliminated. In addition, tumor resection helps in pain relief, decreases the occurrence of life-threatening bleedings, and relieves compressions of many vital organs (brain, spinal cord, trachea …), helping the organs to regain their function and avoiding distressing symptoms. Subsequently, the margins of the tumor are the biggest challenges of the surgical method; this requires the use of an adjuvant therapy such as chemotherapy or radiation (Reson, 2008).

1.5.2 Radiation Therapy

Radiation therapy is a cancer treatment strategy that went into clinical trials after World War II, after discovering the possibility to direct X-rays at narrow fields of radiation to target primary tumors without affecting normal tissue. It is mainly used to treat localized solid tumors when surgery is not feasible. Ionizing radiation kills cancer cells by transferring energy to tissues, discarding electrons from biologically important molecules like DNA. This breaks the DNA strand and stops its replication during mitosis. Extensive DNA damage leads to apoptosis (Birgisson et al, 2007).

1.5.3 Chemotherapy

The most common approach for treating different cancers is chemotherapy. In most cases, it is combined with surgery or radiation. Chemotherapy is more recent than the other techniques as it emerged in the 1940s after discovering antimetabolites that interfere with the normal function of enzymes producing metabolites in the cells. These include purine or pyrimidine analogs that incorporate themselves during DNA synthesis thereby disrupting the normal DNA biosynthesis (Choi et al., 2008). Aside from purine and pyrimidine analogs, antimetabolites can interfere with microtubule assembly and are effective as anti-cancer agents. These work by blocking microtubule breakdown at the end of mitosis. Others work the opposite direction, by preventing the initial assembly of microtubules. Antimetabolites interfering with microtubules assembly and breakdown are mainly used to treat different lymphomas, lung cancers, and squamous cell carcinomas

(Weinberg, 2013). Chemotherapeutic agents directly damage DNA, interfering with cell division and as a result leading to apoptosis. Other chemotherapeutic agents sequester nucleotides in a way to block DNA synthesis. The reason why chemotherapy is very common is because approaches, using one or multi-agent therapies appear to be applicable even in cancer patients who are above 80 years old (Coluccia et al., 1993). Over the past 20 years, chemotherapy has evolved from being a potentially toxic treatment to one that is resulting in significantly positive results. However, chemotherapy has been showing numerous limitations. These include but are not limited to:

1- Toxicity: chemotherapy can injure normal tissues, especially the ones that contain cells that divide more frequently than others such as bone marrow, gonads, and hair follicles, thereby the side effects become predictable: Nausea and vomiting, hair loss, stomatitis, diarrhea, and myelosuppression. Plus, the irony of cancer treatments that is also found in radiation therapy is that most agents used are carcinogens themselves (Gavhane et al., 2011).

2- Poor penetration of the drugs in solid tumors: The safe and efficient doses of anticancer drugs are usually hard to reach, since most of these agents require high concentrations to be efficient, that they become dangerous when treating patients. In addition, the unusual vascularization of tumors is a factor that limits the uptake of the chemotherapeutic agents (Dreicer et al., 2008; Kovacs et al., 2007).

3- Tumor drug resistance: malignant cells have tendency to resist drug administration. They mainly do so by pumping the drug out of the cell through overexpressing membrane glycoproteins (a non-specific mechanism that can confer resistance to any type of drug), thereby limiting the effectiveness of anticancer agents in general, rather than immunotherapy alone (Gavhane et al., 2011).

1.5.4 Metal-Based Compounds in Cancer Therapy

Metal-based compounds have been known since ancient Egyptians used gold salts as potential anti-disease agents (Nobili et al., 2010). Traditional Chinese medicine also uses arsenic trioxide (ATO) as antiseptic agents for diseases such as syphilis, rheumatoid arthritis and psoriasis. These were also used for treatment against leukemia in the 18^{th} and 19^{th} centuries (Dilda et al., 2007).

1.5.4.1 Cisplatin in Cancer Therapy

In 1969, cisplatin was discovered as an antibacterial agent that was essential in the formation of platinum electrodes and eventually showed potency against tumors (Weinberg, 2013; Rosenberg et al., 1969). Cisplatin itself generates covalent intra-strands cross links in DNA, usually between 2 adjacent guanines generating a significant bent in the DNA (Hannon, 2007). Cisplatin is a molecule bearing a Pt(II) metal center connected to 2 molecules of ammonia and 2 chloride atoms in a *cis* conformation (figure 4). After injection in the serum, cisplatin remains in its neutral form. However, once it is inside the cell, one or both Cl ligands can be dislodged by one or two water molecules, thus attributing a cationic charge to cisplatin and abolishing its neutral state. This new cationic complex interferes with nucleotides, specifically with the N7 of guanine and adenine. In most cases (70%), the intercalation of cisplatin moves 2 adjacent bases on the same strand in a bifunctional manner, creating a 45^{o} nick in the DNA double strand; this is called the G-G 1,2 intra-strand adduct (Takahara et al., 1995). As with any anticancer agent, cisplatin is not free of adverse effects that are believed to be due to the platination of sulfur residues on proteins. These side effects include nephrotoxicity, nausea, and numbness of the limbs. Fortunately, they can be encountered by the use of sulfur-rich "rescue agents" (Hannon, 2007).

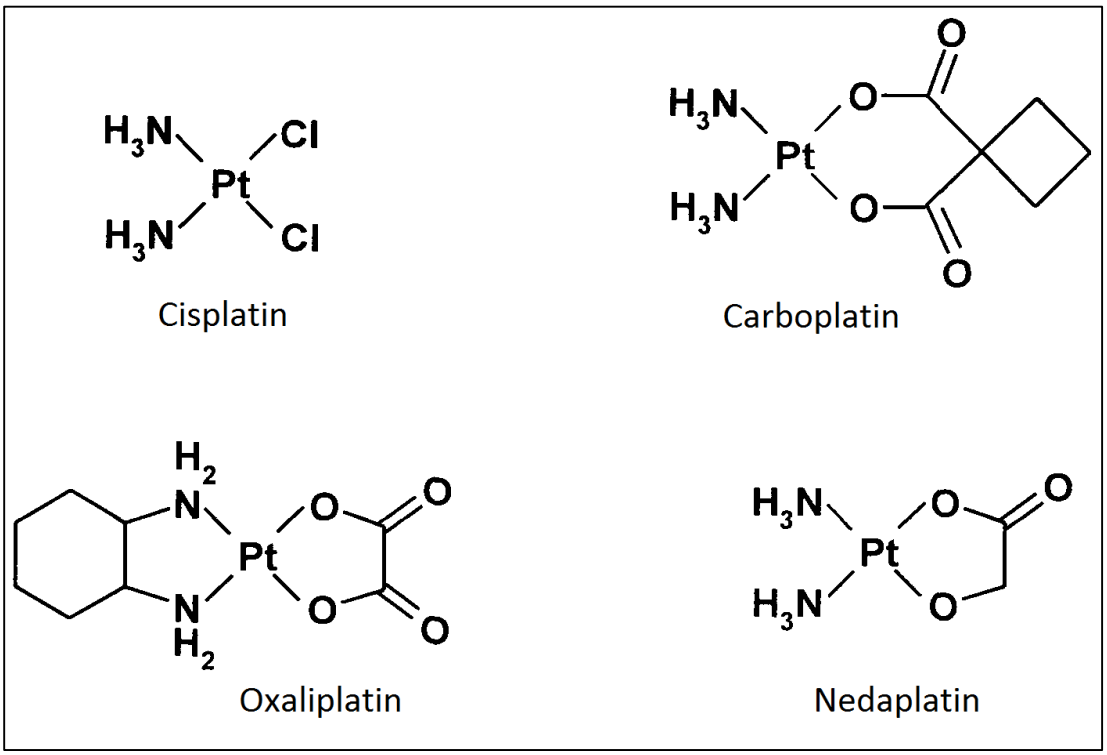

Figure 3: Original *cis*-platinum compounds. (Hannon, 2007)

The cis conformation of cisplatin played an important role in its potency, unlike the trans conformation, which led to the use of the square-planer Pt(II) center connected to 2 amino groups in a cis conformation, along with 2 good relatively leaving groups such as chloride ions. This form seems to be the most efficient, and led to many derivatives including carboplatin, nedaplatin, and oxaliplatin (figure 4). These agents were able to make it to the market. Later on, it was shown that the exact structure described previously was not mandatory for activity; compounds with *trans* conformation were shown to be efficient also, even though they do not follow the classical structure-activity relationship depicted with *cis* conformations (Hannon, 2007; Jakupec et al., 2005). These non-classical agents include 3 different classes of *trans*-platinum (II) complexes: The first class contains pyridine ligands, the second contains an isopropylamine and an alkylamine, and the third contains iminoether ligands Hannon, 2007; Farrell et al., 1989; Montero et al., 1999; Coluccia et al., 1993). These unconventional *trans*-platinum agents showed, in addition to their in-vitro activity similar to cisplatin, an activity against cell lines that were resistant to it. Moreover, the types of DNA lesions caused by cisplatin are constitutionally different from those caused by the *trans* conformation (Hannon, 2007).

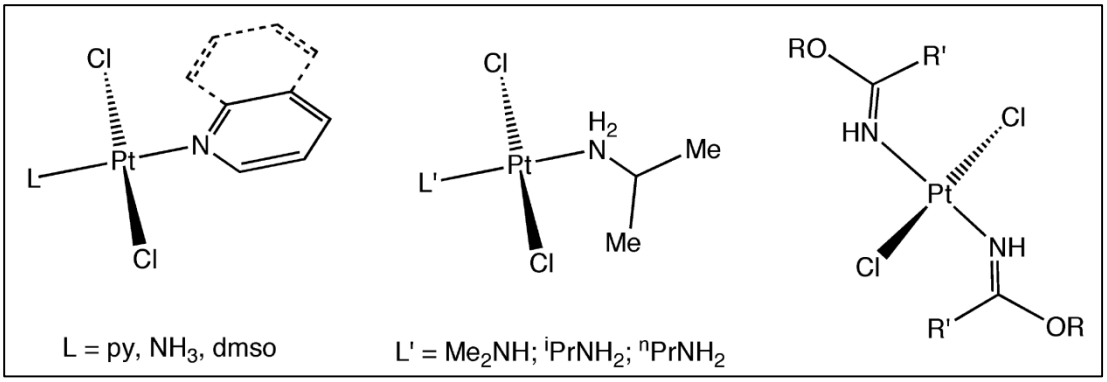

Figure 4: Classes of active unconventional *trans*-platinum (II) complexes.
Left: pyridine-containing; **Middle:** isopropylamine-containing; **Right:** iminoether-containing. (Hannon, 2007)

Another class of active unconventional platinum agents includes the di- and tri-platinum compounds that were developed by Farrel in 2004. In these molecules, the metal centers are connected by flexible diamine chains. These compounds have poly-cationic characteristics in addition to having more than one nucleus, and do not contain platinum centers with *cis* leaving groups. This class of compounds showed increased activity relatively to cisplatin against numerous cell lines including those that were resistant to cisplatin. They induce their effects by generating intra- and inter-strand long range bifunctional moves. They also showed a high ability in changing the DNA from being right-handed (B) to left-handed (Z) (Kloster et al., 1999).

The newer-generation metal based compounds are platinum analogs named oxaliplatin and carboplatin. These, and cisplatin constitute some of the most important chemotherapic agents (Kelland, 2007; Jungwirth et al., 2011). Cisplatin made a huge success in the fields of cancer therapies. An example would be its effect on the cure rate for testicular cancer: prior to the use of carboplatin, a drug derived from cisplatin, only 10% of testicular cancers were cured. After the use of cisplatin-related agents, the cure rate of this cancer increased to 95% (Weinberg, 2013).

1.5.4.2 Non-Platinum-Based Compounds in Cancer Therapy

Following this remarkable success, researchers decided to explore other compounds based on several metals mainly gold, titanium, vanadium, cobalt, and ruthenium, and are currently yielding satisfying outcomes in clinical trials (Jungwirth et al., 2011).

Non-platinum metal-based compounds have been explored ever since cisplatin showed positive results. Among these, those with Ruthenium center were the subject of interest. They had significant anti-cancer activity and numerous benefits:

- Its ability to coordinate with different ligands allows the synthesis of a wide array of new complexes.
- Its rate of ligand exchange is comparable to that of platinum.
- Unlike Platinum, that has a planar geometry, Ruthenium forms an octahedral geometry when bound to ligands, thereby having different mode of function than platinum.
- Under physiological conditions, Ruthenium has 3 oxidation states (+II, +III, and +IV), allowing it to form pro-drugs at the +III oxidation state that can be reduced once the target is reached.
- Finally, Ruthenium has the ability to mimic iron and bind to albumin and transferrin, thus reducing its cytotoxic effects compared to Platinum (Hannon, 2007; Jakupec et al., 2005; Jungwirth et al., 2011; Bergamo et al., 2012).

Ruthenium-Based Compounds

Ruthenium based compounds are administered at first as Ru(III) compounds and once the target is reached, they get reduced to the Ru(II) oxidation state and become more kinetically reactive, following a process called "activation by reduction". This lowers the toxicity of most ruthenium-containing compounds. This is thought to occur in the reductive environment of the proliferating hypoxic cells in the core of the solid tumor where inadequate angiogenesis is present (Jakupec et al., 2005; Schluga et al, 2006). NAMI-A and KP1019 (figure 6) are the 2 Ru(III) compounds that are currently under clinical trials. NAMI-A, the first to enter clinical trials is an anionic complex bearing an octahedral geometry: the center of this molecule, (Ru(III)), is connected to one DMSO and one imidazole ligands, along with 4 chloride ions. NAMI-A was active against cancer cell lines and more importantly had a significant effect on metastasis (Hannon, 2007). NAMI-A's mechanism of action when binding to DNA is different than other Ru-based complexes. It possesses anti-angiogenic activities through scavenging liberated nitric oxide (NO) from epithelial cells, as well as anti-invasive properties that originate from the interaction of

NAMI-A with extracellular membrane receptors (Bergamo et al., 2012; Jungwirth et al., 2011).

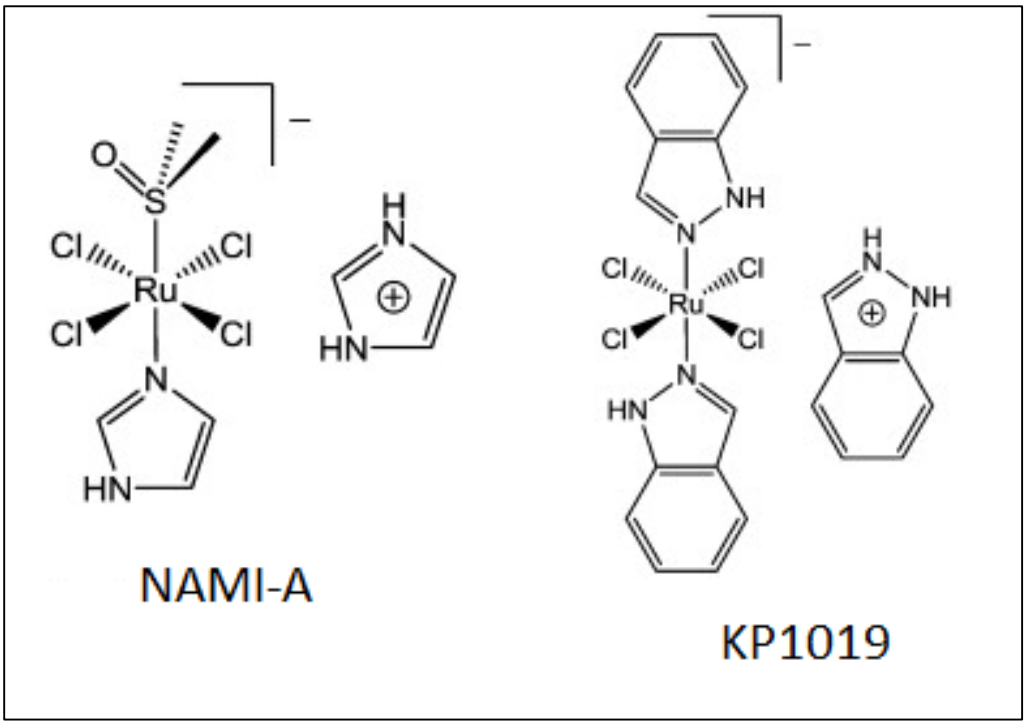

Figure 5: NAMI-A and KP1019 structures. (Bergamo et al., 2012)

Ruthenium and Photodynamic Therapy

Photodynamic therapy (PDT) is a technique that relies on activating photosensitive agents by light in order to kill cancer cells. Their activity is determined by the type of interaction between the PDT agents and the components of the tumor cell (DNA, cell membrane, proteins, biopolymers…). One example of the PDT's mechanism of action is damaging DNA through electron transfer from the excited state of the PDT to DNA. Another example is substituting ligands in a way to make the complex release a biologically active molecule or itself binding to the target molecule after photo-activation (Clarke, 2003). The complexes that are inert in the dark are more efficient in PDT since they display larger phototoxicity indices. Ideally, these complexes should readily switch from the ground state to excited state in the photodynamic therapy window (Clarke, 2003). PDT applied in anticancer approaches primarily target DNA through several mechanisms: non-covalent hydrophobic interaction and covalent binding, DNA intercalation, and the binding between a positively-charged complex and DNA (Manning, 1978; Manning et al.,

1998; Yang et al., 1997) Ru(II) complexes connected to *N*-heterocyclic ligands can be efficient PDT agents since they can have long-lasting excited states and because of their fast metal-to-ligand charge transfer transitions (Clarke, 2003; Pacor, 1991).

1.6 Study Objectives

The purpose of this study is to test the effect of Ru(II) metal-based compounds bound to *N*-heterocyclic ligands against solid tumor cell lines in order to establish a photochemical model related to these compounds. This will be done by first, studying the relationship between structure and activity of the Ru(II) based compounds, relating that to their potency against different solid tumor cell lines. Second, once the compounds show efficiency in killing cancer cells, the type of cell death will be determined. Third, to detect if these compounds possess any photochemical potential, they will be photo-activated once applied to the different solid tumor cell lines, and the type of cell death will be eventually determined. Finally, the goal of this research project is to provide an initiative for future approaches targeting some solid tumors.

CHAPTER TWO

Materials and Methods

2.1 Cells and Cell Lines

Human solid tumor cell lines Astrocytoma cells (SF), Melanoma (B16), Human Breast Adenocarcinoma cells (MDA-MB-231, MCF-7), Colorectal cells (CaCo-2) and Lung carcinoma cells (A549) were obtained from the American Type Culture Collection (ATCC) and grown as described previously in DMEM 1640 supplemented with 10% FBS and 5% Penicillin/Streptomycin at 37°C, 5% CO_2 (Pellizzari et al., 1999).

2.2 Compounds

Compounds were synthesized by Dr. Rony Khnayzer and his research group at the Lebanese American University. They were provided in the lyophilized powder form, dissolved and aliquoted in stocks of 1, 2, 5 or 10 mM in DMSO. Aliquots were stored at -80°C for a maximum of 2 months or 3 freeze-thaw cycles.

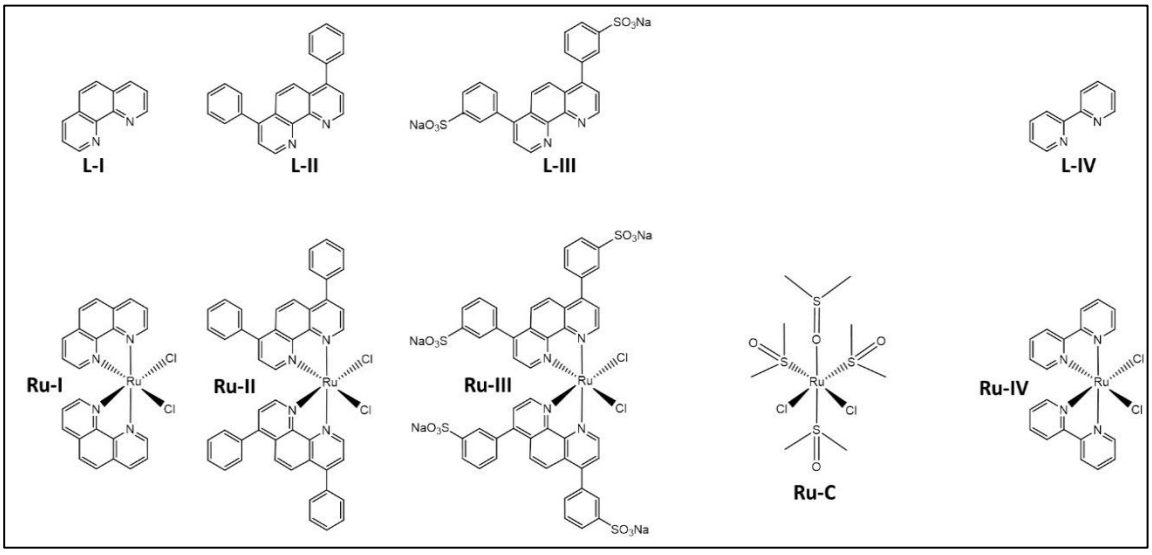

<u>Figure 6:</u> Ligands, ligand-free Ru(II) control and Ru(II) precursor complexes.
Ligands: **L-I**: 1,10-Phenanthroline; **L-II**: 4,7-Diphenyl-1,10-phenanthroline; **L-III**: 4,7-Diphenyl-1,10-phenanthroline disulfonic acid; **L-IV**: 2,2-Bipyridine; *Ligand-free Ru(II) control:* **Ru-C**: $RuCl_2(DMSO)4$; *Ru(II) precursor complexes:* **Ru-I**: $[Ru(II)(1,10\text{-phenanthroline})_2Cl_2]$; **Ru-II**: $[Ru(II)(4,7\text{-diphenyl-}1,10\text{-phenanthroline})_2Cl_2]$; **Ru-III**: $[Ru(II)(4,7\text{-diphenyl-}1,10\text{-phenanthroline-disulfonate})_2Na_2]^{2-}$; **Ru-IV**:$[Ru(II)(2,2'\text{-bipyridine})_2Cl_2]$.

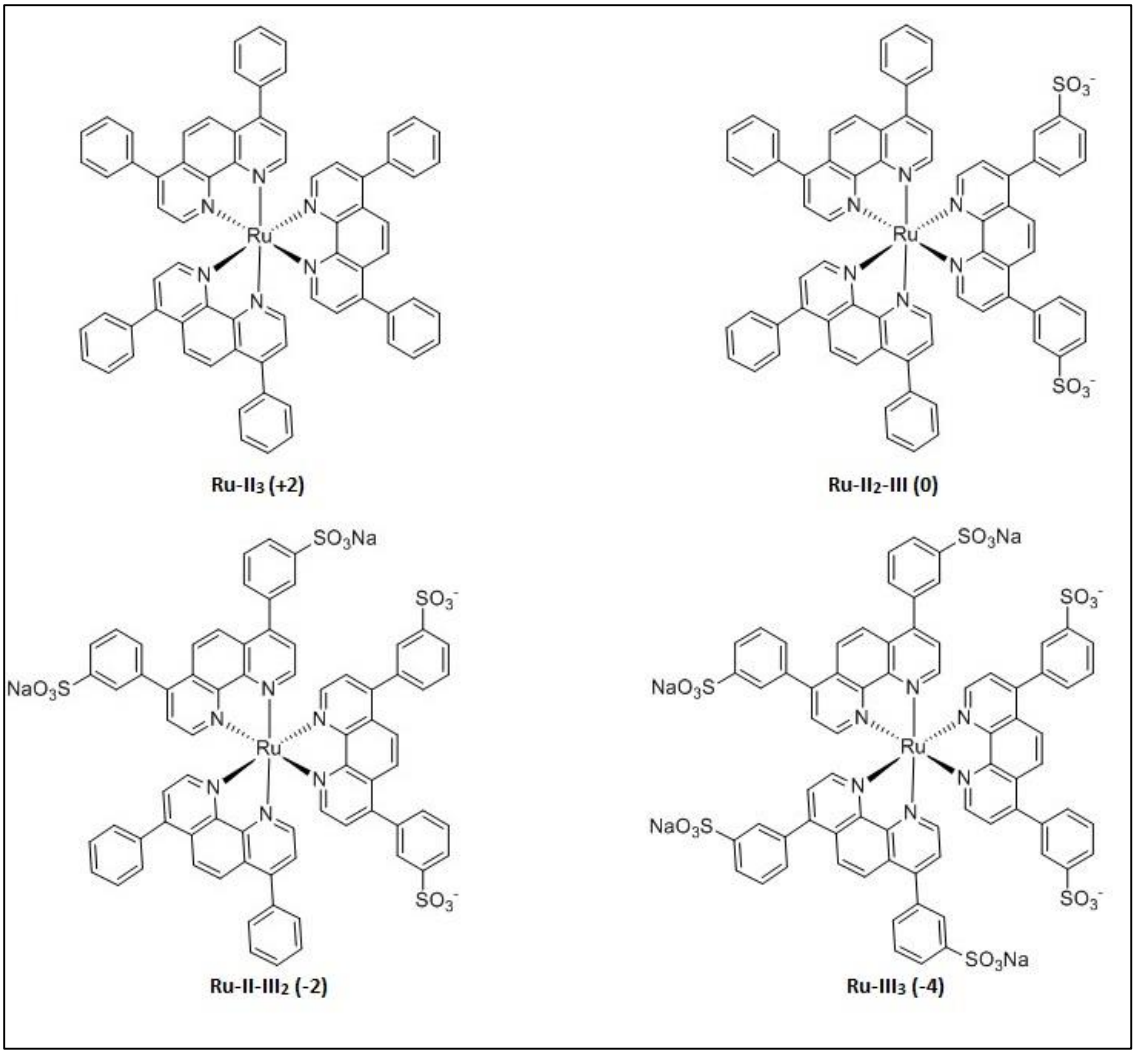

Figure 7: Different structures of the photochemically-active Ru(II) final (Tris) complexes.
Ru-II$_3$: [Ru(II)(4,7-diphenyl-1,10-phenanthroline)$_3$]$^{2+}$; **Ru-II$_2$-III**: [Ru(II)(4,7-diphenyl-1,10-phenanthroline)$_2$(4,7-diphenyl-1,10-phenanthroline-disulfonate)]; **Ru-II-III$_2$**: [Ru(II)(4,7-diphenyl-1,10-phenanthroline)(4,7-diphenyl-1,10-phenanthroline-disulfonate)$_2$]$^{2-}$; **Ru-III$_3$**: [Ru(II)(4,7-diphenyl-1,10-phenanthroline-disulfonate)$_3$]$^{4-}$.

2.3 Metal Uptake by Flow Cytometry

Cellular uptake of auto-fluorescent Ru-containing complexes was measured by flow cytometry. The SF cells were plated in 24-well plates at a density of 2.5 x10^5 cells in 250 µL cell culture medium in each well. The cells were allowed to recover for 24h at 37°C/5% CO_2, then 250 µL of compounds diluted in medium were added. The plates were incubated at 37°C with 5% CO_2 for the needed amount of time before being harvested and run for fluorescence detection on the FL3-H channel on a C6 flow cytometer (BD Accuri, Ann

Arbor, MI). The threshold was set to 500,000 on FSC-H, and 5,000 to 20,000 events were run per sample.

2.4 Proliferation Inhibition Assay (Cytotoxicity)

Sensitivity of the used cell lines to the compounds listed above was determined using a proliferation inhibition assay. Briefly, aliquots of 2 to 3 $x10^4$ cells/well in 100 µL of cell culture medium were plated in a flat-bottom 96-well plate (Corning Inc. Corning, NY). The cells were allowed to recover for 24h, before 50 µl of compound in media were added to each well to yield concentrations ranging from 200 µM to 3 nM. In the experiments involving light activation, the plates containing cells and compounds were exposed to blue light (430-490 nM) at 10 V for 30 min at room temperature. Following an incubation at 37°C/5% CO_2 till the appropriate time-point of the experiment, 10 µL of WST cell proliferation reagent (Roche, Basel, Switzerland) were added to each well 2h before the end of the intended incubation period, and the cells were incubated as above for the remaining 2h. Absorbance was then read at 450 nm using a microplate reader (Thermo Fisher Scientific, Waltham, MA). Nominal absorbance and percent maximal absorbance were plotted against the log of concentration and a non-linear regression with a variable slope sigmoidal dose-response curve was generated along with IC_{50} using GraphPad Prism 5 software (GraphPad Software, San Diego, CA).

2.5 Type of Cell Death Determination

The type of cell death was determined using fluorescin Isothiocyanate (FITC)-conjugated Annexin V antibody (Annexin V-FITC) and PI staining (apoptosis detection kit, Abcam, Cambridge, MA) as described previously (Abi-Habib et al. 2005). Annexin V is a calcium-dependent phospholipid binding protein specific to Phosphatidylserine (PS). PS is a component of the phospholipid membrane that, under normal conditions, faces the cytosolic side of the membrane due to the activity of the enzyme flippase. During apoptosis, flippase loses its activity on PS, allowing it to spontaneously flip and face the extracellular domain. As a result, macrophages recognize and engulf the cell. When the cells die, their cytoplasm becomes permeable to Propiduim idodide (PI), an auto-

fluorescent DNA intercalating agent that can be detected using flow cytometry on the FL2-channel (y axis). As for Annexin V, it can be detected using flow cytometry on the FL1-H channel (x axis). To differentiate between late-apoptosis and necrosis, caspase cascade activity is tested. To do so, an approach that uses flow cytometry called fluorescence inhibition of caspase is used. A fluorescent pan caspase inhibitor binds to reactive cysteine residues of active caspases and the levels of fluorescent caspase inhibitors are measured FL1-H channel (x axis).

The presence of active caspases in SF268 cells was detected using a cell permeable, FITC-conjugated active caspase inhibitor (R&D systems) on flow cytometry as described previously (Abi-Habib et al, 2005). Briefly, $3x10^5$ cells/well were plated in 250 µL of culture medium in a 24-well plate and were left to recover for 24 hours at 37°C/5% CO_2. They were later incubated with either 250 µL of media alone (control cells) or media containing different concentrations of L-II, Ru-II, Ru-II_3, Ru-II_2-III, Ru-II-III_2 and Ru-III_3 for 24, 48 and/or 72 hours at 37°C/5% CO_2. In the experiments involving light activation, the plates containing cells and compounds were exposed to blue light (430-490 nM) at 10 V for 30 min at room temperature. Cells were then either harvested and incubated with FITC-conjugated annexin V antibody (2.5 mg/ml) and PI (5 mg/ml) in antibody binding buffer for 45 minutes at 37°C, or incubated with a FITC-conjugated active caspase inhibitor (ApoStat Apoptosis Detection Kit, R&D Systems, Abingdon, England) for 60 minutes then harvested. Cells were then read using a C6 flow cytometer (BD Accuri, Ann Arbor, MI). Annexin V/PI data was analyzed on FL1-H versus FL2-H scatter plot and caspase activation was detected on FL1-H. Unstained cells were used as negative control. Cells were gated on width versus forward scatter. Cells had to show positive annexin V staining, negative PI staining and positive active caspase staining to be considered apoptotic, while cells positive for both annexin V and PI staining and negative for active caspase staining were considered non-apoptotic/necrotic.

2.6 Cell Cycle Analysis

The impact of Ru-II_3, Ru-II_2-III, Ru-II-III_2 and Ru-III_3 treatment in the dark and light on the cell cycle of SF cells was determined using Propidium Iodide (PI)-staining on flow cytometry as described previously (Abi-Habib et al, 2005). Briefly, cells (10^6 cells/well in 1 mL growth medium) incubated with different concentrations of L-II, Ru-II, Ru-II_3, Ru-II_2-III, Ru-II-III_2, Ru-III_3 or media alone in 6-well plates (Corning Inc. Corning, NY) for 72 hours at 37°C/5% CO_2, were harvested and fixed in 70% ethanol for a minimum of 24 hours at -20°C. In the experiments involving light activation, the plates containing cells and compounds were exposed to blue light (430-490 nM) at 10 V for 30 min at room temperature before the harvesting step. Cells were then incubated in 500 µL PI staining solution (50 µg/ml) for 40 minutes at 37°C. Samples were then read on a C6 flow cytometer (BD Accuri, Ann Arbor, MI) and cell DNA content was measured on FL2-A. The target cell population, excluding fragments and doublets, was gated on width versus forward scatter. Percent of cells in G0/G1, S and G2/M phase as well as percent cells in pre-G0/G1 phase (dead) was determined in control cells and in cells treated with the different concentrations of Ru-II_3, Ru-II_2-III, Ru-II-III_2 and Ru-III_3 at the different time points.

CHAPTER THREE

Results

3.1 Cellular uptake of the Ru-II Precursor Complex

Testing the uptake of Ru-II was done by using the flow cytometry assay after treating SF268 cell line. This compound itself is auto-fluorescent and can be detected on the FL3-H channel, and its uptake was detectable at early time points after treatment of the cells (30 min and 60 min), as well as at later time points (2h, 4h, 6h and 24h) (figure 14). The uptake was significant at the late time points, starting 4h and up posttreatment. Thus, deducing that the uptake of the compound is necessary for inducing a cytotoxic effect in the cells.

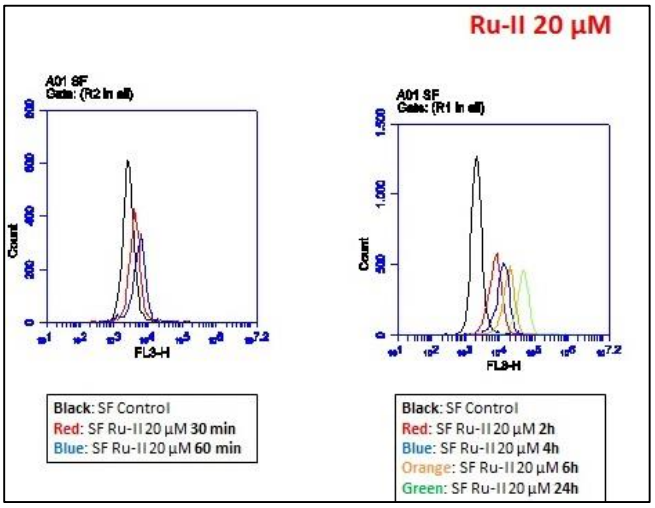

Figure 8: Detection of cellular uptake of Ru-II at early and late time points after treatment of SF268 cell line. **Ru-II** found intracellularly through flow cytometry on FL3-H at 0.5, 1, 2, 4, 6 & 24h post treatment. The emission fluorescence is near 600 nm.

3.2 Cytotoxic Effect of the Ligands and Ru(II) Precursor Complexes on Human Solid Tumor Cell Lines

The Ru(II) precursor complexes were tested on 6 different solid tumor cell lines, along with their respective free ligands which are derivatives of phenanthroline and bipyridine. In figure 8, data showed that L-I and Ru-I had no significant effect on the cell lines except B16 and MDA-MB-231. However, all cell lines were sensitive to L-II and Ru-II as depicted in figure 9. L-III, Ru-III, L-IV and Ru-IV showed no potency on the cell lines except for L-IV showing significant potency against B16 cell line (figures 10 & 11). As for the ligand-free metal control Ru-C, data from figure 12 showed no toxicity on the tested cell lines. IC_{50} averages were calculated and only the compounds that showed potency were summarized in table 1.

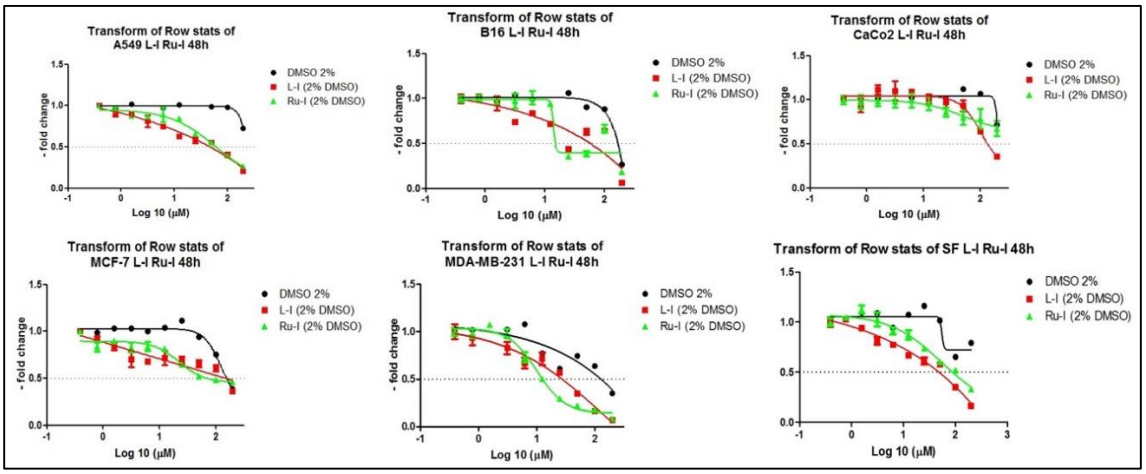

Figure 9: Cytotoxic effect of the free ligand L-I and its corresponding precursor complex Ru-I on 6 representative Solid Tumor cell lines at 48h.

Nonlinear regression curves for the cytotoxicity of **L-I** & **Ru-I** vs DMSO (solvent) on A549, B16, Caco2, MCF-7, MDA-MB-231 and SF268, respectively. Percentage of v/v DMSO is 2% at the highest dosage of each tested compound.

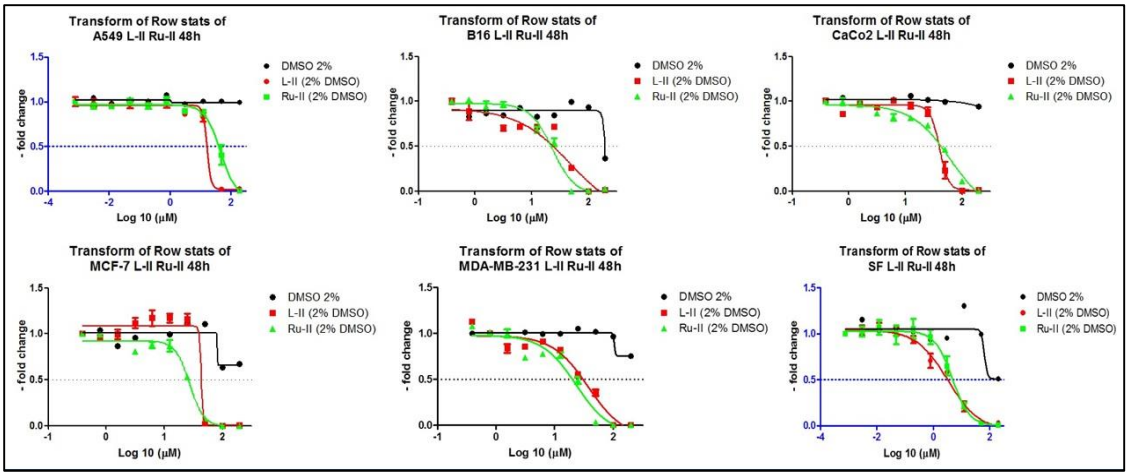

Figure 10: Cytotoxic effect of the free ligand L-II and its corresponding precursor complex Ru-II on 6 representative Solid Tumor cell lines at 48h.

Nonlinear regression curves for the cytotoxicity of **L-II** & **Ru-II** vs DMSO (solvent) on A549, B16, Caco2, MCF-7, MDA-MB-231 and SF268, respectively. Percentage of v/v DMSO is 2% at the highest dosage of each tested compound.

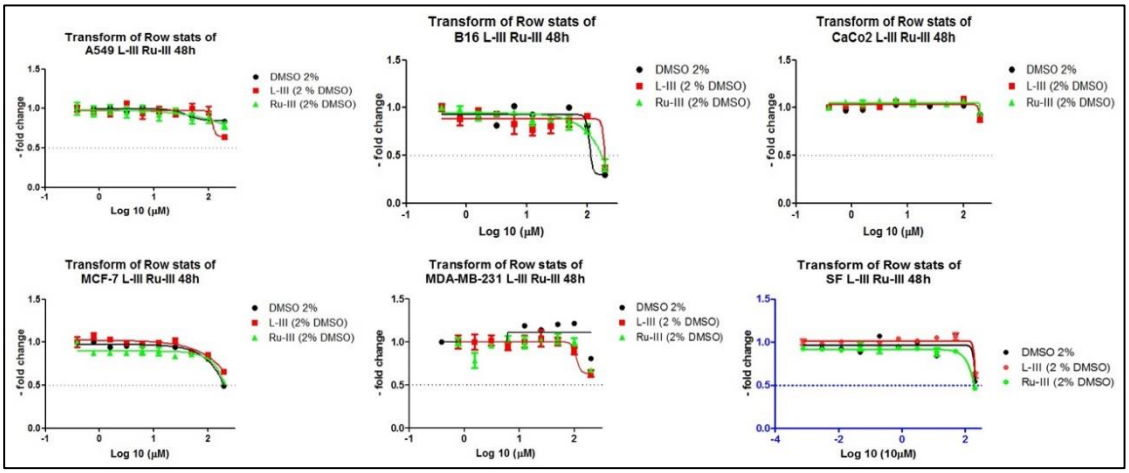

Figure 11: Cytotoxic effect of the free ligand L-III and its corresponding precursor complex Ru-III on 6 representative Solid Tumor cell lines at 48h.

Nonlinear regression curves for the cytotoxicity of **L-III** & **Ru-III** vs DMSO (solvent) on A549, B16, Caco2, MCF-7, MDA-MB-231 and SF268, respectively. Percentage of v/v DMSO is 2% at the highest dosage of each tested compound.

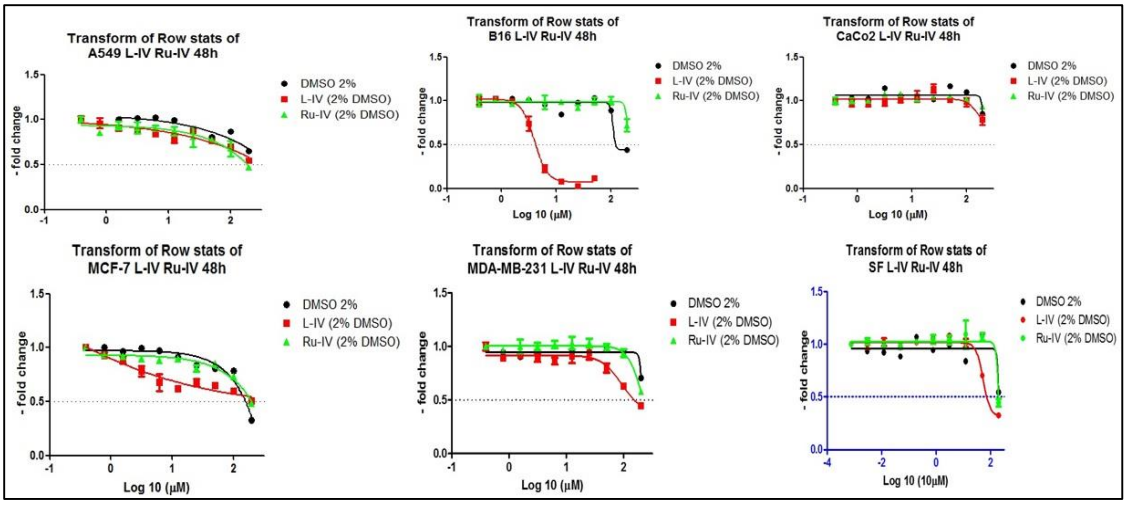

Figure 12: Cytotoxic effect of the free ligand L-IV and its corresponding precursor complex Ru-IV on 6 representative Solid Tumor cell lines at 48h.

Nonlinear regression curves for the cytotoxicity of **Ru-C** vs DMSO (solvent) on A549, B16, Caco2, MCF-7, MDA-MB-231 and SF268, respectively. Percentage of v/v DMSO is 2% at the highest dosage of each tested compound.

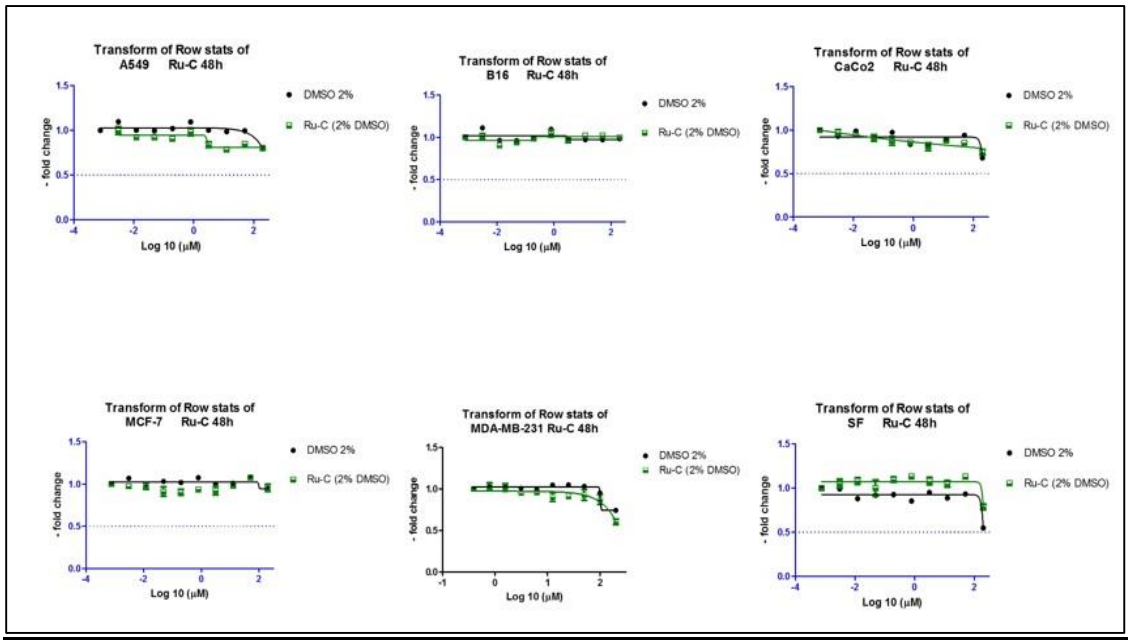

Figure 13: Cytotoxic effect of the ligand-free Ru(II) metal core on 6 representative Solid Tumor cell lines at 48h.

Nonlinear regression curves for the cytotoxicity of **Ru-C** vs DMSO (solvent) on A549, B16, Caco2, MCF-7, MDA-MB-231 and SF268, respectively. Percentage of v/v DMSO is 2% at the highest dosage of each tested compound.

Table 1: Average IC_{50} (µM) at 48h

	L-I	Ru-I	L-II	Ru-II	L-IV
A549	63	62	22	38	>200
B16	21.5	21	28	27.5	4.5
Caco2	140	>200	20	30	>200
MCF-7	>200	>200	37.5	27	>200
MDA-MB-231	31	12.5	24.4	22	>200
SF268	63	107	4	5	105

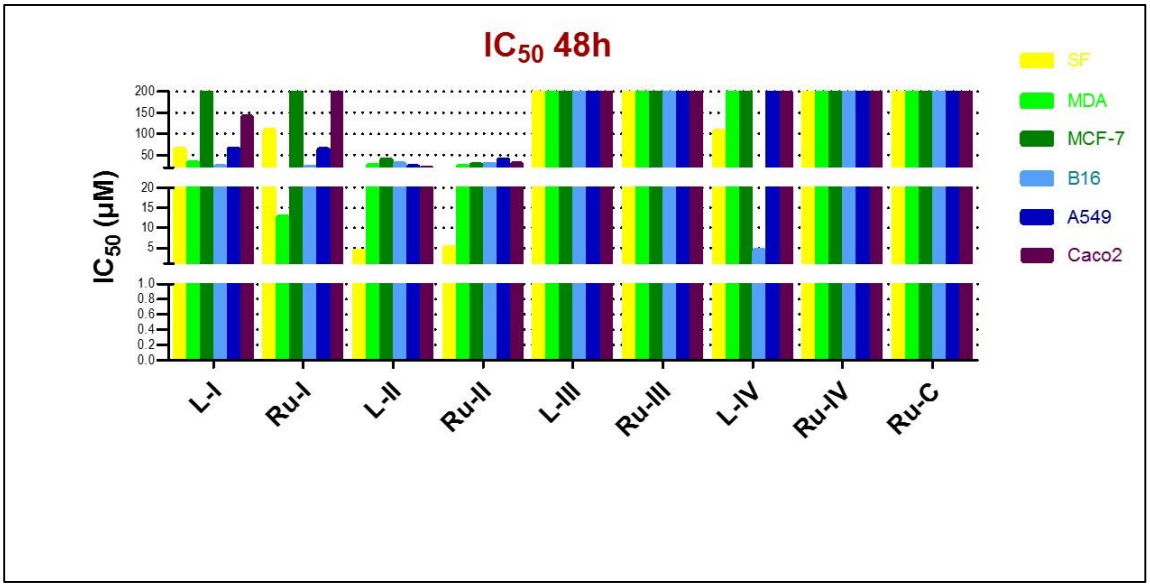

Figure 14: **Ru-I shows high potency against MDA-MB-231 cell line, L-II and Ru-II against SF268 cell line, L-IV against B16 cell line and the ligand-free Ru-C is biologically inert.**
IC_{50} (µM) at 48h of the different compounds obtained from 6 solid tumor cell lines.

3.3 Type of Cell Death Determination of the Action of the Free L-II Ligand and Ru-II Precursor

One method to determine the type of cell death involves Annexin V labeled with a fluorescent probe. As a result, cells that stain negative for Annexin V and PI are the healthy population, cells staining positive for Annexin V and negative for PI are cells undergoing apoptosis, whereas cells staining positive for both are late-apoptotic cells and the cells positive for PI stain only are necrotic.

Flow cytometry is used to determine the type of cell death of SF268 cell line when treated with L-II and Ru-II at 24h and 48h. These are non-conclusive results and this experiment is still under process (Figures 15 & 16). However, from these preliminary data, at 24h no cell death is observed by L-II and Ru-II, same goes for Ru-II at 48h. On the other hand, in the case of L-II at 48h, small traces of late-apoptotic cell death is shown by these cells, however the values are non-significant (control; 2.2%; treatment with low concentration: 5.9%; treatment with high concentration: 7.3%).

As for the caspase assay at 48h, for both compounds, L-II and Ru-II, data showed lack of caspase cascade activation meaning no detection of apoptosis.

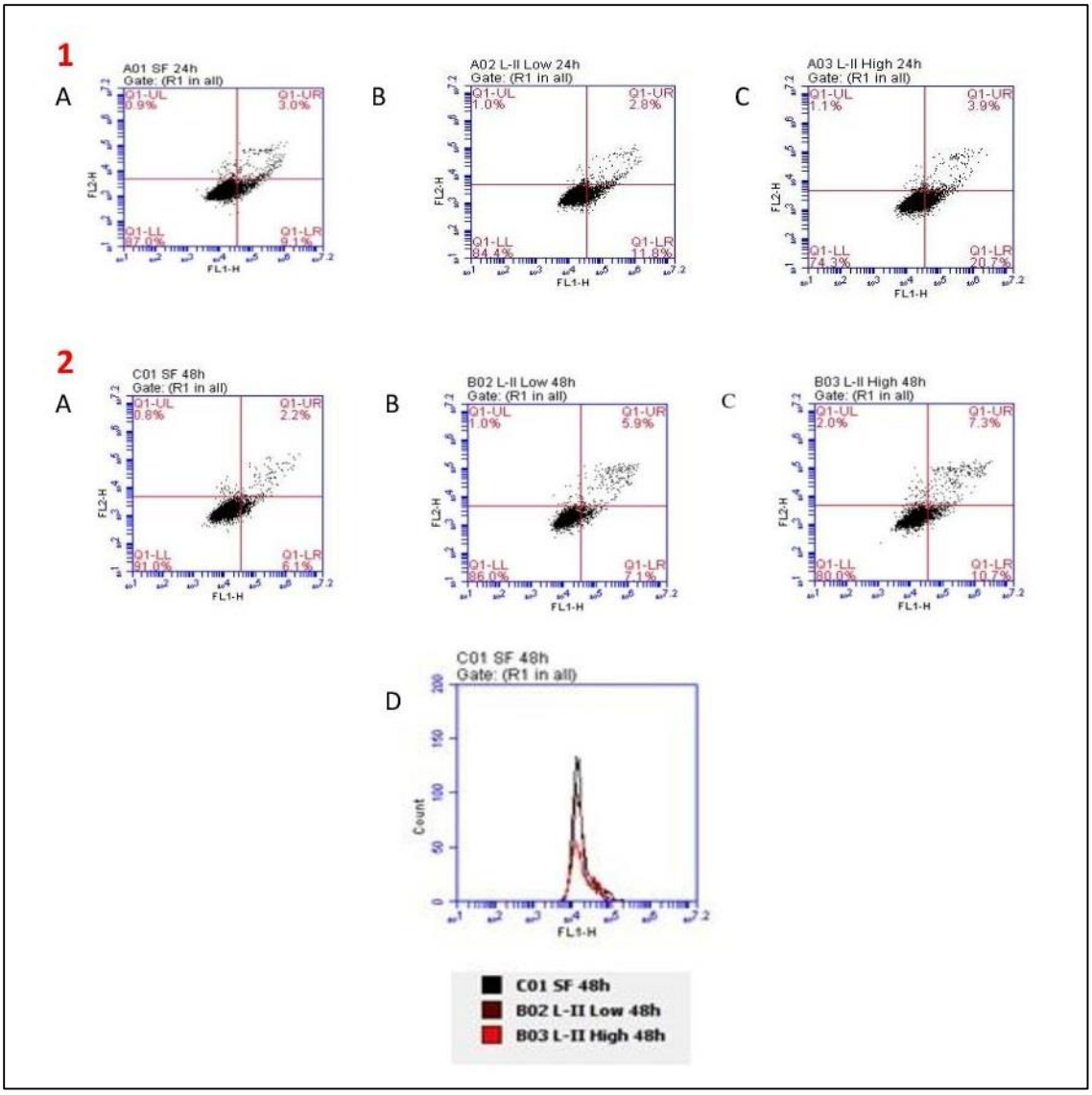

Figure 15: Preliminary results of the type of cell death caused by L-II.
Annexin-PI (1A –1C & 2A-2C) & Caspase Activation (D) at 48h. SF268 Control (1A & 2A). **L-II** – 4.5 µM (1B & 1C) & 9 µM (2B & 2C). Normal cell population (LL), early-apoptotic cell population (LR), late-apoptotic / necrotic cell population (UR).

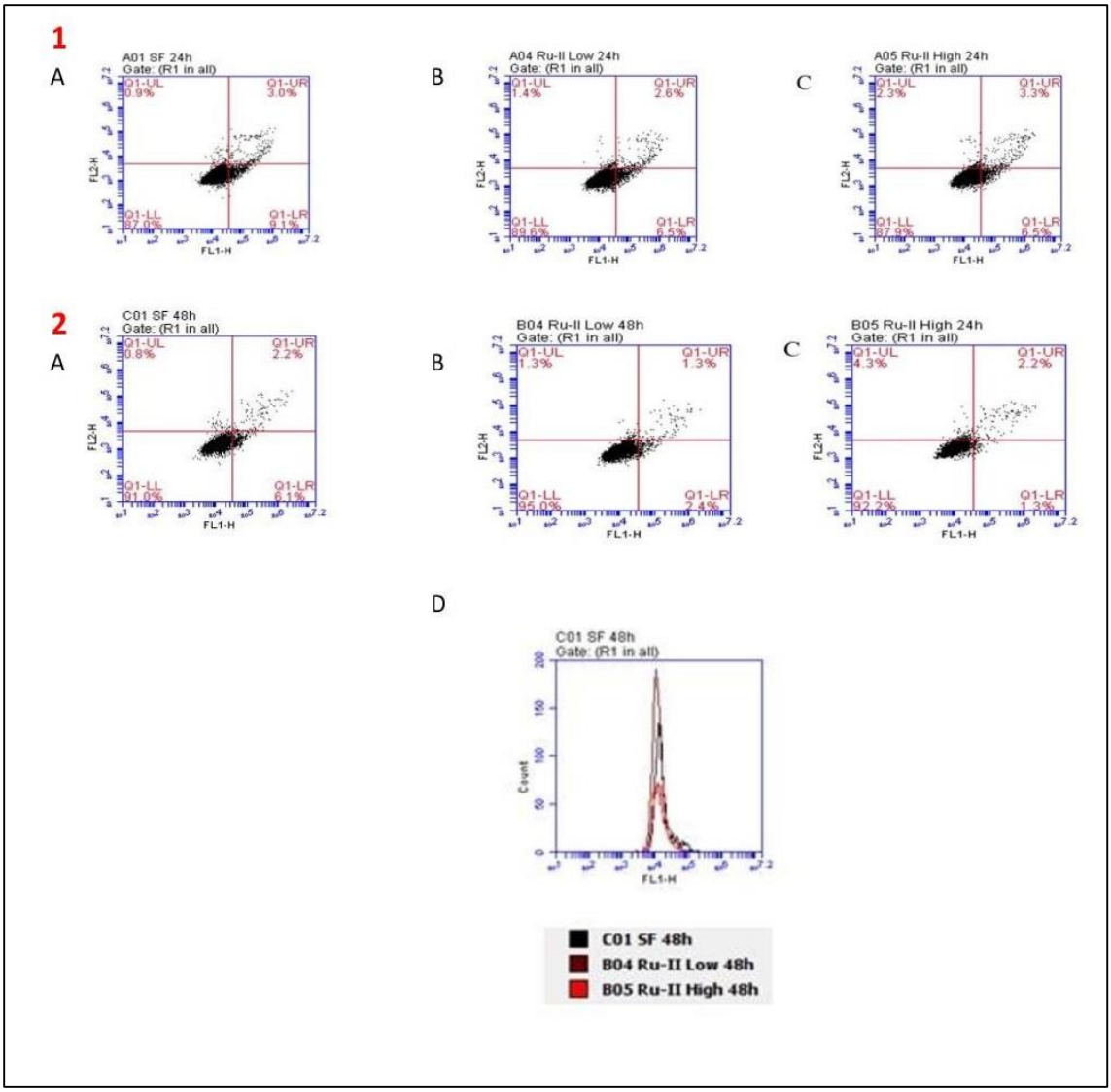

<u>Figure 16:</u> Preliminary results of the type of cell death caused by Ru-II.
Annexin-PI (1A –1C & 2A-2C) & Caspase Activation (D) at 48h. SF268 Control (1A & 2A). **Ru-II** – 5 µM (1B & 1C) & 10 µM (2B & 2C).

3.4 Cellular uptake of the Final (Tris-) Complexes in the Dark

Intracellular levels of uptake, as described above, were observed for all 4 compounds at early and late time points post-treatment in SF268 cell line. The data of Ru-II_3 & Ru-II_2-III were only shown (Figures 24 & 25), where significant cellular uptake was detected at the late time points. In the case of Ru-II_3, it was detected at 60 min posttreatment, whereas for Ru-II_2-III, it was detected 2h after treating the cells. Same results were obtained for Ru-II_2-III & Ru-II_3, however the data are not shown.

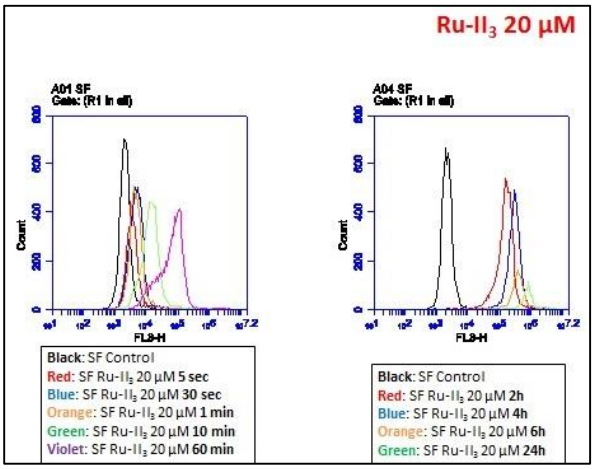

Figure 17: Detection of cellular uptake of Ru-II_3 at early and late time points after treatment.
Ru-II_3 found intracellularly through flow cytometry on FL3-H at 60 min, 2, 4, 6 & 24h post treatment. The emission fluorescence is near 600 nm.

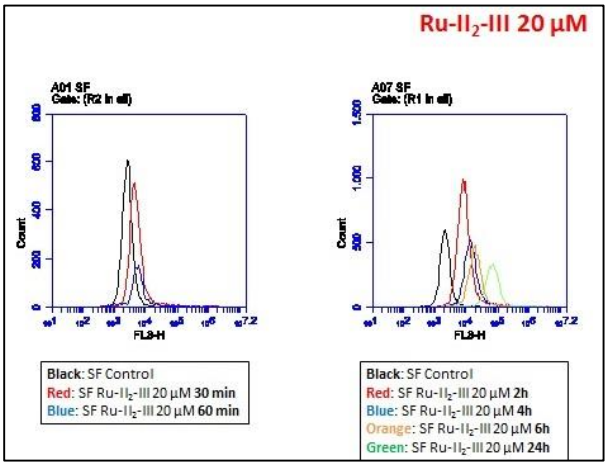

Figure 18: Detection of cellular uptake of Ru-II_2-III at early and late time points after treatment.
Ru-II_2-III found intracellularly through flow cytometry on FL3-H at 2, 4, 6 & 24h post treatment. The emission fluorescence is near 600 nm.

3.5 Cytotoxicity of the Final (Tris-) Complexes in the Dark

The final (Tris-) complexes were tested on the 6 solid tumor cell lines using the cell viability assay. The effect of cisplatin was also tested on the same cell lines and the results were used as positive control as shown in figures 17, 18, 19, 20, 21 & 23. Data showed that all final complexes that have more L-II ligands conjugated to the Ru(II) metal had a significant potency against solid tumor cell lines in the dark, especially Ru-II_3 more than Ru-II_2-III. These 2 final compounds do not bear a negative charge in their structure. In addition, the tested cell lines had a higher sensitivity to Ru-II_3, as their IC_{50} values were in the low µM range, and in the case of SF268, IC_{50} values reached the low nM range, while the other 2 final complexes, Ru-II-III_2 and Ru-III_3, showed little or no effect as expected (figure 23 & table 2). Regarding A549 and Caco2 cell lines, they showed resistance to cisplatin while having significant sensitivity to Ru-II_3, and in the case of A549 to Ru-II_2-III as shown in figures 17 and 19, respectively.

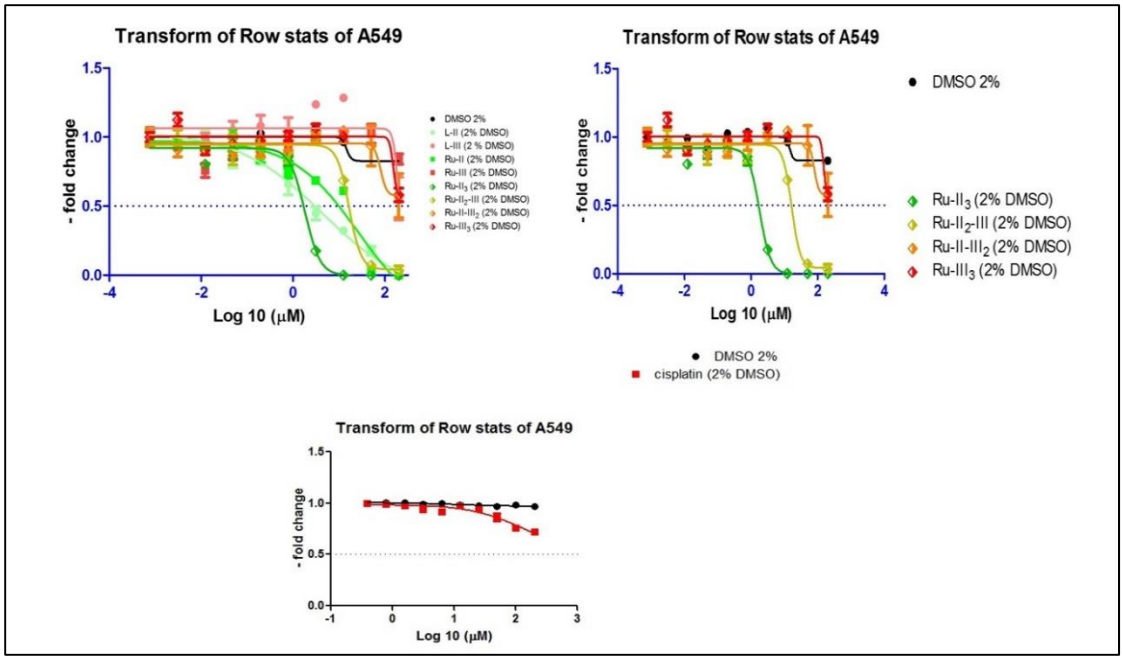

Figure 19: Cytotoxic effect of the final Ru(II) complexes vs. ligands, precursors and cisplatin on A549 solid tumor cell line at 72h in the dark.

Nonlinear regression curves for the cytotoxicity of **L-II**, **L-III**, **Ru-II**, **Ru-III**, **Ru-II$_3$**, **Ru-II$_2$-III**, **Ru-II-III$_2$**, **Ru-III$_3$ and cisplatin** vs DMSO on A549.

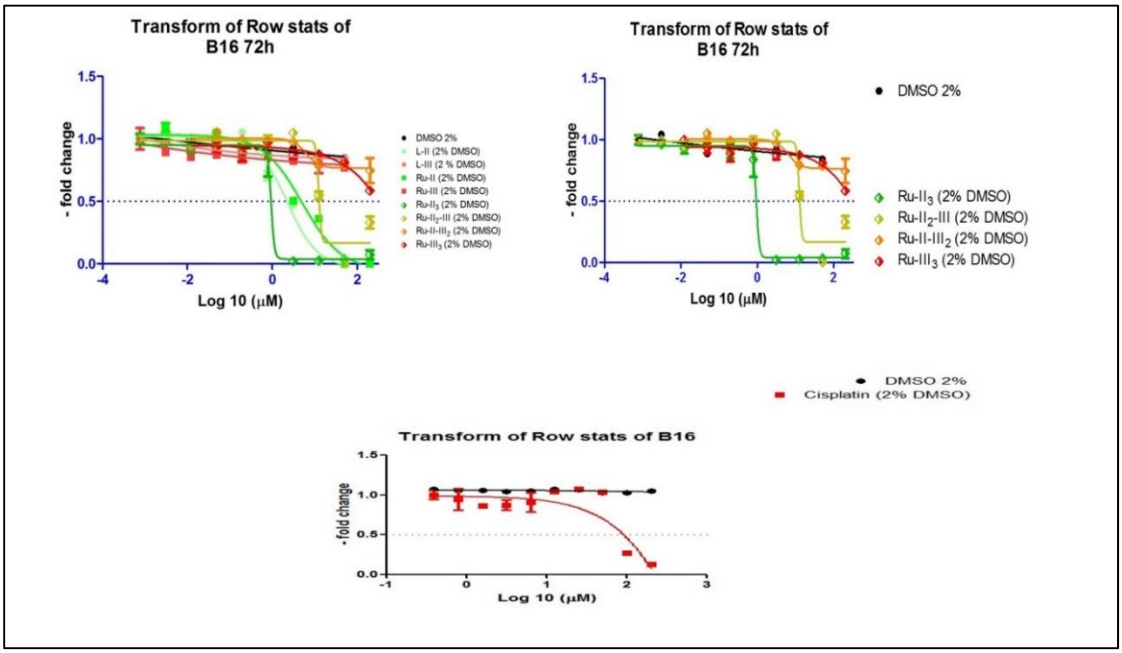

Figure 20: Cytotoxic effect of the final Ru(II) complexes vs. ligands, precursors and cisplatin on B16 solid tumor cell line at 72h in the dark.

Nonlinear regression curves for the cytotoxicity of **L-II**, **L-III**, **Ru-II**, **Ru-III**, **Ru-II$_3$**, **Ru-II$_2$-III**, **Ru-II-III$_2$**, **Ru-III$_3$ and cisplatin** vs DMSO on B16.

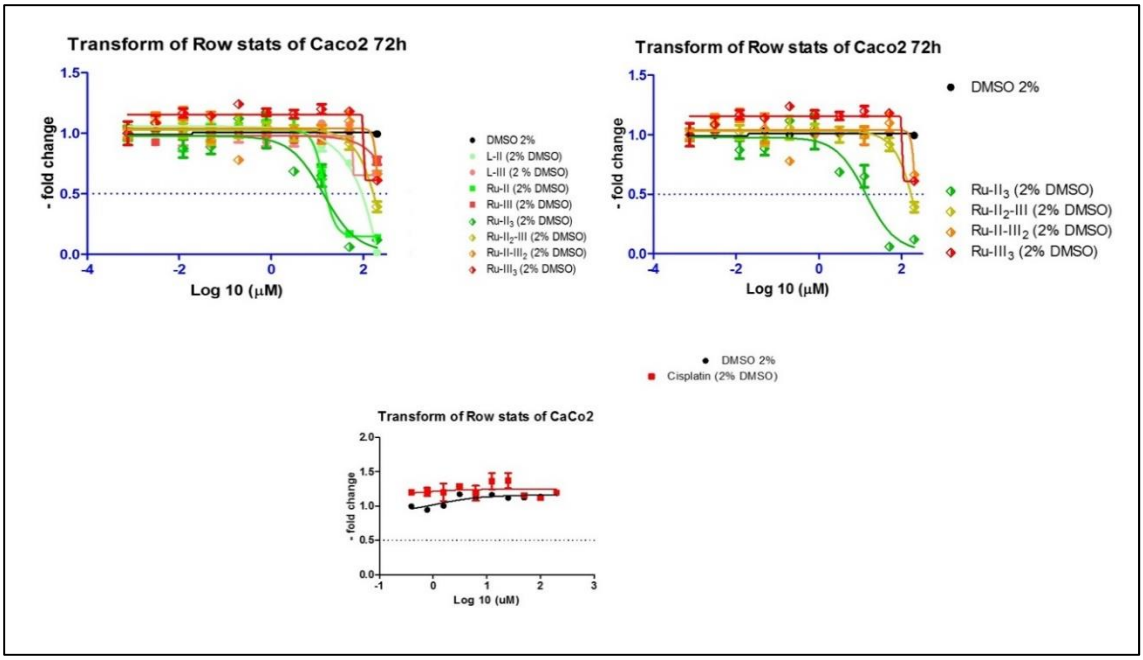

Figure 21: **Cytotoxic effect of the final Ru(II) complexes vs. ligands, precursors and cisplatin on Caco2 solid tumor cell line at 72h in the dark.**

Nonlinear regression curves for the cytotoxicity of **L-II**, **L-III**, **Ru-II**, **Ru-III**, **Ru-II$_3$**, **Ru-II$_2$-III**, **Ru-II-III$_2$**, **Ru-III$_3$ and cisplatin** vs DMSO on Caco2.

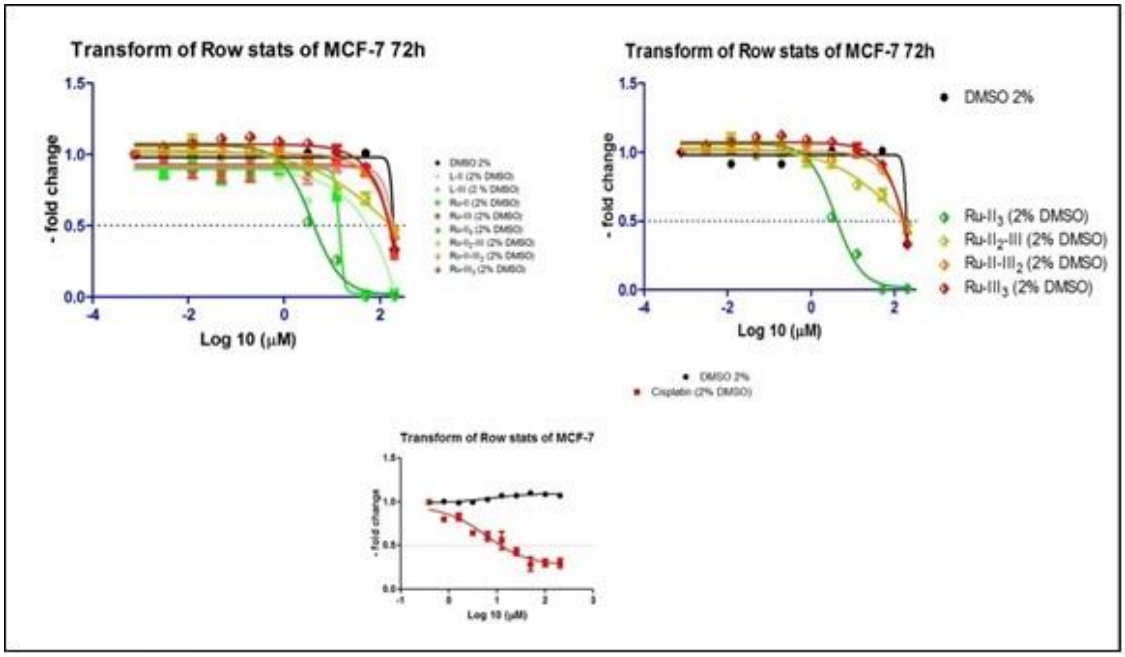

Figure 22: **Cytotoxic effect of the final Ru(II) complexes vs. ligands, precursors and cisplatin on MCF-7 solid tumor cell line at 72h in the dark.**

Nonlinear regression curves for the cytotoxicity of **L-II**, **L-III**, **Ru-II**, **Ru-III**, **Ru-II$_3$**, **Ru-II$_2$-III**, **Ru-II-III$_2$**, **Ru-III$_3$ and cisplatin** vs DMSO on MCF-7.

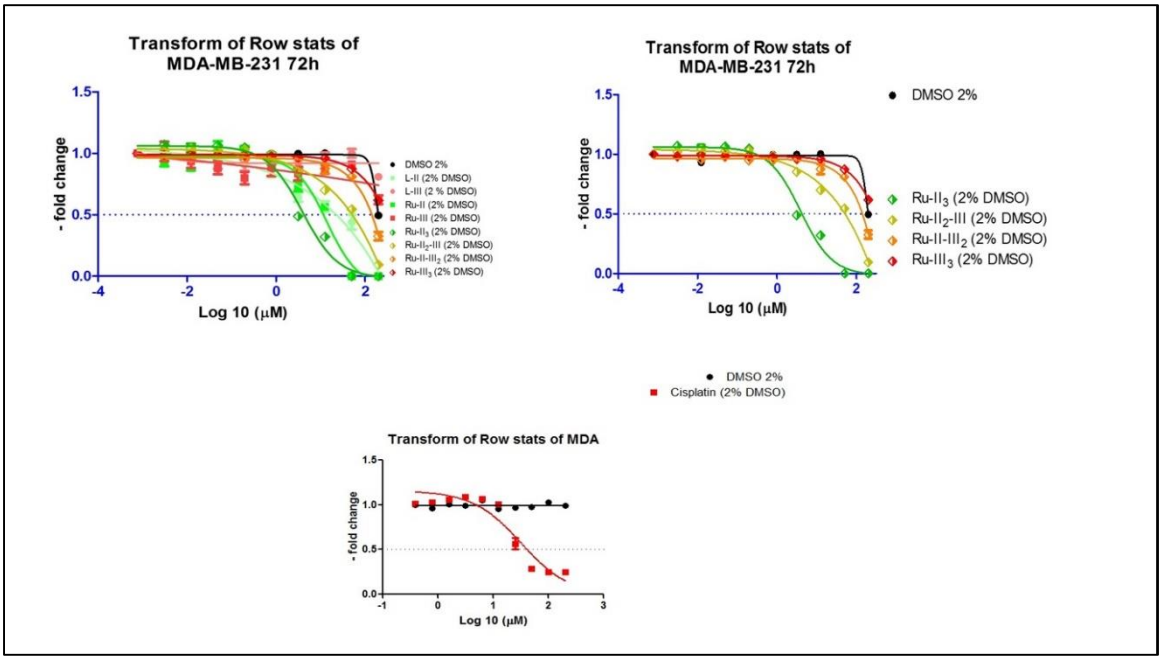

Figure 23: Cytotoxic effect of the final Ru(II) complexes vs. ligands, precursors and cisplatin on MDA-MB-231 solid tumor cell line at 72h in the dark.
Nonlinear regression curves for the cytotoxicity of **L-II**, **L-III**, **Ru-II**, **Ru-III**, **Ru-II$_3$**, **Ru-II$_2$-III**, **Ru-II-III$_2$**, **Ru-III$_3$ and cisplatin** vs DMSO on MDA-MB-231.

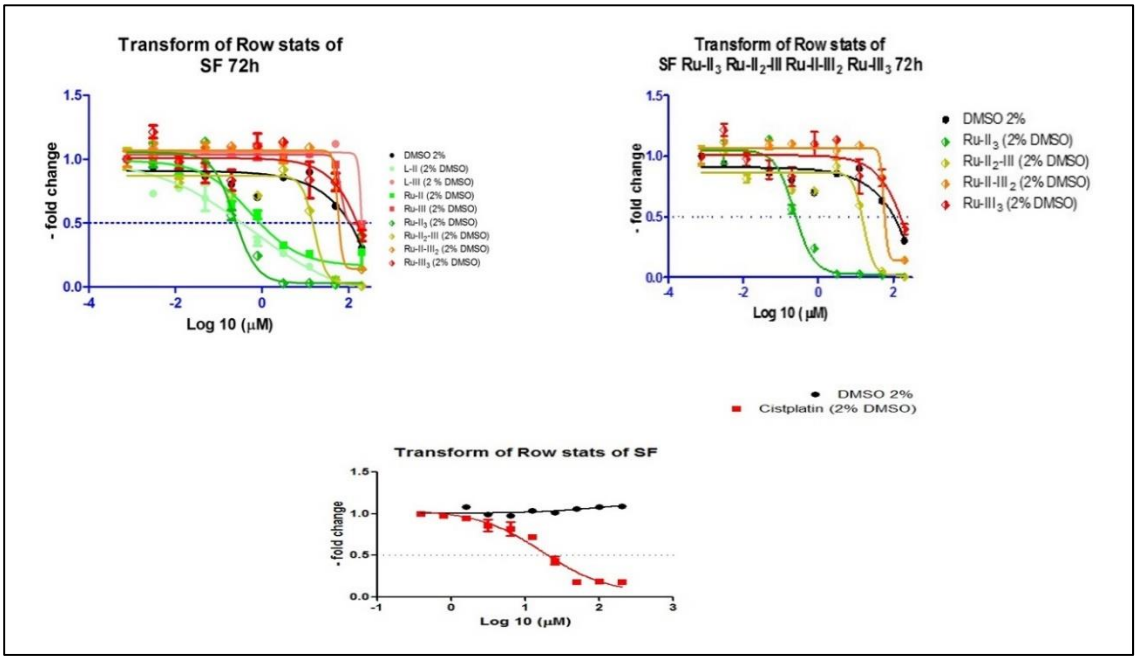

Figure 24: Cytotoxic effect of the final Ru(II) complexes vs. ligands, precursors and cisplatin on SF268 solid tumor cell line at 72h in the dark.
Nonlinear regression curves for the cytotoxicity of **L-II**, **L-III**, **Ru-II**, **Ru-III**, **Ru-II$_3$**, **Ru-II$_2$-III**, **Ru-II-III$_2$**, **Ru-III$_3$ and cisplatin** vs DMSO on SF268.

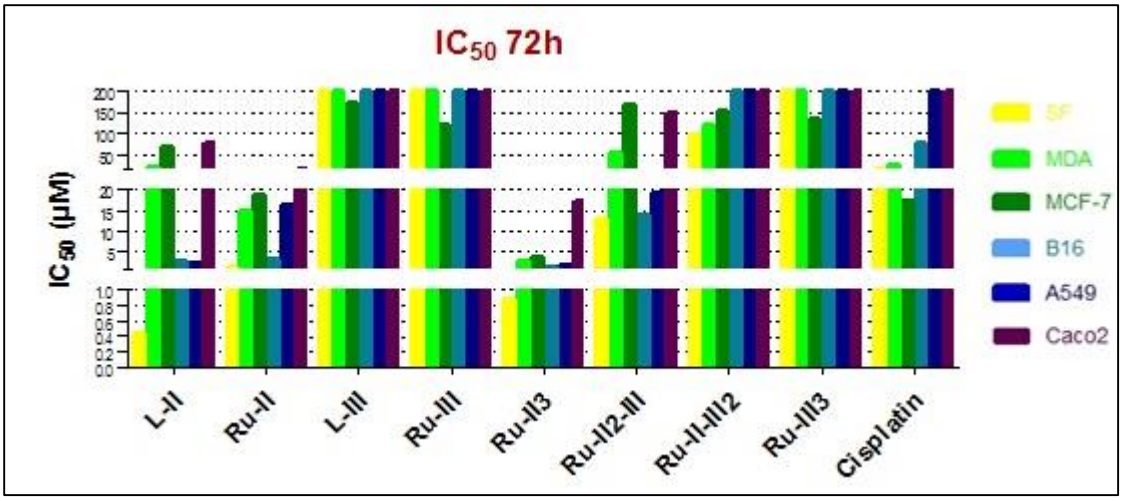

Figure 25: **L-II, Ru-II and the final complexes Ru-II_3 & Ru-II_2-III (that have more L-II ligands conjugated) show potency against solid tumor cell lines in the dark.**
IC_{50} (µM) at 72h of the different compounds and cisplatin on 6 solid tumor cell lines.

Table 2: **Average IC_{50} (µM) at 72h**

	L-II	Ru-II	L-III	Ru-III	Ru-II_3	Ru-II_2-III	Ru-II-III_2	Ru-III_3
A549	2	16	>200	>200	1.5	19	>200	>200
B16	2.5	3.5	>200	>200	1.5	14	>200	>200
Caco2	>200	20	>200	>200	17	>200	>200	>200
MCF-7	>200	18	>200	>200	3.5	>200	>200	>200
MDA-MB-231	>200	15	>200	>200	3	>200	>200	>200
SF268	0.5	1	>200	>200	1	13	>200	>200

3.6 Type of Cell Death Determination of the Action of the Final Ru(II) Complexes Active in the Dark

The two final complexes that showed activity in the dark, as well as the other two inactive compounds, were applied on SF268 cell line, and flow cytometry was used to determine the type of cell death at 24h, 48h and 72h and cell cycle analysis at 72h as described earlier.

Results showed that the type of cell death of **Ru-II$_3$** in the dark was non-apoptotic as observed in figure 26, at 24h, 48h and 72h since most of the cells were late apoptotic/necrotic and the caspase assay confirms the lack of apoptosis due to the absence of cascade activation. Same goes for **Ru-II$_2$-III** where no signs of apoptosis were detected (Figure 27), whereas **Ru-II-III$_2$** and **Ru-III$_3$**, as previously demonstrated in the previous experiments, showed no type of cell death as expected (figure 28).

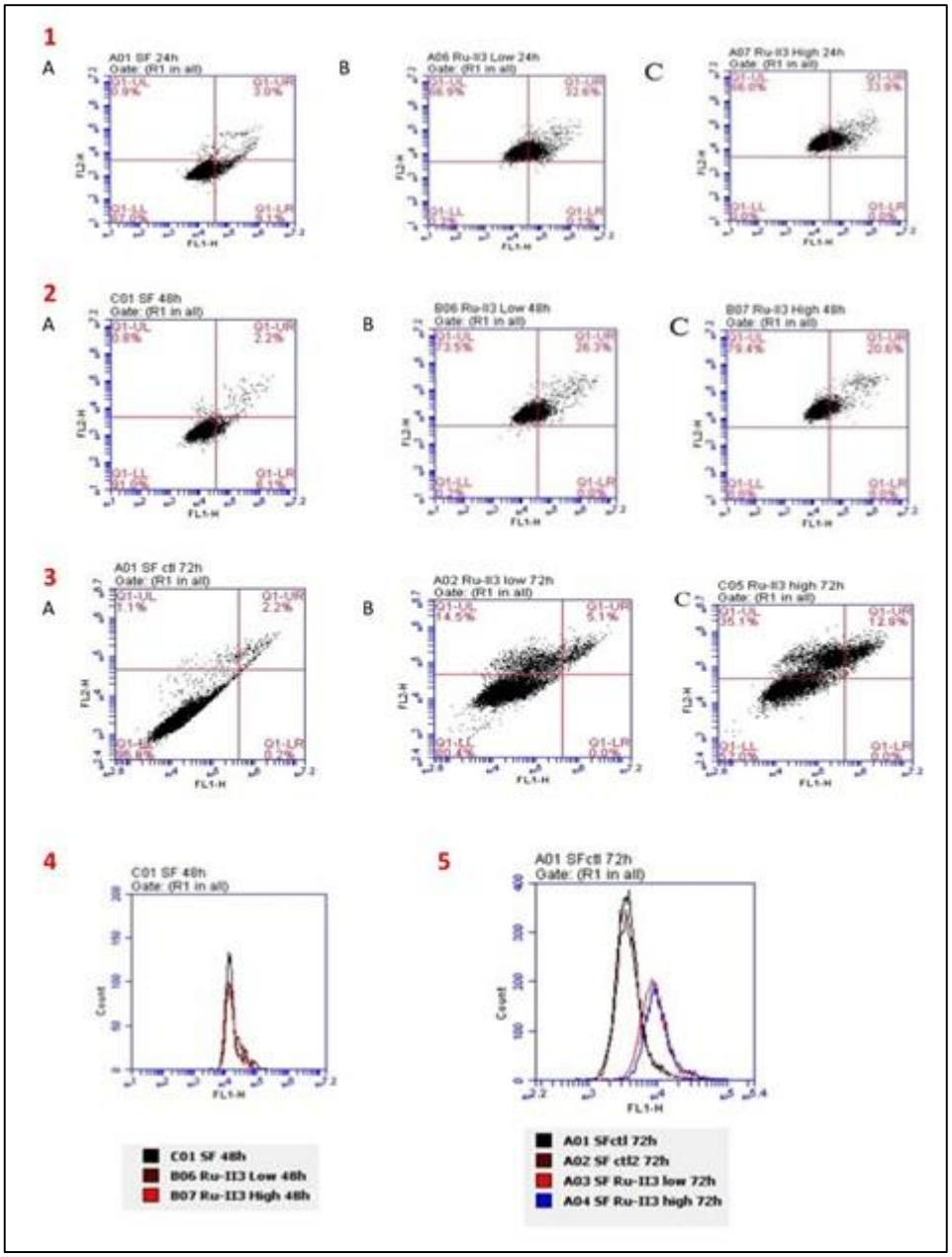

Figure 26: Cell death caused by Ru-II$_3$ is non-apoptotic in the dark.
Annexin-PI at 24h (1), 48h (2) and 72h (3) & Caspase Activation at 48h (4) and 72h (5). SF268 Control (1A, 2A &3A). **Ru-II$_3$** – 1.5 µM (1B, 2B & B) & 3 µM (1C, 2C & 3C).

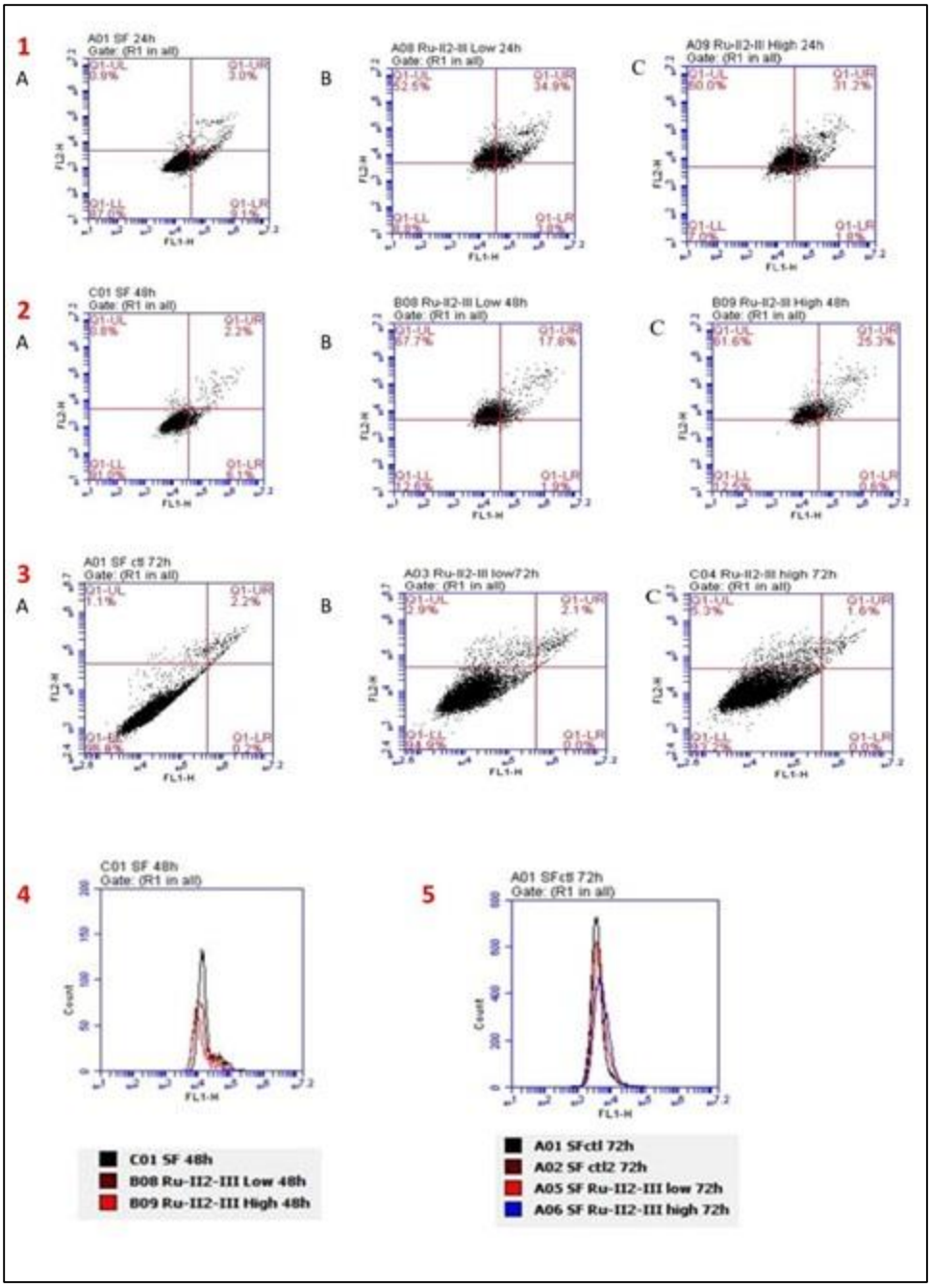

<u>Figure 27:</u> Cell death caused by Ru-II$_2$-III is non-apoptotic in the dark.
Annexin-PI at 24h (1), 48h (2) and 72h (3) & Caspase Activation at 48h (4) and 72h (5). SF268 Control (1A, 2A &3A). **Ru-II$_2$III** – 12 µM (1B, 2B & B) & 24 µM (1C, 2C & 3C).

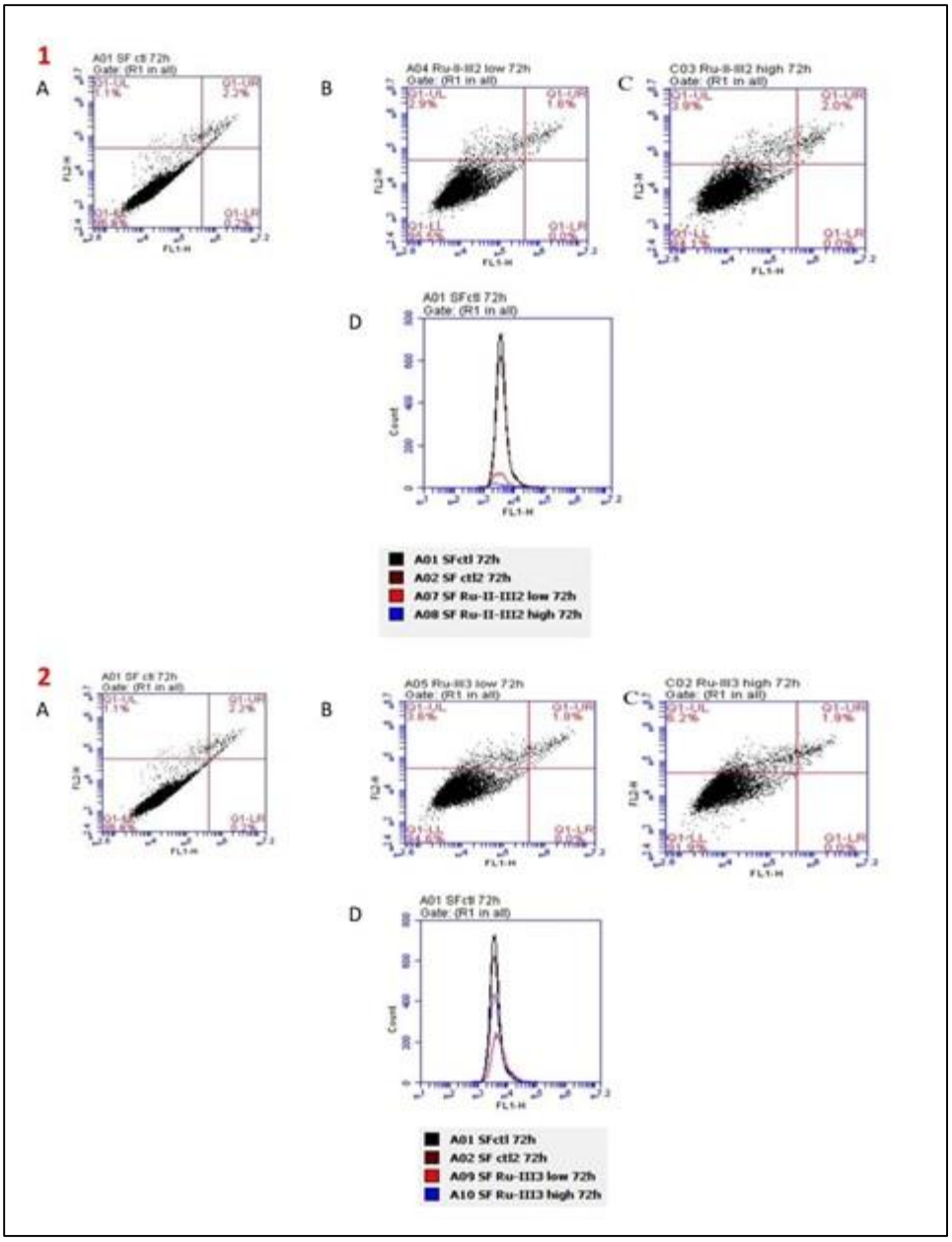

<u>Figure 28:</u> No cell death caused by Ru-II-III$_2$ and Ru-III$_3$ in the dark.

Annexin-PI at 72h (1A-B & 2A-B) & Caspase Activation at 72h (1D & 2D). SF268 Control (1A & 2A). **Ru-II-III$_2$** – 10 µM (1B) & 20 µM (2B) and **Ru-III$_3$** – 7 µM (1C) & 14 µM (2C) (Random dosages)

3.7 Cell Cycle Analysis of the Action of the Final Ru(II) Complexes Active in the Dark

Cell cycle analysis data in figure 29 are preliminary results. This experiment is still a work in progress. However, it was shown that there is a significant decrease of cell cycle arrest at G1 at high concentrations of **Ru-II$_3$** & **Ru-II$_2$-III** at 72h when tested on SF268 cell line. In contrast, **Ru-II-III$_2$** and **Ru-III$_3$** did not show this decrease as expected since they are inert in the dark. These data are non-conclusive and need to be further elucidated.

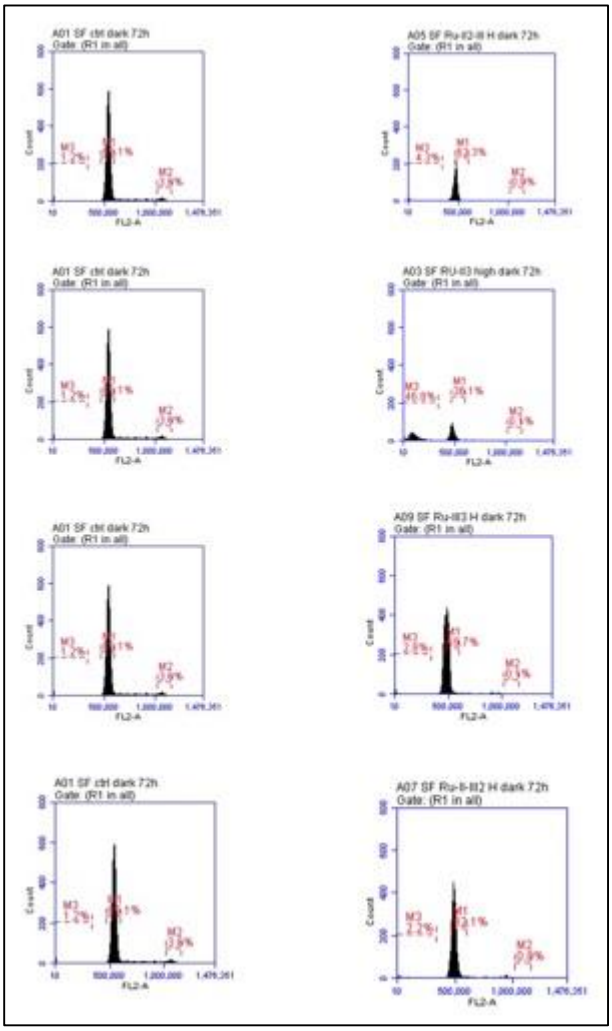

Figure 29: Preliminary results of Cell cycle analysis of the 4 (Tris-) compounds in the dark.
Cell Cycle Analysis – PI Staining at 72h. SF268 Control (A, D, G & K). **Ru-II$_3$** – 1.5 µM (B) & 3 µM (C), **Ru-II$_2$III** – 3 µM (E) & 6 µM (F), **Ru-II-III$_2$** – 7 µM (H) & 14 µM (I), **Ru-III$_3$** – 1 µM (L) & 2 µM (M).

3.8 Cytotoxicity of the Final (Tris-) Compounds with Light Activation against SF268

The 4 final (Tris-) compounds were tested on SF268 cell line in the dark and after exposure to blue light as described above at 6h, 12h and 24h post-treatment. Previous data showed that only **Ru-II$_3$** and **Ru-II$_2$-III** had a cytotoxic effect on cells in the dark and the other 2 were inert. However, upon photo-activating the 4 compounds at the different time points as mentioned above, all of them showed activity including the DMSO solvent (figure 26). Cell death was observed in the cells exposed to DMSO alone at the earliest time points of photo-activation, and its "cytotoxic effect" appeared to diminish at the later time points, specifically at 24h post-treatment light activation (figure 29).

In table 3, results show the differences between the 4 compounds' IC_{50} values and in figures 31 & 32 the significant increase or initiation of their cytotoxic action at the 24h time point. In the case of **Ru-II$_3$** and **Ru-II$_2$-III**, their potent activity increased, occurring at earlier time points, whereas **Ru-II-III$_2$** and **Ru-III$_3$** acquired potency.

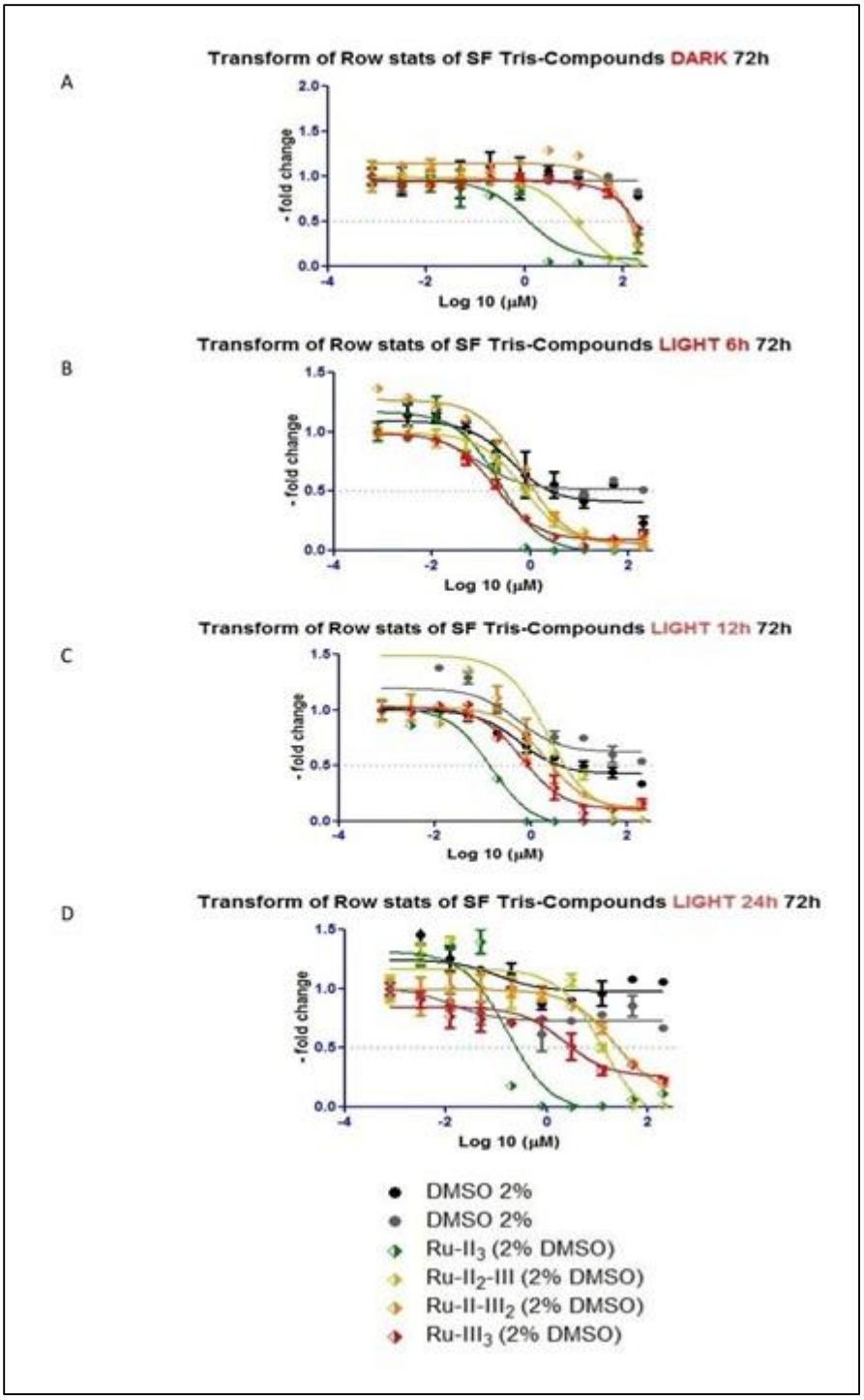

<u>Figure 30:</u> Effect of all final complexes is significantly potentiated after exposure to blue light.
Nonlinear regression curves for the cytotoxicity of **Ru-II$_3$**, **Ru-II$_2$-III**, **Ru-II-III$_2$** & **Ru-III$_3$** vs DMSO (solvent) on SF268 in the dark (A), with light activation at T=6h (B), at T=12h (C) and at T=24h (D). All readings of the cell viability experiment were done at 72h.

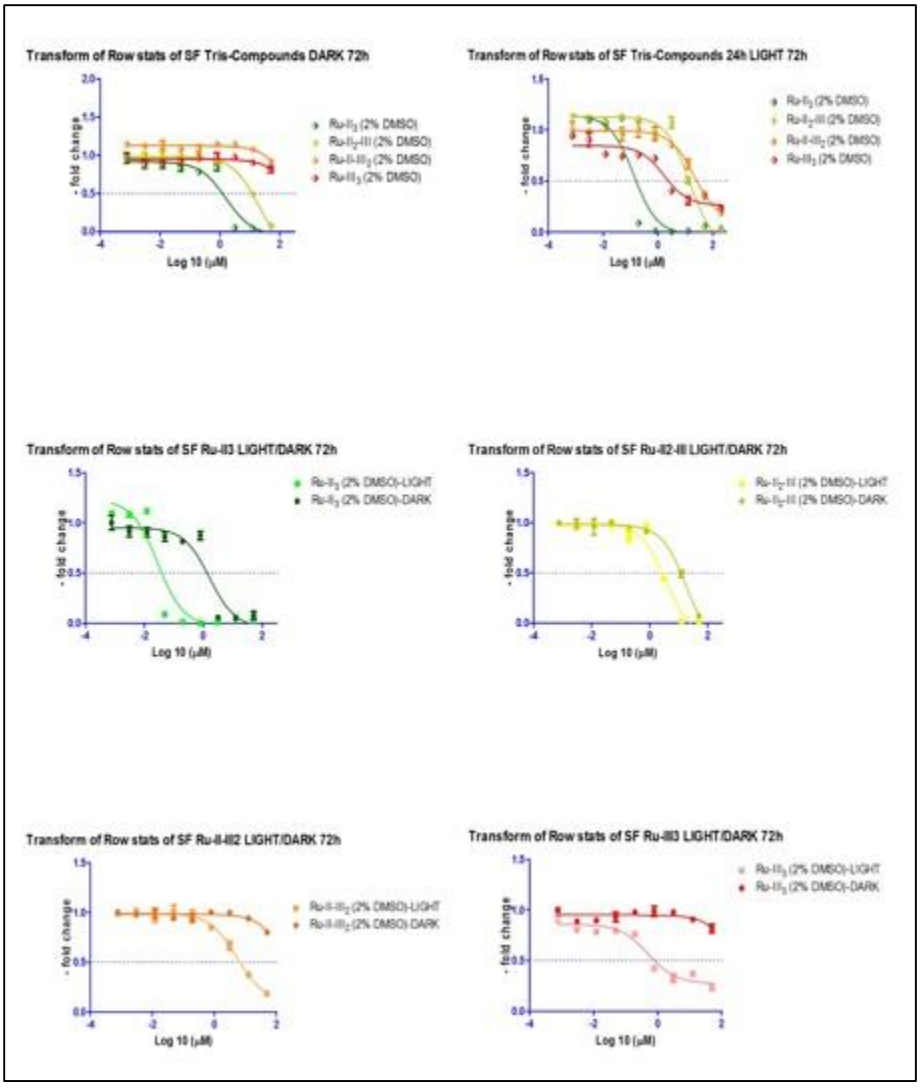

<u>Figure 31:</u> Comparison of the effect of all final complexes in the dark and after exposure to blue light 24h posttreatment.

Nonlinear regression curves for the cytotoxicity of **Ru-II$_3$**, **Ru-II$_2$-III**, **Ru-II-III$_2$** & **Ru-III$_3$**, dark vs light at 24h on SF268.

All readings of the cell viability experiment were done at 72h.

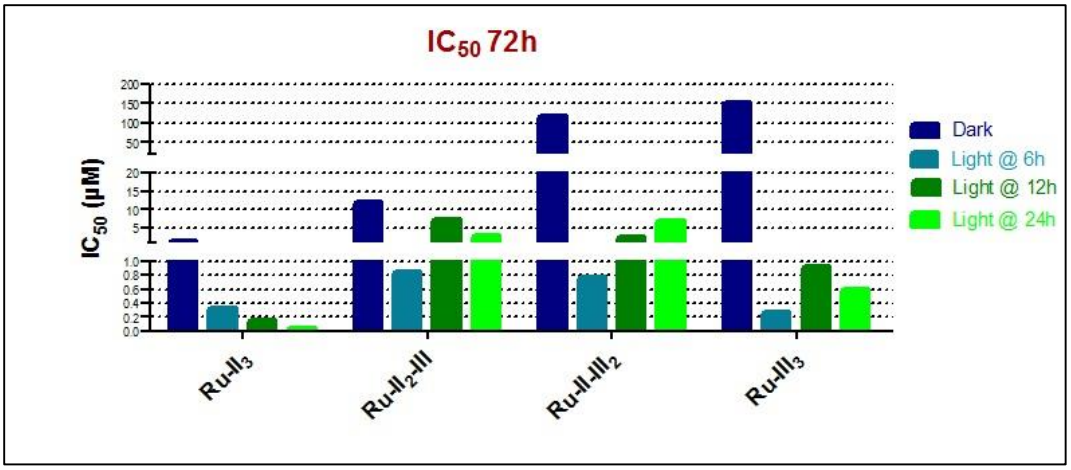

Figure 32: **IC_{50} values in the nM and µM range after activating all of the final complexes at 24h post-treatment.**

Table 3: **Average IC_{50} (µM) at 72h – Dark vs Light @ 24h – SF268 cell line.**

SF268					
Compounds	**DARK**	**BLUE LIGHT 10V/30 min @6h**	**BLUE LIGHT 10V/30 min @ 12h**	**BLUE LIGHT 10V/30 min @24h**	**Photo-toxicity index @ 24h**
Ru-II_3	**1.5**	**0.3**	**0.2**	**0.03**	**50**
Ru-II_2-III	**12**	**0.8**	**7**	**3**	**4.5**
Ru-II-III_2	**>200**	**0.8**	**2.5**	**7**	**>200**
Ru-III_3	**>200**	**0.3**	**1**	**0.6**	**>200**

The Photo-toxicity Index is the ratio of the IC_{50} value in the dark to that in the light.

3.9 Type of Cell Death Determination of the Action of the Final Ru(II) Complexes Active in the Light

The 4 final complexes were applied on SF268 cell line, and flow cytometry was used to determine the type of cell death at 72h as described earlier, with photo-activation using the blue light at 24h post-treatment.

Results showed that the type of cell death of **Ru-II$_3$** in the dark was also non-apoptotic as shown in figure 33, at 72h, since most of the cells were late apoptotic/necrotic. Also, the caspase assay showed no caspase cascade activation thus indicating no apoptosis. In the case of **Ru-II$_2$-III**, no signs of apoptosis were detected at 72h (Figure 34) since the majority of cells were necrotic and lack of apoptosis was confirmed by the caspase assay. Same goes for the inert compounds in the dark, once applying blue light on plates treated with **Ru-II-III$_2$** and **Ru-III$_3$** at 24h as previously stated, these compounds were activated and showed no sign of apoptosis (figure 34).

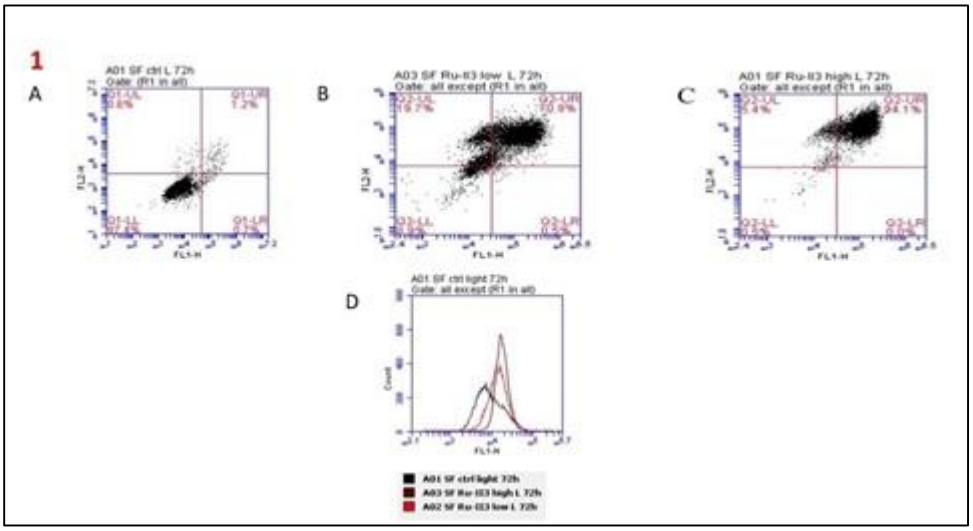

Figure 33: Cell death caused by Ru-II$_3$ is predominantly non-apoptotic after blue light exposure at 24h.
Annexin-PI (A-C) & Caspase Activation (D) at 72h. SF268 Control (1A). **Ru-II$_3$** – 0.1 µM (1B) & 0.2 µM (1C).

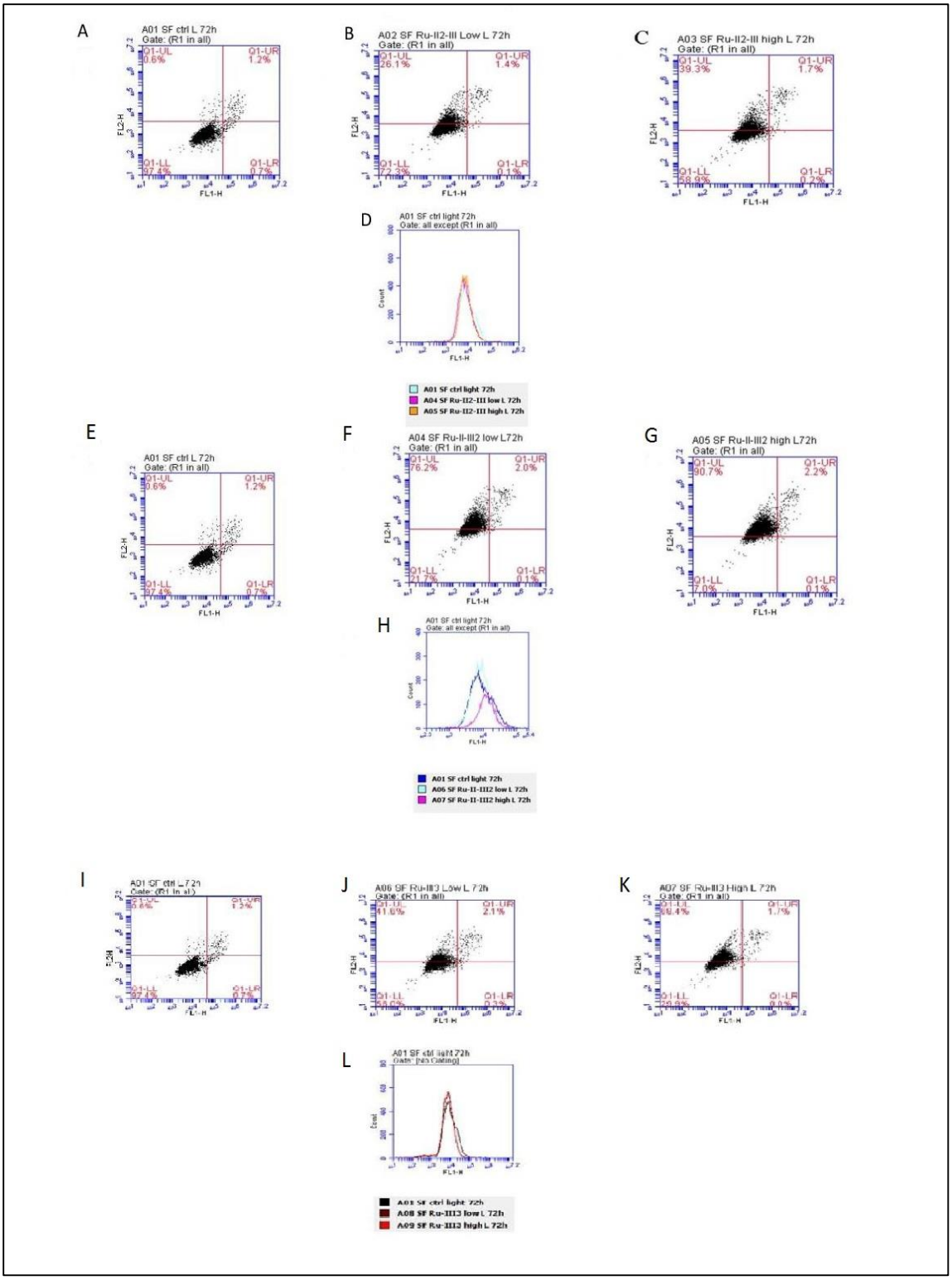

<u>Figure 34:</u> Cell death caused by Ru-II$_2$-III, Ru-II-III$_2$ and Ru-III$_3$ is non-apoptotic after blue light exposure at 24h.

Annexin-PI at 72h (A-C, E-G, I-K) & Caspase Activation at 72h (D, H & L). SF268 Control (A, E &I). **Ru-II$_2$III** – 3 µM (B) & 6 µM (C), **Ru-II-III$_2$** – 7 µM (F) & 14 µM (G), **Ru-III$_3$** – 1 µM (J) & 2 µM (K).

3.10 Cell Cycle Analysis of the Action of the Final Ru(II) Complexes Active in the Light

Cell cycle analysis data shown in figure 35 are preliminary results. This experiment is still a work in progress. However, it was shown that there is a significant increase of cell cycle arrest at sub-G and significant decrease at G1 at high concentrations of all the (Tris-) compounds at 72h when tested on SF268 cell line. These data are non-conclusive and need to be further elucidated.

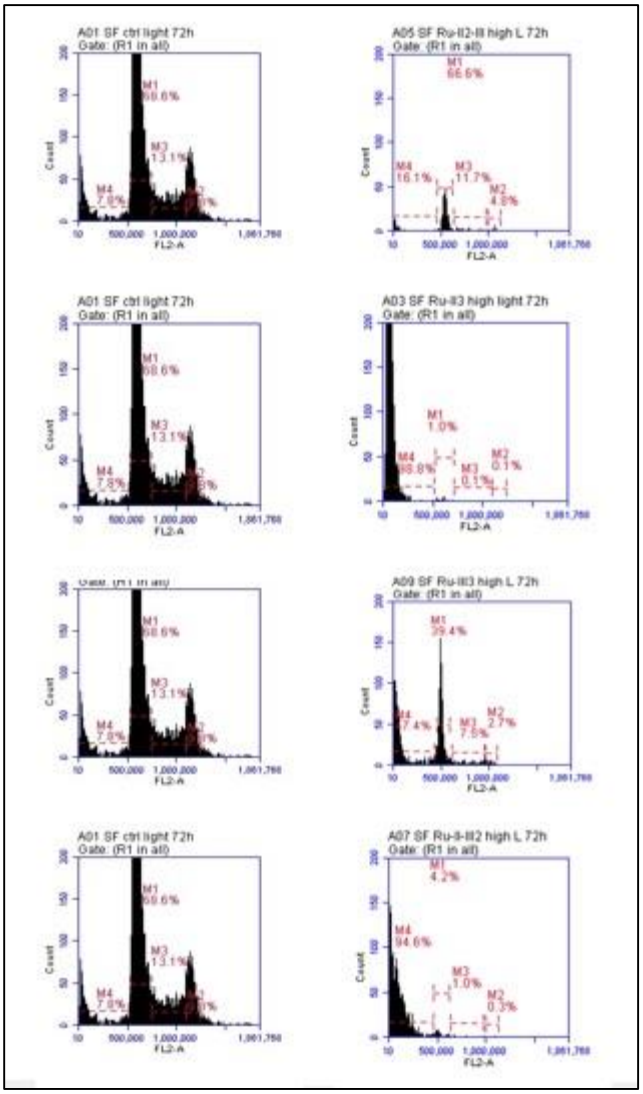

Figure 35: Preliminary results of Cell cycle analysis of the 4 (Tris-) compounds after photo-activation.
Cell Cycle Analysis – PI Staining at 72h. SF268 Control (A, D, G & K). **Ru-II$_3$** – 0.1 µM (B) & 0.2 µM (C), **Ru-II$_2$III** – 3 µM (E) & 6 µM (F), **Ru-II-III$_2$** – 7 µM (H) & 14 µM (I), **Ru-III$_3$** – 1 µM (L) & 2 µM (M).

CHAPTER FOUR

Discussion

4.1 Establishing a Structure-Activity Relationship in the Dark

Cell viability assays were applied on the ligand-free Ru(II) metal control, the free phenanthroline and bipyridine derivative ligands along with their corresponding Ru(II) metal complexes in order to test whether a cytotoxic effect is detected against the 6 solid tumor cell lines.

These different compounds differ from each other in their structures as followed:

L-I & Ru-I are hydrophobic and bulky, L-II & Ru-II are more hydrophobic and bulkier, respectively. L-III and Ru-III, with the exception of having negatively-charged sulfonated groups on the phenyls, have more or less a similar structure to L-II and Ru-II, respectively. The addition of these sulfonated groups attributed an anionic characteristic to these compounds, causing them to be repulsed by the negatively charged backbone of the DNA, thus inhibiting their intercalation. The results obtained in the cytotoxicity assays confirmed this theory by showing an effect similar to that of DMSO (inert) on all the tested cell line. However, L-I, L-II, Ru-I and Ru-II showed different sensitivity on the tested cell lines, whereas L-IV was selective to only one cell line (B16). This leads to the assumption that L-I, L-II and L-IV have the selective ability to intercalate DNA in specific solid tumors cell lines. When conjugating 2 L-I ligands to Ru-I, not the same significant activity was displayed, same goes for conjugating 2 L-II ligands to Ru-II, but when conjugating 2 L-IV ligands to Ru-IV, no activity was detected. Thus, diphenylphenanthroline, a molecule that results when 2 phenyl groups are added to phenanthroline, can significantly increase the activity of phenanthroline-derived compounds to become more effective DNA intercalating agents.

Table 4: Binding constants for trisbidentate complexes of Ru(II).

Complex	K	Site size	Enantio-selectivity	Likely intercalator
$[Ru(bpy)_3]^{2+}$	7×10^2	6–12	no	no
$[Ru(bpy)(tpy)(H_2O]^{2+}$	6.6×10^2			no
$[Ru(bpy)_2phen]^{2+}$	7×10^2	10–14	Δ	no
$[Ru(bpy)_2dip]^{2+}$	1.7×10^3	12–18	Δ	yes
$[Ru(bpy)_2ppz]^{2+}$	5.5×10^3	3–4	yes	partial
$[Ru(bpy)_2qpy]^{2+}$	1.3×10^4	2–3	no	yes
$[Ru(bpy)_2Me_2qpy]^{4+}$	2.8×10^4	3	yes	yes
$[Ru(phen)_3]^{2+}$	3×10^4	3–4	Δ	no(?)
$[Ru(NH_3)_4dppz]^{2+}$	1.24×10^5			yes
$[Ru(bpy)_2phi]^{2+}$	1.6×10^5	4	yes	yes
$[Ru(tpy)dppz(H_2O)]^{2+}$	7.3×10^5			yes
$\{(dpp)[(NH_3)_4Ru(II)]_2\}^{4+}$	8.3×10^5	6		yes
$[Ru(phen)_2dppz]^{2+}$	$\sim 10^8$	2	yes	yes

(From Clarke, 2002)

Trisbidentate complexes of Ru(II), also known as molecules containing an Ru core conjugated to three ligands have been reviewed in 2002 by Clarke et al. Some of these compounds were reported as poor DNA intercalators: $[Ru(bpy)_3]^{2+}$ (Ru core connected to three bipyridine ligands) and $[Ru(phen)_3]^{2+}$ (Ru core connected to three phenanthroline ligands) (Table 4). The results obtained are in accordance with what was stated earlier as the compounds tested, Ru-IV $\{[Ru(bpy)_2Cl_2]^{2+}\}$ and Ru-I $\{[Ru(phen)_2Cl_2]^{2+}\}$, that share high similarities with $[Ru(bpy)_3]^{2+}$ and $[Ru(phen)_3]^2$, respectively, were not DNA intercalating agents since they showed low or no activity against the tested cell lines (figure 13). In addition, when one phenanthroline and two bipyridine molecules are connected to the Ru metal core forming $[Ru(bpy)_2phen]^{2+}$ showed no DNA intercalating potential. At the same time, another similar compound, where the phenanthroline ligand is replaced with a diphenylphenanthroline ligand $\{[Ru(bpy)_2dip]^{2+}\}$ was an effective DNA intercalator (Table 4). The results obtained confirmed what was state previously since $\{[Ru(dip)_2Cl_2]^{2+}\}$, in which the Ru core is connected to two diphenylphenanthroline ligands, showed significant activity against the majority of the tested cell lines. All the previous data and results indicate that one diphenylphenanthroline ligand connected to the Ru core is enough to confer intercalative activity. In addition, Clarke et al (2002) showed that some combinations of ligands are also active in intercalating DNA (table 4).

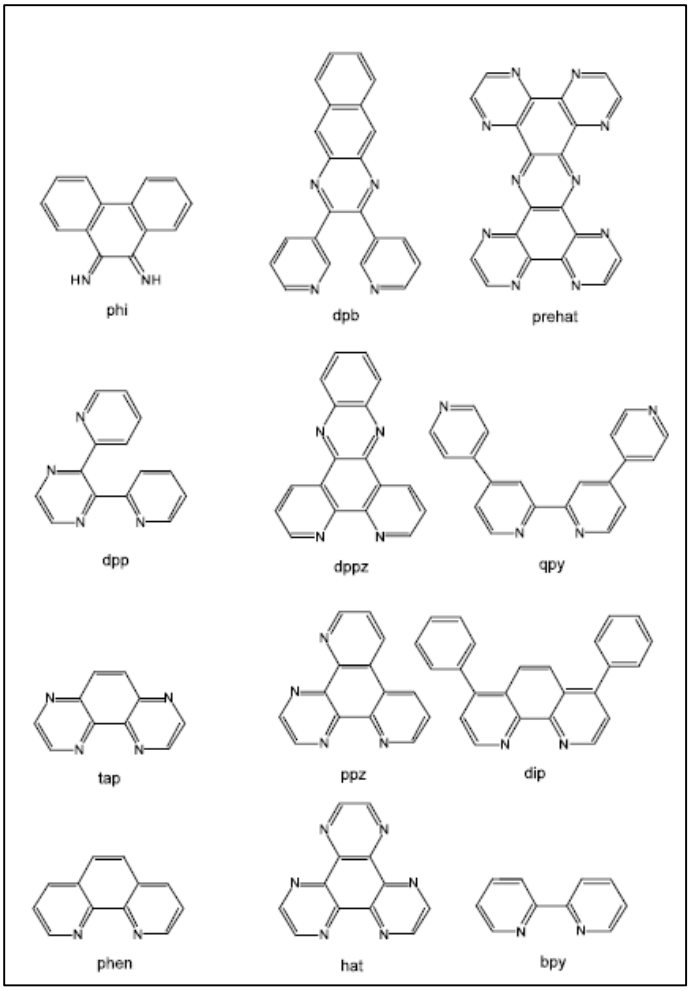

Figure 36: Structures of N-heteroaromatic ligands. (From Clarke M. J., 2002)

The general structure-activity relationship is still conserved in the final (Tris-) compounds in the dark. The compounds bearing 3 L-II and 2 L-II ligands in their structure showed very high potency, as predicted since they are cationic and neutral, respectively. This allows them to play a significant role as intercalating agents. Whereas the 2 other (Tris-) compounds bearing more L-III ligands are anionic and unable to intercalate the DNA.

4.2 Type of Cell Death and Cell Cycle Analysis of the Final (Tris-) Compounds in the Dark

Our data obtained from the flow cytometry assay showed a non-apoptotic type of cell death of the treated SF268 cells with Ru-II_3 and Ru-II_2-III in the dark. Additional investigation and experiments should be done to further understand the type of cell death elucidated by these 2 compounds on solid tumors (necrosis, autophagy, test for apoptotic markers by western blots,…), as well as test again for any cell cycle arrest occurring in cells when treated with the different compounds.

4.3 Photo-Activation and an Activity Profile that does not obey the Structure-Activity Relationship

When photo-activated with blue light, the activity of the anionic compounds (Ru-II-III_2 and Ru-III_3) was altered, thereby acquiring potency against SF268 cell lines. Thus, these complexes are very promising for photodynamic therapies (PDT) since in the dark, they act as inactive pro-drugs, and this inert activity is terminated once exposed to blue light. A suggested mechanism is that, upon photo-activation, reactive oxygen species are liberated, causing this cytotoxic effect. This still needs to be investigated by additional biological experiments such as detecting levels of ROS release by flow cytometry assay or others.

4.4 Type of Cell Death and Cell Cycle Analysis of the Final (Tris-) Compounds after Photo-Activation

Our data obtained from the flow cytometry assay showed also a non-apoptotic type of cell death of the treated SF268 cell lines with all 4 final (Tris-) compounds after exposure to the blue light. Additional investigation and experiments should be done to further understand the type of cell death elucidated by these 4 complexes on solid tumors (necrosis, autophagy, test for apoptotic markers by western blots,…), as well as check for any cell cycle arrest occurring in cells when treated with the different compounds.

4.5 Conclusion

In conclusion, different ruthenium precursors, final complexes and free phenanthroline- or bipyridine-derived ligands were tested against 6 solid tumor cell lines. Mainly, the Ru-II precursor has shown most potency on all cell lines and specifically on SF268, since it bears two diphenylphenanthroline ligands, while the rest of the precursors showed low potency or none. As for the free ligands, significant activity was detected with L-II (diphenylphenanthroline) on most of the cell lines while L-I (phenanthroline) showed less activity on fewer cell lines, whereas L-III was biologically inert after adding the sulfonate groups to its structure. L-IV showed no activity at all, similarly to its precursor. These data suggest that the phenanthroline-derived metal-based complexes act as DNA intercalating agents and exert their potent action. And since the unconjugated Ru(II) metal core alone did not affect any of the tested cell lines, it can be deduce that any activity detected is due to the ligands that are bound to the ruthenium metal. Moreover, the four final tris-bidentate compounds, Ru-II_3, Ru-II_2-III, Ru-II-III_2 and Ru-III_3, were studied in the dark and after exposure to blue light. In the dark, only Ru-II_3 was active against all the tested cell lines, Ru-II_2-III showed moderate toxicity against three cell lines (A549, B16, and SF268), while the others showed no effect. After exposure of SF268 treated cells to the blue light, all four compounds showed high levels of potency, including Ru-II-III_2 and Ru-III_3 that were biologically inert in the dark. It is assumed that the (Tris-) final compounds' cytotoxic action is due to the release of Reactive Oxygen Species (ROS), thus affecting the cells' metabolism and causing DNA damage, thereby leading to cell death. Notably, Ru-II-III_2 and/or Ru-III_3 seem promising in being successfully developed as photo-dynamic therapeutic agents, due to the absence of potency when in the dark and their sudden switch to activity when photo-activated. Further investigation and studies need to be done in order to further understand their detailed underlying mechanisms of action in the dark and when exposed to blue light by examining at which stage of mitosis cell cycle arrest is occurring, as well as the type of cell death they cause. Finally, these studies will constitute a beginning in the quest of finding the most selective and potent complex, and the possibility of new targeted photodynamic therapies against solid tumors.

References

Alteri, R., Bertaut, T., Brooks, D., Chambers, W., Chang, E., Desantis, C. … Zou, J. (2015). *Cancer facts & Figures* 2015. Atlanta, GA: American Cancer Society.

Anand, P., Kunnumakara, B., Sundaram, C., Harikumar, B., Tharakan, T., Lai, S., & Aggarwal, B. (2008). "Cancer is a preventable disease that requires major lifestyle changes. *Pharm. Res., 25*(9), 116-2097. doi:10.1007/s11095-008-9661-9.

Arndt, A. (2010). Skin Care and Repair. In Chestnut Hill, MA:Harvard Health Publications.

Ashraf, S., Conaghan, P., Wilding, J., & Bodmer, W. (2008). Reply: In vitro and in vivo anticancer efficacy of unconjugated humanised anti-CEA monoclonal antibodies. *Br J Cancer, 99*(5), 839-840. doi: 10.1038/sj.bjc.6604549.

Astin M, Griffin, T, Neal, RD, Rose, P, Hamilton, W. (May 2011). "The diagnostic value of symptoms for colorectal cancer in primary care: a systematic review". *The British Journal of General Practice, 61*(586), 231–43. doi:10.3399/bjgp11X572427.

Bergamo, A., Gaiddon, C., Schellens, J. H. M., Beijnen, J. H., & Sava, G. (2012). Approaching tumour therapy beyond platinum drugs. *Journal of Inorganic Biochemistry, 106*(1), 90–99. doi.org/10.1016/j.jinorgbio.2011.09.030.

Bickle, K., Glass, F., Messina, L., Fenske, A., & Siegrist, K. (2004). Merkel cell carcinoma: a clinical, histopathologic, and immunohistochemical review. *Seminars in cutaneous medicine and surgery*, *23*(1), 46-53. doi:10.1016/s1085-5629(03)00087-7.

Birgisson, H., Påhlman, L., Gunnarsson, U., & Glimelius, B. (2007). Late adverse effects of radiation therapy for rectal cancer - a systematic overview. *Acta Oncol*, *46*(4), 504-516. doi:10.1080/02841860701348670.

Brown, M., & Wilson, W. (2004). Exploiting tumour hypoxia in cancer treatment. *Nature Reviews Cancer*, *4*, 437-447. doi:10.1038/nrc1367.

Clarke, M. J. (2003). Ruthenium metallopharmaceuticals. *Coordination Chemistry Reviews*, *236*(1), 209–233.

Coluccia, M., Nassi, A., Loseto, F., Boccarelli, A., Mariggio, M. A., Giordano, D., … Natile, G. (1993). A trans-platinum complex showing higher antitumor activity than the cis congeners. *Journal of Medicinal Chemistry*, *36*(4), 510–512.

Connolly, J., Schnitt, S., Wang, H., Longtine, J., Dvorak, A., & Dvorak, H. (2003). *Holland-Frei Cancer Medicine* (6th ed.). Hamilton: BC Decker.

Cunningham, D., Atkin, W., Lenz, H., Lynch, H., Minsky, B., Nordlinger, B., Starling N. (2010). Colorectal cancer. *Lancet, 375*(9719), 1030–47. doi:10.1016/S0140-6736(10)60353-4.

Degroot, P., & Munden, F. (2012). Lung cancer epidemiology, risk factors, and prevention. *Radiol Clin North Am*, *50*(5), 76-863. doi:10.1016/j.rcl.2012.06.006.

Dilda, P. J., & Hogg, P. J. (2007). Arsenical-based cancer drugs. *Cancer Treatment Reviews*, *33*(6), 542–564. doi.org/10.1016/j.ctrv.2007.05.001.

Dreicer, R. (2008). Current status of cytotoxic chemotherapy in patients with metastatic prostate cancer. *Urol Oncol*, *26*(4), 426-429. doi:10.1016/j.urolonc.2007.11.005.

El-Zein, R., Minn, A., Wrensch, M., & Bondy, M. (2002). Epidemiology of Brain Tumors. , 252-266. Stupp, R., Reni, M., Gatta, G., Mazza, E., & Vecht, C. (2007). Anaplastic astrocytoma in adults. *Critical Reviews in Oncology/Hematology*, *63*(1), 72-80. doi:10.1016/j.critrevonc.2007.03.003.

Farrell, N., Ha, T. T., Souchard, J. P., Wimmer, F. L., Cros, S., & Johnson, N. P. (1989). Cytostatic trans-platinum(II) complexes. *Journal of Medicinal Chemistry, 32*(10), 2240–2241.

Ferlay, J., Shin, HR., Bray, F., Forman, D., Mathers, C., & Parkin, DM. (2010). GLOBOCAN 2008: Cancer Incidence and Mortality Worldwide. *IARC CancerBase, 127*(12), 2893-917. doi: 10.1002/ijc.25516.

Ferlay, J., Soerjomataram, I., Ervik, M., Dikshit, R., Eser, S., Mathers, C. … Bray, F. (2014). GLOBOCAN 2012: Cancer Incidence and Mortality Worldwide. *IARC CancerBase, 136*(5), 359-386. DOI: 10.1002/ijc.29210.

Fogh, J., & Trempe, G. (1975). *New Human Tumor Cell Lines* (pp. 115-159). New York, NY: Springer US.

Gavhane, N., Shete, S., Bhagat, K., Shinde, R., Bhong, K., Khaimar, A., & Yadav, A. (2011). Solid Tumors: Facts, Challenges and Solutions. *International Journal of Pharma Sciences and Research, 2*(1), 1-12.

Giard, J., Aaronson, A., Todaro, J., Amstein, P., kersey, H., Dosik, H., & Parks, P. (1973). In vitro cultivation of human tumors: Establishment of cell lines derived from a series of solid tumors. *Journal of the National Cancer Institute, 51*(5), 23-1417. doi:10.1093/jnci/51.5.1417.

Haim, A., & Portnov, B. (2013). *Light Pollution as a New Risk Factor for Human Breast and Prostate Cancers.* Netherlands: Springer Netherlands.

Hannon, M. J. (2007). Metal-based anticancer drugs: From a past anchored in platinum chemistry to a post-genomic future of diverse chemistry and biology. *Pure and Applied Chemistry, 79*(12), 2243-2261. doi.org/10.1351/pac200779122243.

Hidalgo, I., Raub, T., & Borchardt, R. (1989). "Characterization of the human colon carcinoma cell line (Caco-2) as a model system for intestinal epithelial permeability". *Gastroenterology, 96*(3), 736–49.

Hoffman, C., Mauer, M., & Vokes, E. (2000). Lung cancer. *Lancet, 355*(9202), 479-485.

Horn, L., Lovly, C., & Johnson, D. (2015). *Harrison's Principles of Internal Medicine* (19th ed.). N.p: McGraw-Hill Companies.

Jakupec, M. A., Reisner, E., Eichinger, A., Pongratz, M., Arion, V. B., Galanski, M., … Keppler, B. K. (2005). Redox-active antineoplastic ruthenium complexes with indazole: correlation of in vitro potency and reduction potential. *Journal of Medicinal Chemistry, 48*(8), 2831–2837. doi.org/10.1021/jm0490742.

Jawad, N., Direkze, N., & Leedham, SJ. (2011). Inflammatory bowel disease and colon cancer. *Recent Results in Cancer Research, 185*, 99–115. doi:10.1007/978-3-642-03503-6_6.

Jones, W., Harman, C., Ng, A., Shaw, J. (1999)."Incidence of malignant melanoma in Auckland, New Zealand: The highest rates in the world". *World Journal of Surgery, 23*(7), 732-5. doi:10.1007/pl00012378.

Jungwirth, U., Kowol, C. R., Keppler, B. K., Hartinger, C. G., Berger, W., & Heffeter, P. (2011). Anticancer Activity of Metal Complexes: Involvement of Redox Processes. *Antioxidants & Redox Signaling, 15*(4), 1085–1127. doi.org/10.1089/ars.2010.3663.

Kelland, L. (2007). The resurgence of platinum-based cancer chemotherapy. *Nature Reviews. Cancer, 7*(8), 573–584. doi.org/10.1038/nrc2167.

Kloster, M. B., Hannis, J. C., Muddiman, D. C., & Farrell, N. (1999). Consequences of nucleic acid conformation on the binding of a trinuclear platinum drug. *Biochemistry, 38*(45), 14731–14737.

Kovacs, G., Barany, O., Schlick, B., Csoka, M., Gado, J., Ponyi, A., & Erdelyi, D. (2008). Late immune recovery in children treated for malignant diseases. *Pathol Oncol Res, 14*(4), 7-391. doi: 10.1007/s12253-008-9073-5.

Lacroix, M. (2006). Significance, detection and markers of disseminated breast cancer cells. *Endocrine-Related Cancer (Bioscientifica), 13*(4), 67-1033. doi:10.1677/ERC-06-0001.

Lacroix, M., & Leclercq, G. (2004). Relevance of breast cancer cell lines as models for breast tumours: an update. *Breast Research and Treatment, 83*(3), 249–289. doi:10.1023/B:BREA.0000014042.54925.cc.

Levenson, AS., & Jordan, VC. (1997). MCF-7: the first hormone-responsive breast cancer cell line. *Cancer Research, 57*(15), 3071– 3078.

Lozano, R. (2012). "Global and regional mortality from 235 causes of death for 20 age groups in 1990 and 2010: a systematic analysis for the Global Burden of Disease Study 2010". *Lancet, 380*(9859), 2095–128. doi: 10.1016/S0140-6736(12)61728-0.

Manning, G. S. (1978). The molecular theory of polyelectrolyte solutions with applications to the electrostatic properties of polynucleotides. *Quarterly Reviews of Biophysics, 11*(2), 179–246.

Manning, G. S., & Ray, J. (1998). Counterion condensation revisited. *Journal of Biomolecular Structure & Dynamics, 16*(2), 461–476. doi.org/10.1080/07391102.1998.10508261.

Martin, A., & Jiang, G. (2009). Loss of tight junction barrier function and its role in cancer metastasis. *Biochim Biophys Acta, 1788*, 872-891. doi:10.1016/j.bbamem.2008.11.005.

McGuire, A., Brown, A., Malone, C., McLaughlin, R., & Kerin, J. (2015). Effects of age on the detection and management of breast cancer. *Cancers, 7*(2), 29-908. doi: 10.3390/cancers7020815.

McKinnell, R. (2007). *NIH Curriculum Supplement Series*. Bethesda, MD: National Institutes of Health (US).

Montero, E. I., Díaz, S., González-Vadillo, A. M., Pérez, J. M., Alonso, C., & Navarro-Ranninger, C. (1999). Preparation and characterization of novel trans-[PtCl(2)(amine)(isopropylamine)] compounds: cytotoxic activity and apoptosis induction in ras-transformed cells. *Journal of Medicinal Chemistry, 42*(20), 4264–4268.

Nobili, S., Mini, E., Landini, I., Gabbiani, C., Casini, A., & Messori, L. (2010). Gold compounds as anticancer agents: chemistry, cellular pharmacology, and preclinical studies. *Medicinal Research Reviews, 30*(3), 550–580. doi.org/10.1002/med.20168.

Overwijk, W. W., & Restifo, N. P. (2001). B16 as a Mouse Model for Human Melanoma. *Current Protocols in Immunology*, CHAPTER, Unit-20.1. doi.org/10.1002/0471142735.im2001s39.

Pacor, S., Sava, G., Ceschia, V., Bregant, F., Mestroni, G., & Alessio, E. (1991). Antineoplastic effect of mer-trichlorobisdimethylsulphoxideaminorutheniumIII against murine tumors: comparison with cisplatin and with ImH[RuIm2Cl4]. *Chemico-Biological Interactions, 78*(2), 223–234.

Parkin, M., Boyd, L., & Walker, C. (2011). "16. The fraction of cancer attributable to lifestyle and environmental factors in the UK in 2010. *British Journal of Cancer, 105*(2), 77-81. doi:10.1038/bjc.2011.489.

Pellizzari, R., Rossetto, O., Schiavo, G., & Montecucco, C. (1999). Tetanus and botulinum neurotoxins: mechanism of action and therapeutic uses. *Philos. Trans. R. Soc. Lond. B Biol. Sci., 354*(1381), 259–268.doi:10.1098/rstb.1999.0377.

Pinto, M. (1983). "Enterocyte-like differentiation and polarization of the human colon carcinoma cell line Caco-2 in culture". *Biol Cell, 47*, 323–30.

Ribatti, D., & Crivellato, E. (2011). *Mast Cells and Tumours*. Springer Netherlands: Springer Science+Business Media B.V.

Rosenberg, B., VanCamp, L., Trosko, J. E., & Mansour, V. H. (1969). Platinum compounds: a new class of potent antitumour agents. *Nature, 222*(5191), 385–386.

Ross, DT., & Perou, CM. (2001). A comparison of gene expression signatures from breast tumors and breast tissue derived cell lines. *Diseases Markers, 17*(2), 99–109. doi:10.1155/2001/850531.

Saladi, R., Persaud, A. (2005). "The causes of skin cancer: a comprehensive review." *Drugs of today, 41*(1), 37–53. doi:10.1358/dot.2005.41.1.875777.

Sambuy, Y., De Angelis, I., Ranaldi, G., Scarino, M., Stammati, A., & Zucco, F. (2005). "The Caco-2 cell line as a model of the intestinal barrier: influence of cell and culture-related factors on Caco-2 cell functional characteristics". *Cell Biol Toxicol., 21*(1), 1–26. doi: 10.1007/s10565-005-0085-6.

Santoro, E., DeSoto, M., & Hong Lee, J. (2009). *Hormone Therapy and Menopause.* National Research Center for Women & Families.

Schluga, P., Hartinger, C. G., Egger, A., Reisner, E., Galanski, M., Jakupec, M. A., & Keppler, B. K. (2006). Redox behavior of tumor-inhibiting ruthenium(III) complexes and effects of physiological reductants on their binding to GMP. *Dalton Transactions (Cambridge, England: 2003)*, (14), 1796–1802. doi.org/10.1039/b511792e.

Siegel, M., & Chung, E. (2008). Wilms' tumor and other pediatric renal masses. *Magn Reson Imaging Clin N Am., 16*(3), 97-479. doi:10.1016/j.mric.2008.04.009.

Skarin, A. (2003). *Atlas of Diagnostic Oncology*. Philadelphia, PA: Elsevier Science Ltd.

Smith, J., Tachibana, I., Passe, S., Huntley, B., Borell, T., Iturria, N., & Jenkins, R. (2001). PTEN Mutation, EGFR Amplification, and Outcome in Patients With Anaplastic Astrocytoma and Glioblastoma Multiforme. *JNCI J Natl Cancer Inst*, *93*(16), 1246-1256. doi:10.1093/jnci/93.16.1246.

Soule, HD., Vazquez, J., Long, A., Albert, S., & Brennan, M. (1973). A human cell line from a pleural effusion derived from a breast carcinoma. *Journal of the National Cancer Institute*, *51*(5), 1409–1416.

Stewart, B., & Wild, C. (2014). *World Cancer Report*. In World Health Organization.

Stewart, W., & Kleihues, P. (2003). *World Cancer Report*. Lyon, France: IARCPress.

Takahara, P. M., Rosenzweig, A. C., Frederick, C. A., & Lippard, S. J. (1995). Crystal structure of double-stranded DNA containing the major adduct of the anticancer drug cisplatin. *Nature, 377*(6550), 649–652. doi.org/10.1038/377649a0.

Watson, M. (2008). Assessment of suspected cancer. *InnoAiT, 1*(2), 94-107. doi:10.1093/innovait/inn001.

Weigelt, B., Peterse, J., & van't Veer, L. (2005). Breast cancer metastasis: markers and models. *Nature Reviews Cancer, 5,* 591-602. doi: 10.1038/nrc1670.

Weinberg, R. A. (2013). *The biology of cancer* (Second edition). New York: Garland Science, Taylor & Francis Group.

Westphal, M., Harsh, G., Rosenblum, M., & Hammonds, R. (1985). Epidermal growth factor receptors in the human glioblastoma cell line SF268 differ from those in epidermoid carcinoma cell line A4 Parsa, N. (2012). Environmental Factors Inducing Human Cancers. *Iran J Public Health, 41*(11), 1-9.

What You Need To Know About™ Melanoma and Other Skin Cancers (2010). In *National Cancer Institute*.

Yager, D., & Davidson, E. (2006). Estrogen carcinogenesis in breast cancer. *New Engl J Med, 354*(3), 82-270. doi:10.1056/NEJMra050776.

Yamada, T., Alpers, D., Kalloo, A., Kaplowitz, N., Owyang, C., & Powell, D. (2008). *Principles of clinical gastroenterology*. Chichester, West Sussex: Wiley-Blackwell.

Yang, G., Wu, J. Z., Wang, L., Ji, L. N., & Tian, X. (1997). Study of the interaction between novel ruthenium(II)-polypyridyl complexes and calf thymus DNA. *Journal of Inorganic Biochemistry*, *66*(2), 141–144.

Appendix 1

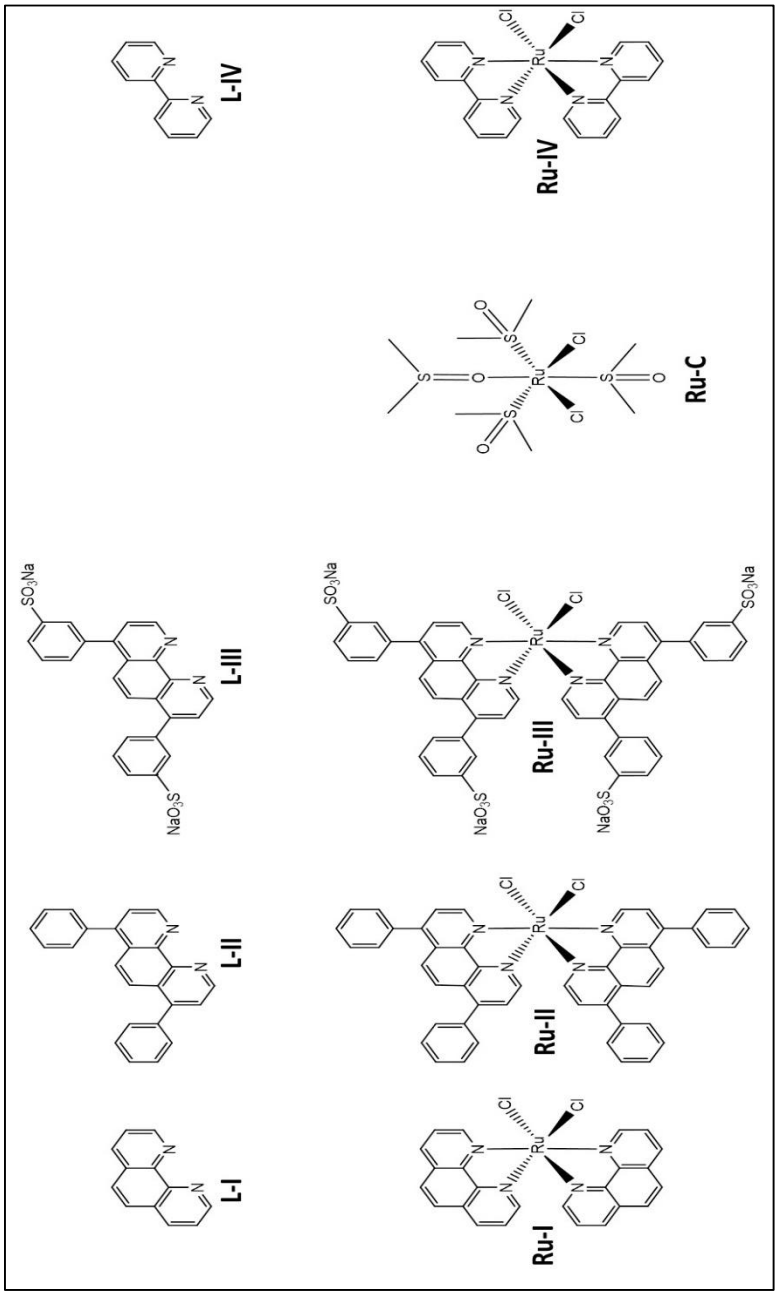

Appendix 2

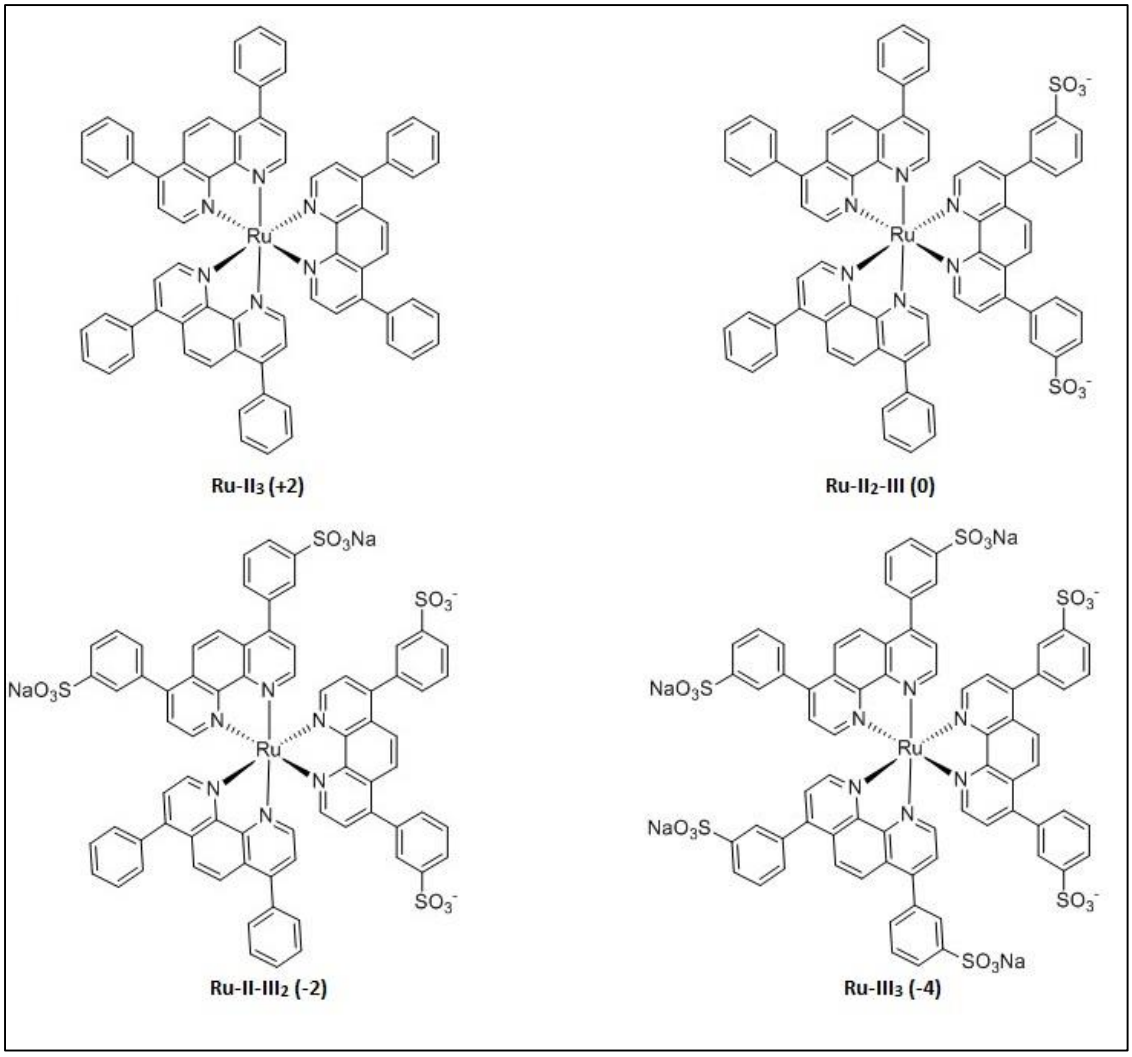

Appendix 3

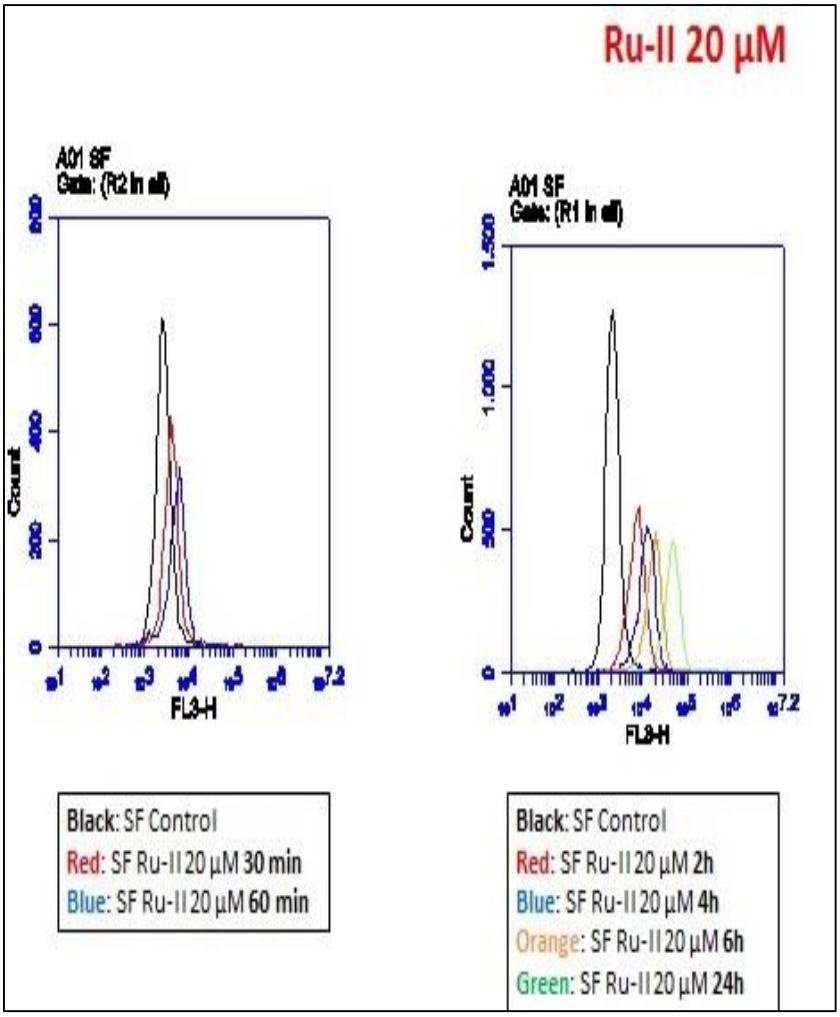
Ru-II 20 µM
A01 SF
Gate: (R2 in all)
Count
FL3-H
Black: SF Control
Red: SF Ru-II 20 µM 30 min
Blue: SF Ru-II 20 µM 60 min
A01 SF
Gate: (R1 in all)
Count
FL3-H
Black: SF Control
Red: SF Ru-II 20 µM 2h
Blue: SF Ru-II 20 µM 4h
Orange: SF Ru-II 20 µM 6h
Green: SF Ru-II 20 µM 24h

Appendix 4

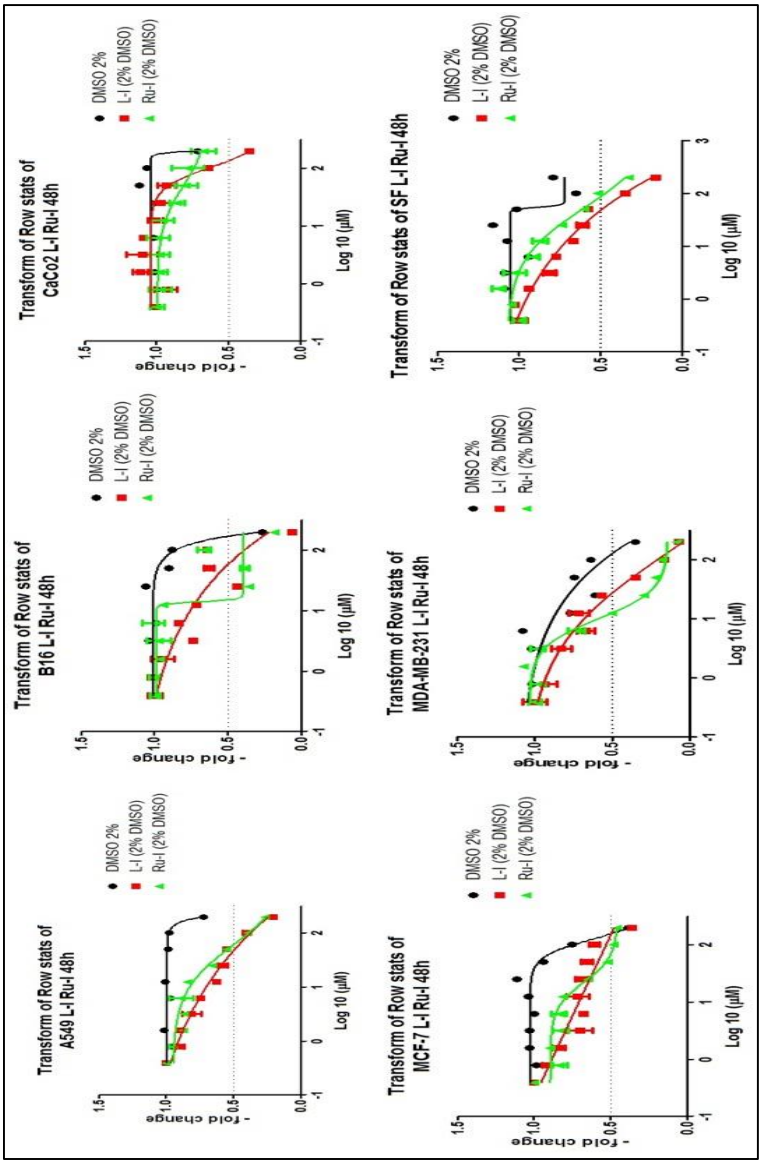
Transform of Row stats of CaCo2 L-I Ru-I 48h
Transform of Row stats of SF L-I Ru-I 48h
Transform of Row stats of B16 L-I Ru-I 48h
Transform of Row stats of MDA-MB-231 L-I Ru-I 48h
Transform of Row stats of A549 L-I Ru-I 48h
Transform of Row stats of MCF-7 L-I Ru-I 48h
DMSO 2%
L-I (2% DMSO)
Ru-I (2% DMSO)
- fold change
Log 10 (µM)

Appendix 5

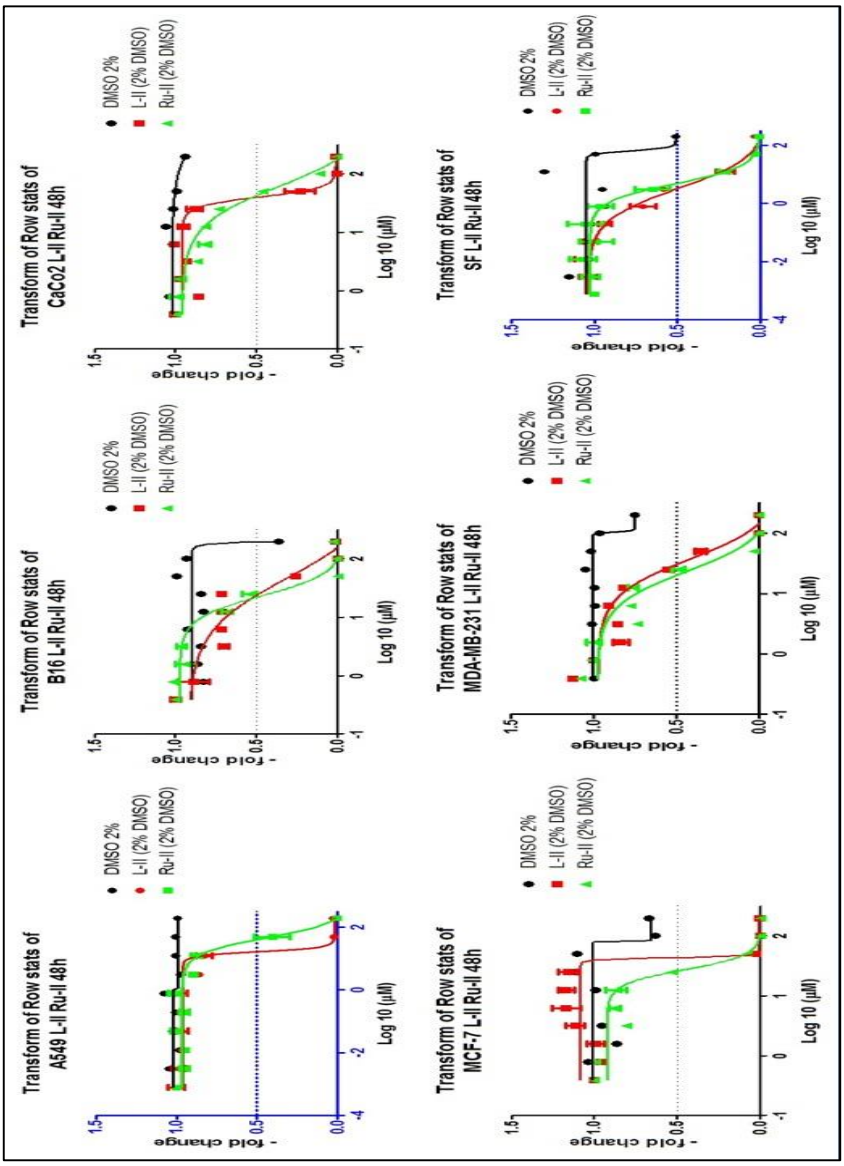
Transform of Row stats of
CaCo2 L-II Ru-II 48h
Transform of Row stats of
SF L-II Ru-II 48h
Transform of Row stats of
B16 L-II Ru-II 48h
Transform of Row stats of
MDA-MB-231 L-II Ru-II 48h
Transform of Row stats of
A549 L-II Ru-II 48h
Transform of Row stats of
MCF-7 L-II Ru-II 48h
DMSO 2%
L-II (2% DMSO)
Ru-II (2% DMSO)
- fold change
Log 10 (µM)

Appendix 6

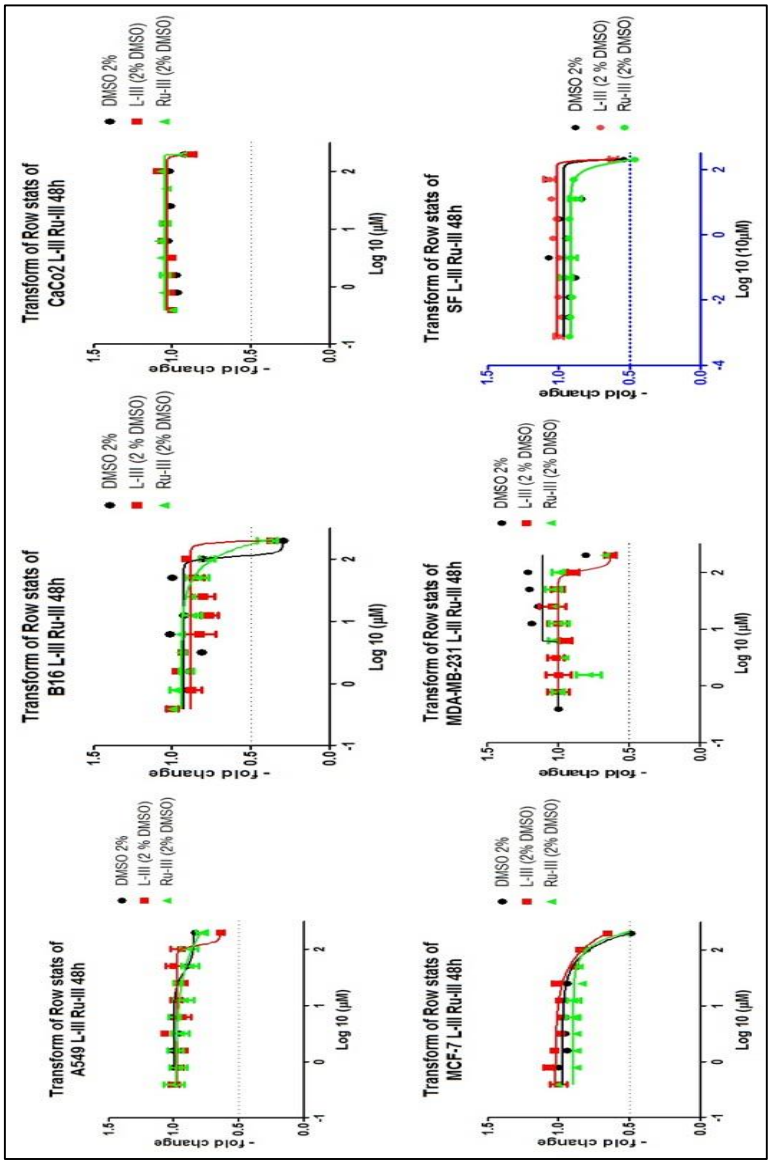
Transform of Row stats of
CaCo2 L-III Ru-III 48h
Transform of Row stats of
SF L-III Ru-III 48h
Transform of Row stats of
B16 L-III Ru-III 48h
Transform of Row stats of
MDA-MB-231 L-III Ru-III 48h
Transform of Row stats of
A549 L-III Ru-III 48h
Transform of Row stats of
MCF-7 L-III Ru-III 48h
DMSO 2%
L-III (2% DMSO)
Ru-III (2% DMSO)
- fold change
Log 10 (μM)
Log 10 (10μM)

Appendix 7

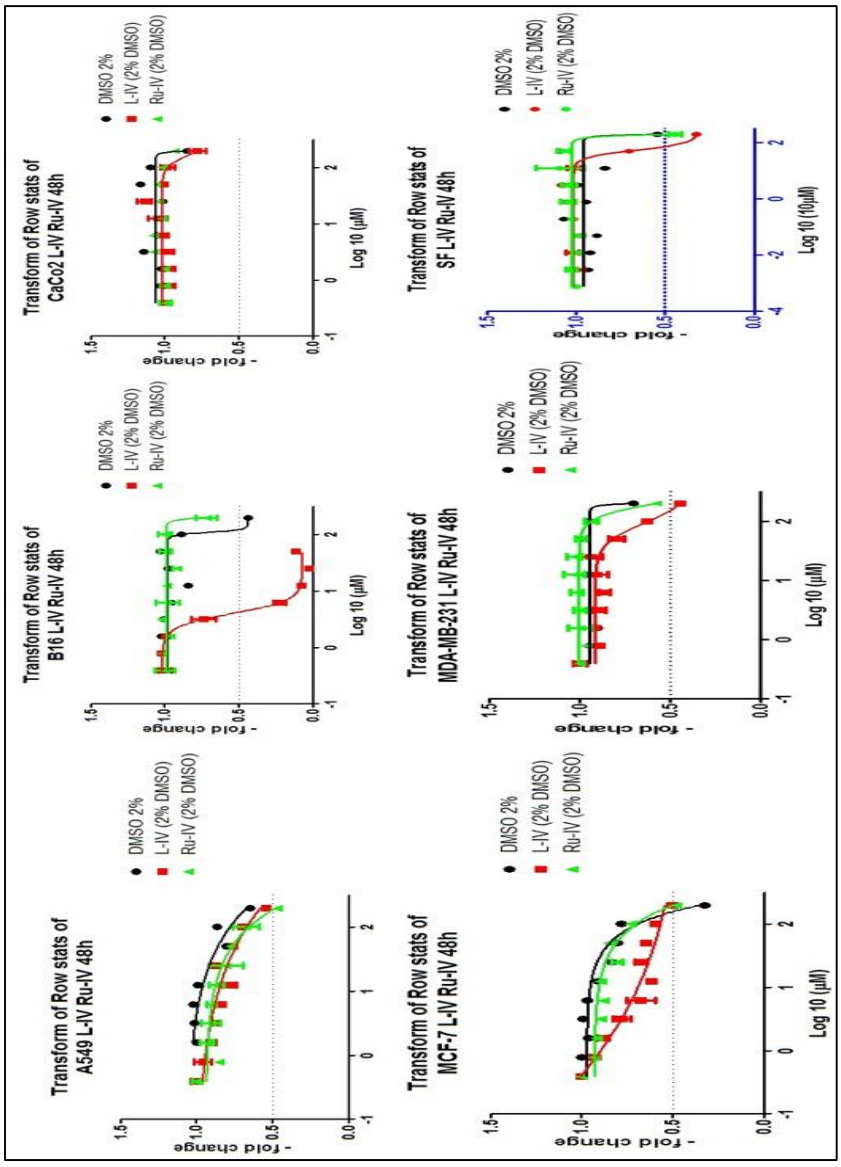
Transform of Row stats of
A549 L-IV Ru-IV 48h
Transform of Row stats of
B16 L-IV Ru-IV 48h
Transform of Row stats of
CaCo2 L-IV Ru-IV 48h
Transform of Row stats of
MCF-7 L-IV Ru-IV 48h
Transform of Row stats of
MDA-MB-231 L-IV Ru-IV 48h
Transform of Row stats of
SF L-IV Ru-IV 48h
DMSO 2%
L-IV (2% DMSO)
Ru-IV (2% DMSO)
- fold change
Log 10 (µM)
Log 10 (10µM)

Appendix 8

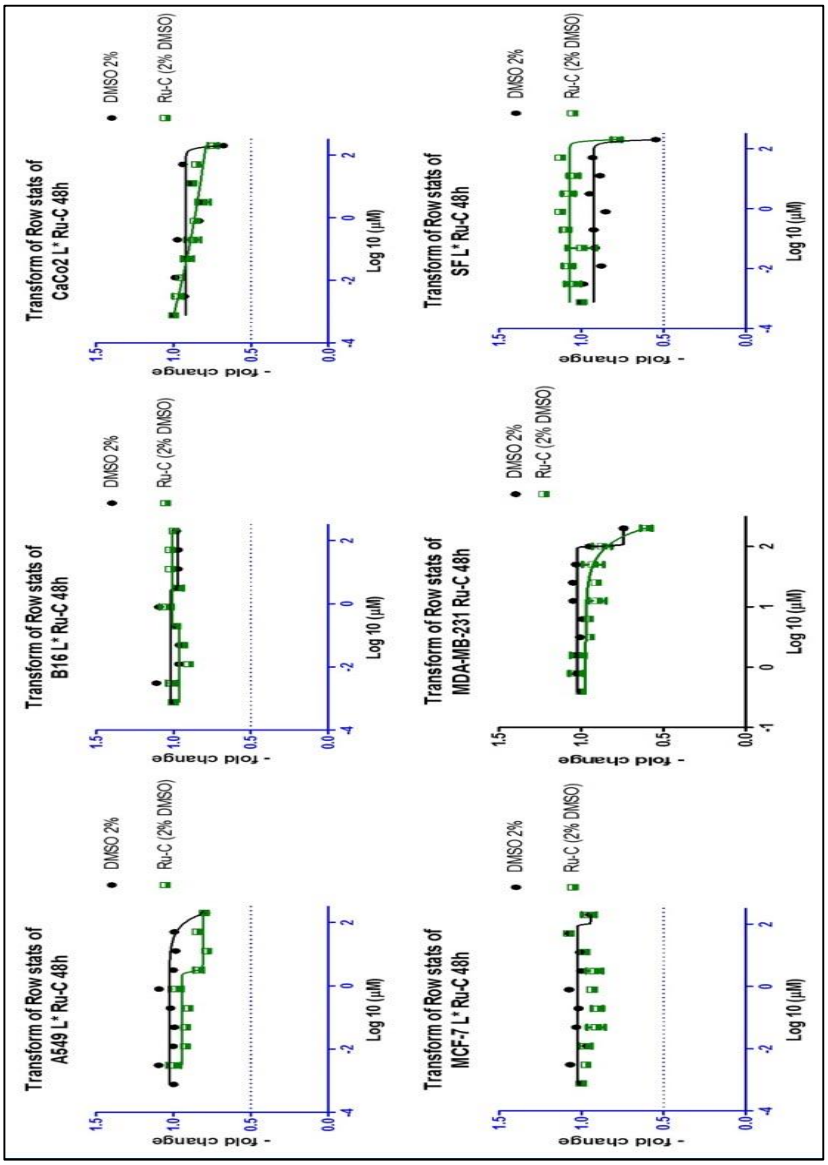
Transform of Row stats of
CaCo2 L* Ru-C 48h
Transform of Row stats of
SF L* Ru-C 48h
Transform of Row stats of
B16 L* Ru-C 48h
Transform of Row stats of
MDA-MB-231 Ru-C 48h
Transform of Row stats of
A549 L* Ru-C 48h
Transform of Row stats of
MCF-7 L* Ru-C 48h
DMSO 2%
Ru-C (2% DMSO)
- fold change
Log 10 (µM)

Appendix 9

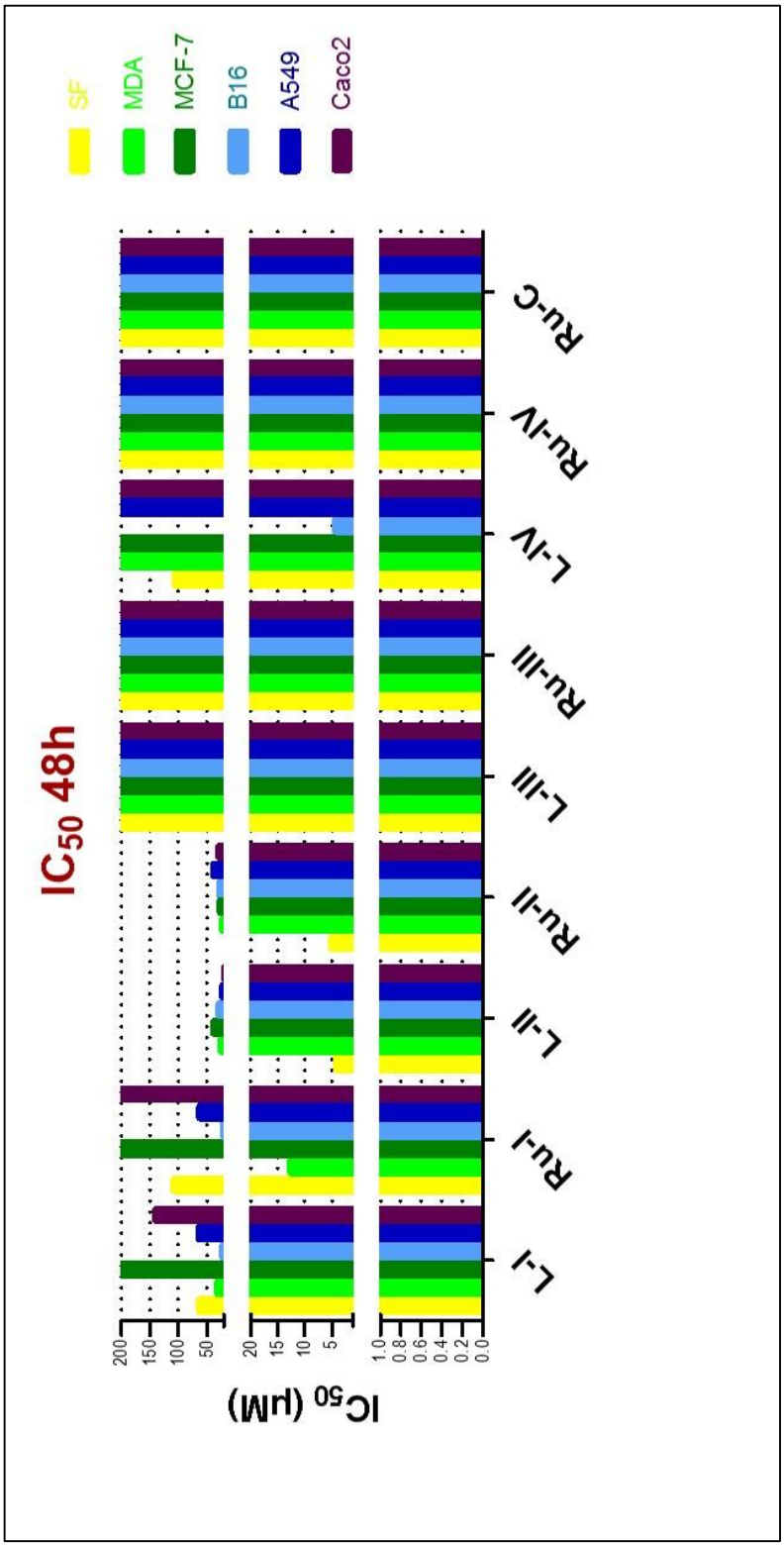
SF
MDA
MCF-7
B16
A549
Caco2
IC50 48h
IC50 (μM)
200
150
100
50
20
15
10
5
1.0
0.8
0.6
0.4
0.2
0.0
L-I
Ru-I
L-II
Ru-II
L-III
Ru-III
L-IV
Ru-IV
Ru-C

Appendix 10

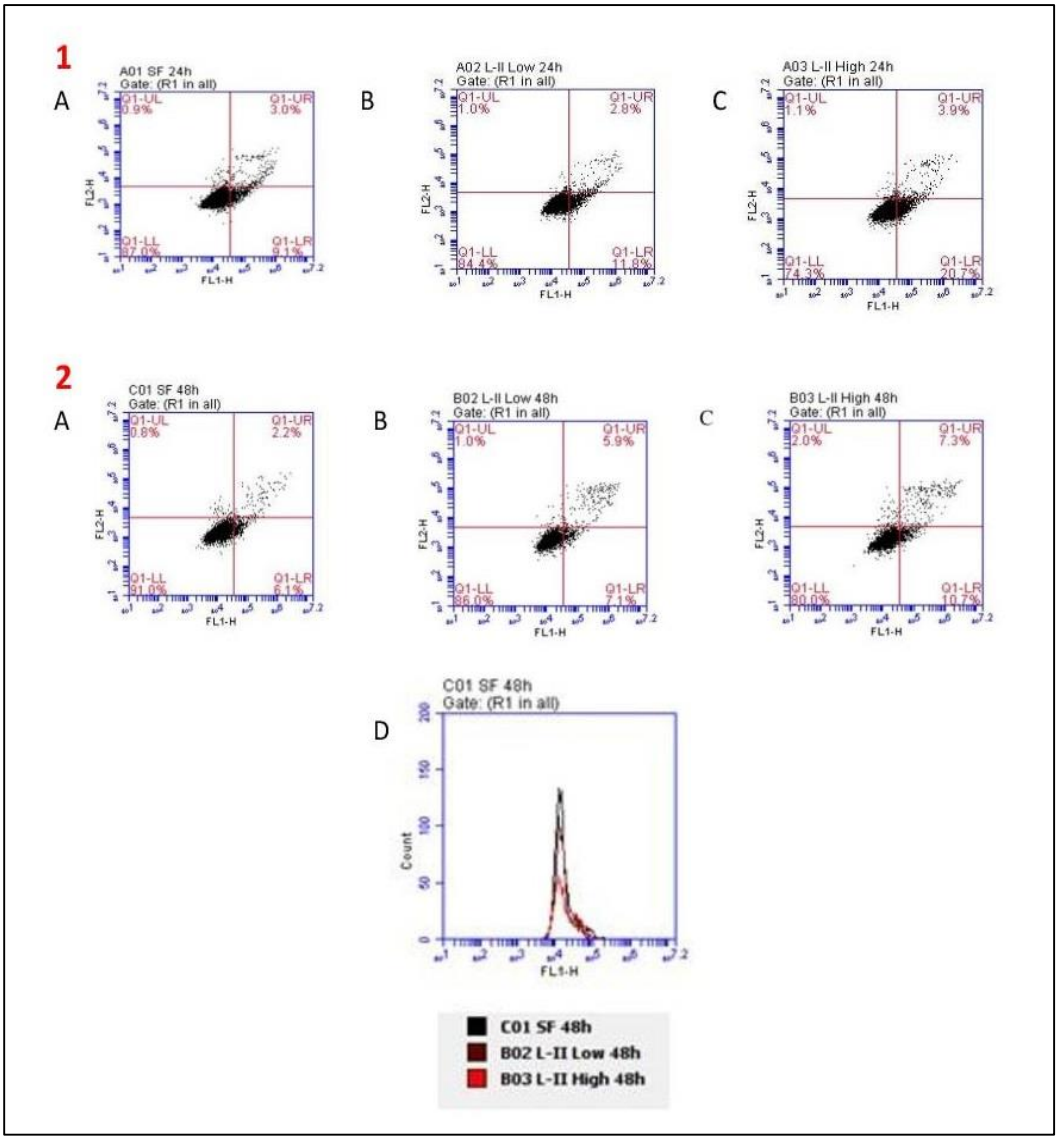
1
A
A01 SF 24h
Gate: (R1 in all)
Q1-UL 0.9%
Q1-UR 3.0%
Q1-LL 97.0%
Q1-LR 9.1%
B
A02 L-II Low 24h
Gate: (R1 in all)
Q1-UL 1.0%
Q1-UR 2.8%
Q1-LL 84.4%
Q1-LR 11.8%
C
A03 L-II High 24h
Gate: (R1 in all)
Q1-UL 1.1%
Q1-UR 3.9%
Q1-LL 74.3%
Q1-LR 20.7%
2
A
C01 SF 48h
Gate: (R1 in all)
Q1-UL 0.8%
Q1-UR 2.2%
Q1-LL 91.0%
Q1-LR 6.1%
B
B02 L-II Low 48h
Gate: (R1 in all)
Q1-UL 1.0%
Q1-UR 5.9%
Q1-LL 86.0%
Q1-LR 7.1%
C
B03 L-II High 48h
Gate: (R1 in all)
Q1-UL 2.0%
Q1-UR 7.3%
Q1-LL 80.0%
Q1-LR 10.7%
D
C01 SF 48h
Gate: (R1 in all)
Count
FL1-H
C01 SF 48h
B02 L-II Low 48h
B03 L-II High 48h

Appendix 11

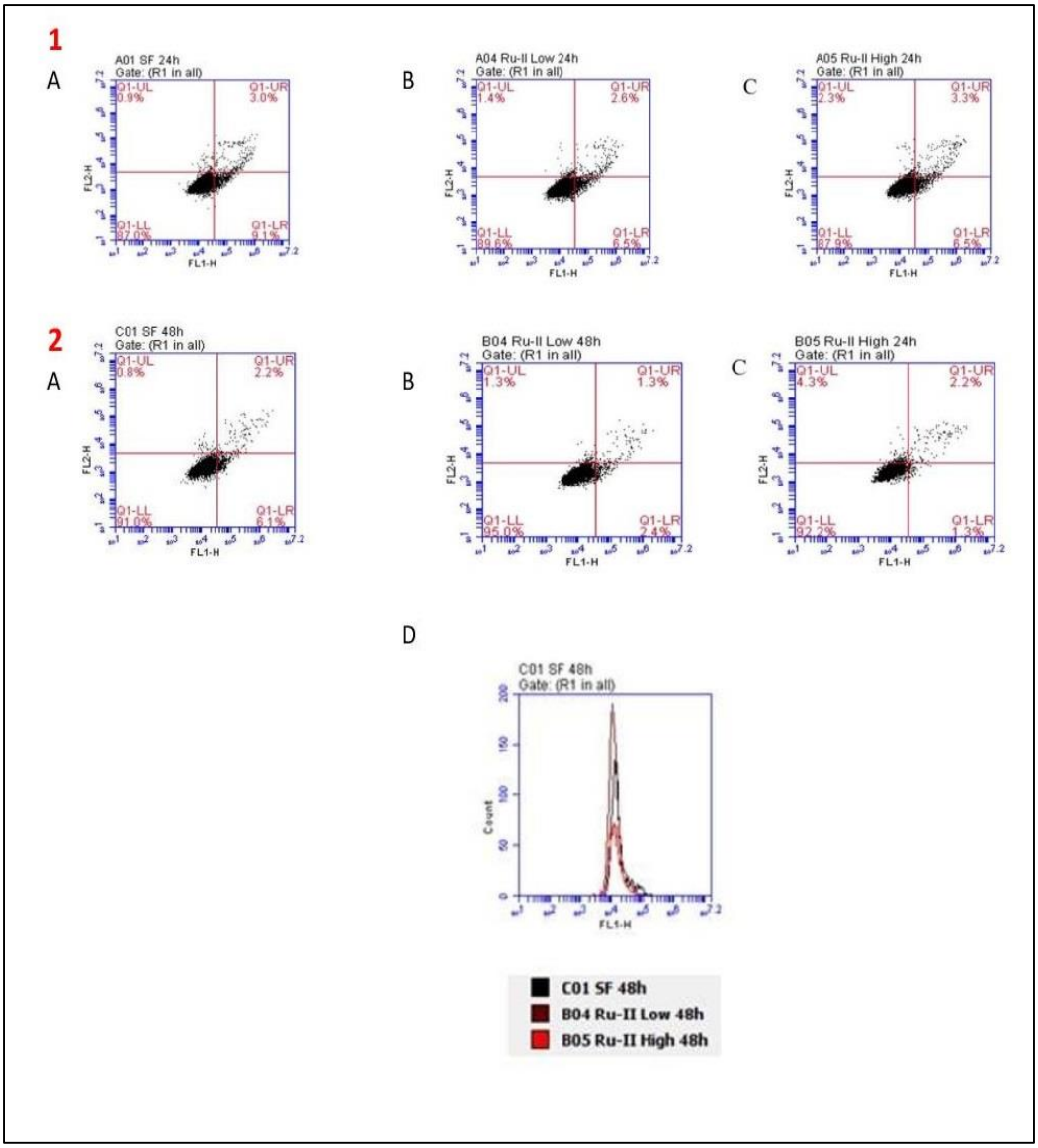
1
A
A01 SF 24h
Gate: (R1 in all)
Q1-UL 0.9%
Q1-UR 3.0%
Q1-LL 97.0%
Q1-LR 0.1%
B
A04 Ru-II Low 24h
Gate: (R1 in all)
Q1-UL 1.4%
Q1-UR 2.6%
Q1-LL 89.6%
Q1-LR 6.5%
C
A05 Ru-II High 24h
Gate: (R1 in all)
Q1-UL 2.3%
Q1-UR 3.3%
Q1-LL 87.9%
Q1-LR 6.5%
2
A
C01 SF 48h
Gate: (R1 in all)
Q1-UL 0.8%
Q1-UR 2.2%
Q1-LL 91.0%
Q1-LR 6.1%
B
B04 Ru-II Low 48h
Gate: (R1 in all)
Q1-UL 1.3%
Q1-UR 1.3%
Q1-LL 95.0%
Q1-LR 2.4%
C
B05 Ru-II High 24h
Gate: (R1 in all)
Q1-UL 4.3%
Q1-UR 2.2%
Q1-LL 92.2%
Q1-LR 1.3%
FL1-H
FL2-H
D
C01 SF 48h
Gate: (R1 in all)
Count
C01 SF 48h
B04 Ru-II Low 48h
B05 Ru-II High 48h

Appendix 12

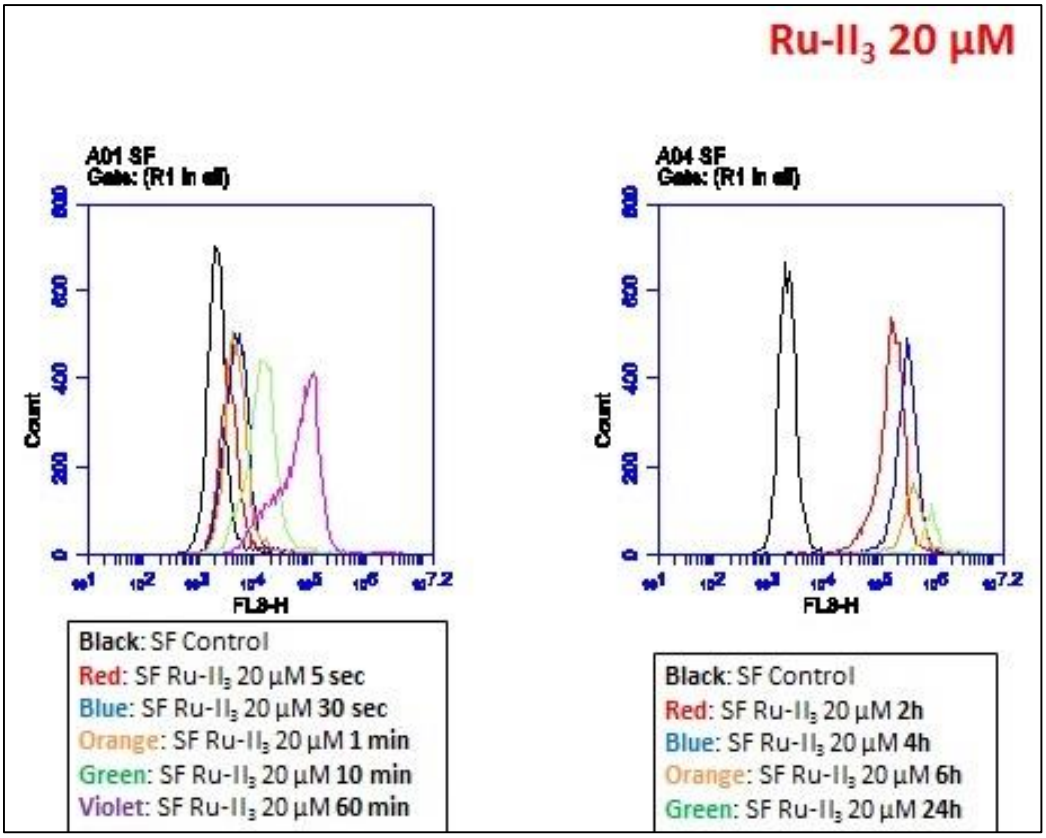
Ru-II3 20 µM
A01 SF
Gate: (R1 in all)
Count
FL3-H
Black: SF Control
Red: SF Ru-II3 20 µM 5 sec
Blue: SF Ru-II3 20 µM 30 sec
Orange: SF Ru-II3 20 µM 1 min
Green: SF Ru-II3 20 µM 10 min
Violet: SF Ru-II3 20 µM 60 min
A04 SF
Gate: (R1 in all)
Count
FL3-H
Black: SF Control
Red: SF Ru-II3 20 µM 2h
Blue: SF Ru-II3 20 µM 4h
Orange: SF Ru-II3 20 µM 6h
Green: SF Ru-II3 20 µM 24h

Appendix 13

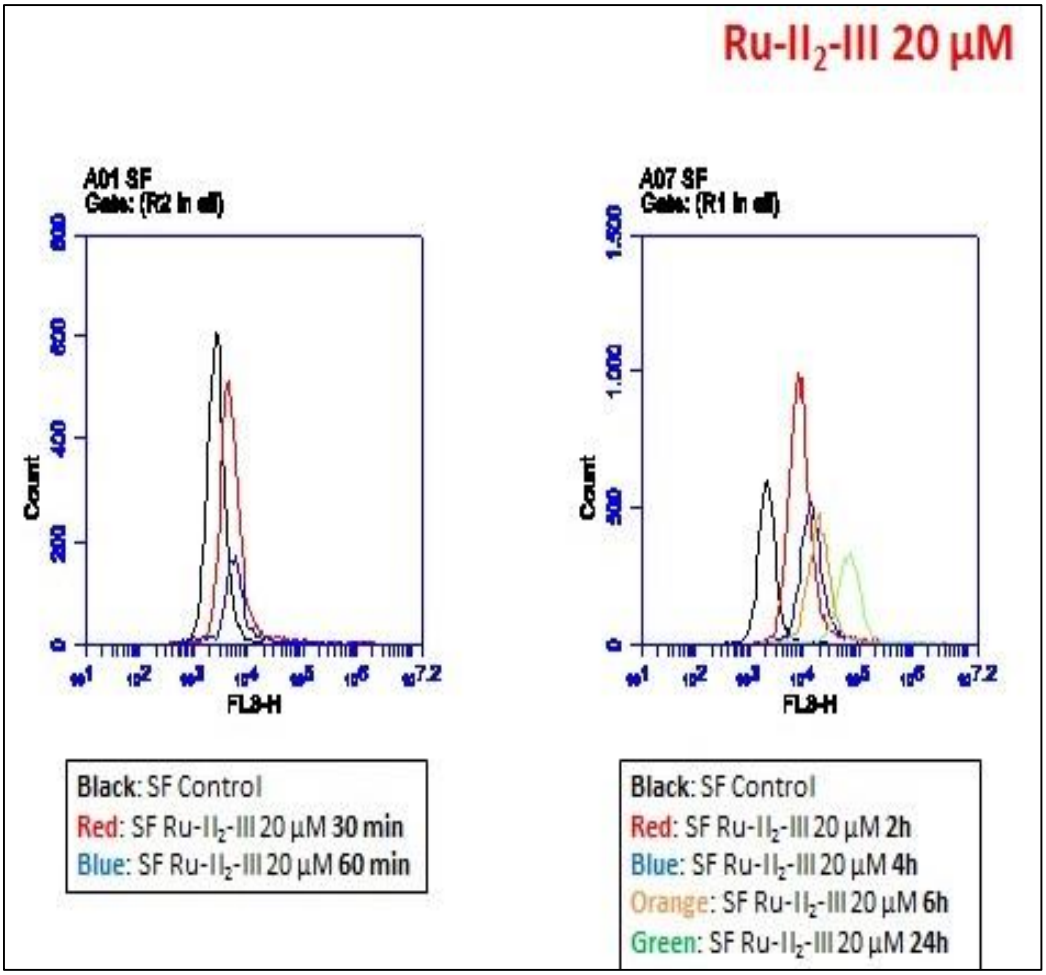
Ru-II2-III 20 µM
A01 SF
Gate: (R2 in all)
Count
FL3-H
Black: SF Control
Red: SF Ru-II2-III 20 µM 30 min
Blue: SF Ru-II2-III 20 µM 60 min
A07 SF
Gate: (R1 in all)
Count
FL3-H
Black: SF Control
Red: SF Ru-II2-III 20 µM 2h
Blue: SF Ru-II2-III 20 µM 4h
Orange: SF Ru-II2-III 20 µM 6h
Green: SF Ru-II2-III 20 µM 24h

Appendix 14

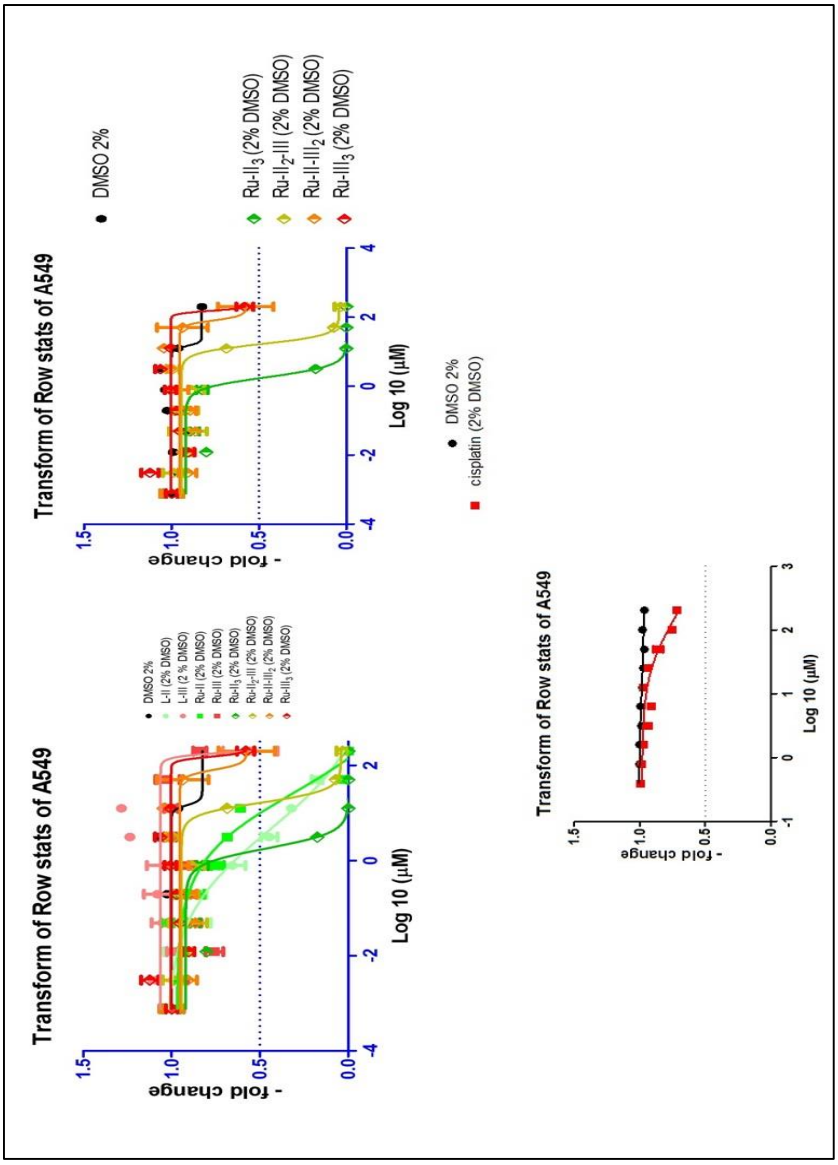
Transform of Row stats of A549
DMSO 2%
Ru-II$_3$ (2% DMSO)
Ru-II$_2$-III (2% DMSO)
Ru-II-III$_2$ (2% DMSO)
Ru-III$_3$ (2% DMSO)
- fold change
Log 10 (µM)
DMSO 2%
cisplatin (2% DMSO)
Transform of Row stats of A549
- fold change
Log 10 (µM)
Transform of Row stats of A549
DMSO 2%
L-II (2% DMSO)
L-III (2 % DMSO)
Ru-II (2% DMSO)
Ru-III (2% DMSO)
Ru-II$_3$ (2% DMSO)
Ru-II$_2$-III (2% DMSO)
Ru-II-III$_2$ (2% DMSO)
Ru-III$_3$ (2% DMSO)
- fold change
Log 10 (µM)

Appendix 15

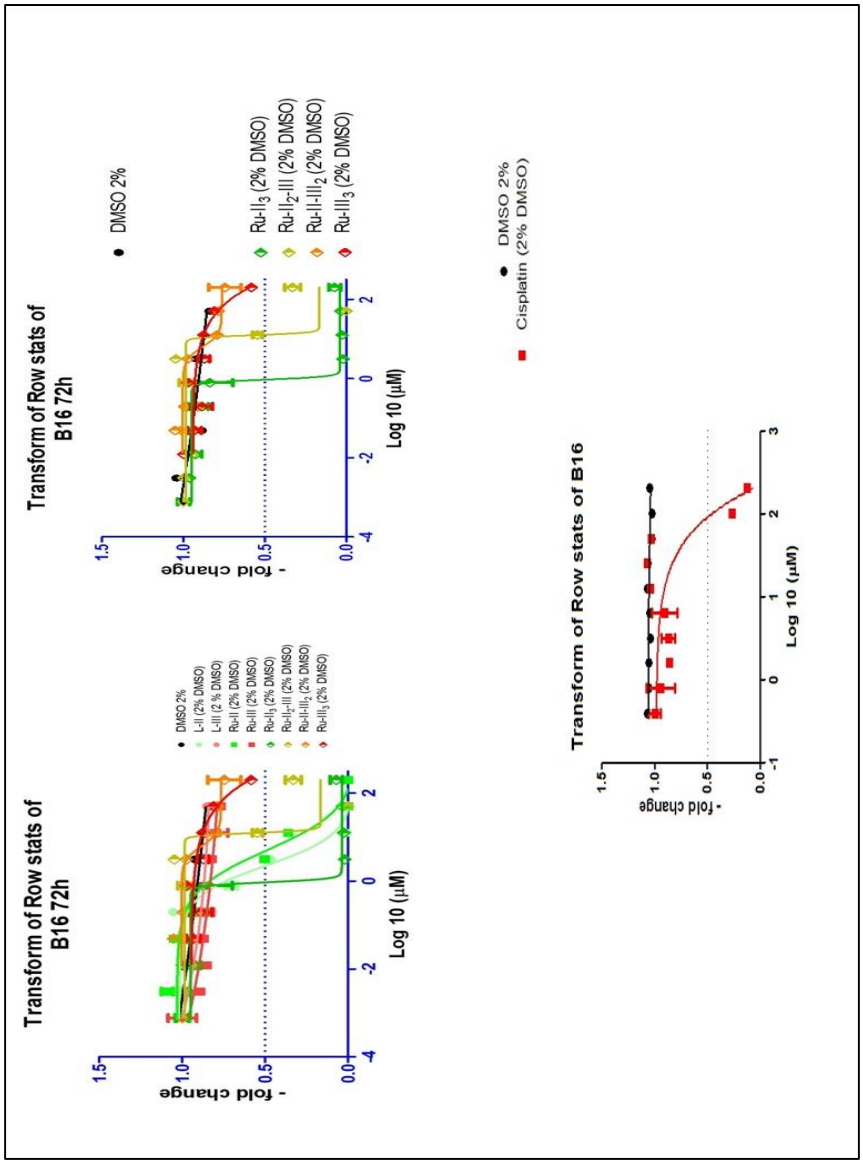
Transform of Row stats of B16 72h
DMSO 2%
Ru-II3 (2% DMSO)
Ru-II2-III (2% DMSO)
Ru-II-III2 (2% DMSO)
Ru-III3 (2% DMSO)
- fold change
Log 10 (µM)
Transform of Row stats of B16 72h
DMSO 2%
L-II (2% DMSO)
L-III (2 % DMSO)
Ru-II (2% DMSO)
Ru-III (2% DMSO)
Ru-II3 (2% DMSO)
Ru-II2-III (2% DMSO)
Ru-II-III2 (2% DMSO)
Ru-III3 (2% DMSO)
- fold change
Log 10 (µM)
Transform of Row stats of B16
DMSO 2%
Cisplatin (2% DMSO)
- fold change
Log 10 (µM)

Appendix 16

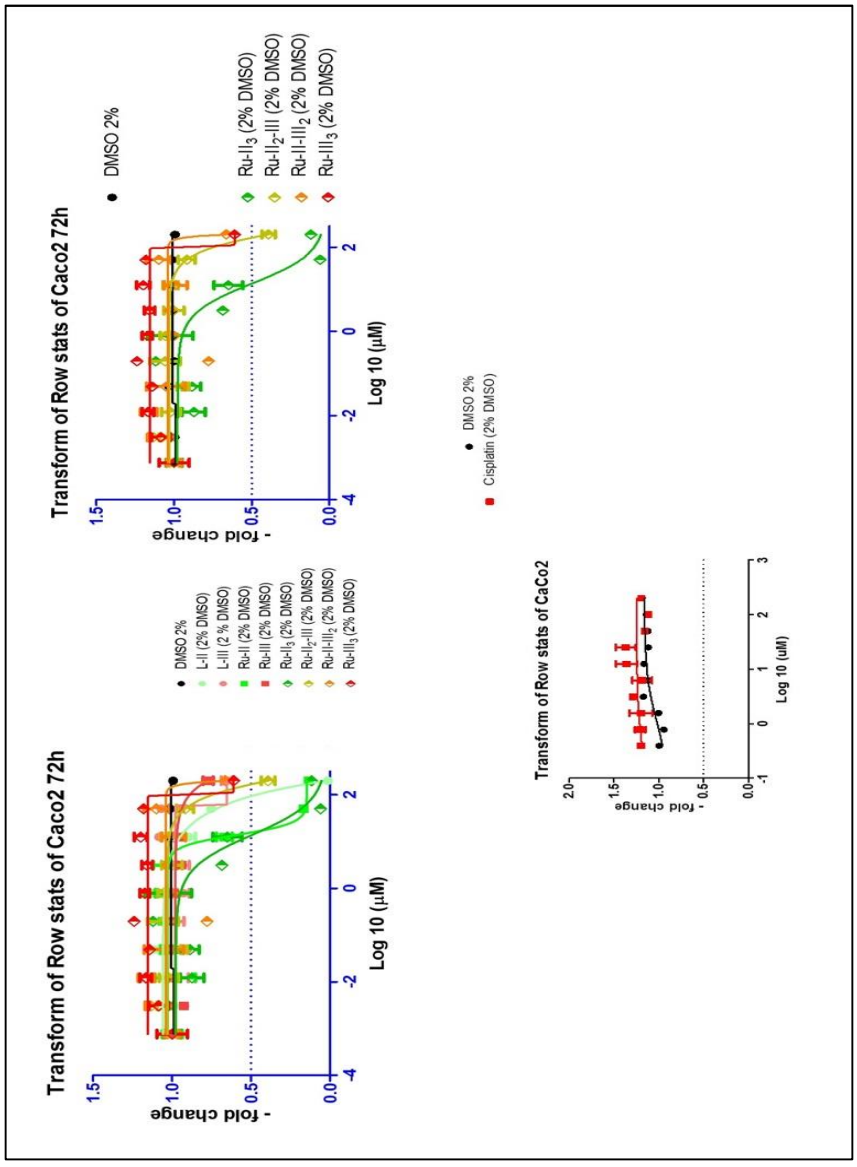
Transform of Row stats of Caco2 72h
DMSO 2%
Ru-II3 (2% DMSO)
Ru-II2-III (2% DMSO)
Ru-II-III2 (2% DMSO)
Ru-III3 (2% DMSO)
- fold change
Log 10 (µM)
Transform of Row stats of Caco2 72h
DMSO 2%
L-II (2% DMSO)
L-III (2 % DMSO)
Ru-II (2% DMSO)
Ru-III (2% DMSO)
Ru-II3 (2% DMSO)
Ru-II2-III (2% DMSO)
Ru-II-III2 (2% DMSO)
Ru-III3 (2% DMSO)
- fold change
Log 10 (µM)
DMSO 2%
Cisplatin (2% DMSO)
Transform of Row stats of CaCo2
- fold change
Log 10 (uM)

Appendix 17

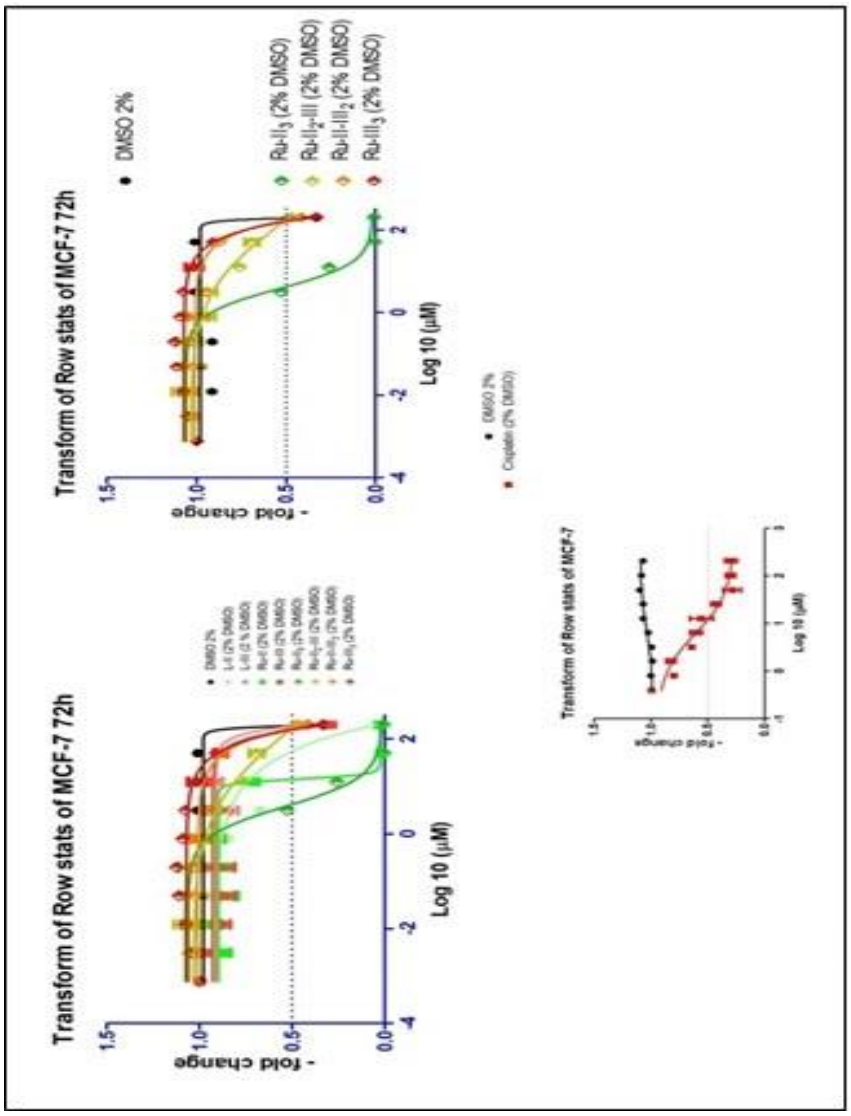
Transform of Row stats of MCF-7 72h
DMSO 2%
Ru-II$_3$ (2% DMSO)
Ru-II$_2$-III (2% DMSO)
Ru-II-III$_2$ (2% DMSO)
Ru-III$_3$ (2% DMSO)
- fold change
Log 10 (µM)
Transform of Row stats of MCF-7 72h
- fold change
Log 10 (µM)
Transform of Row stats of MCF-7

Appendix 18

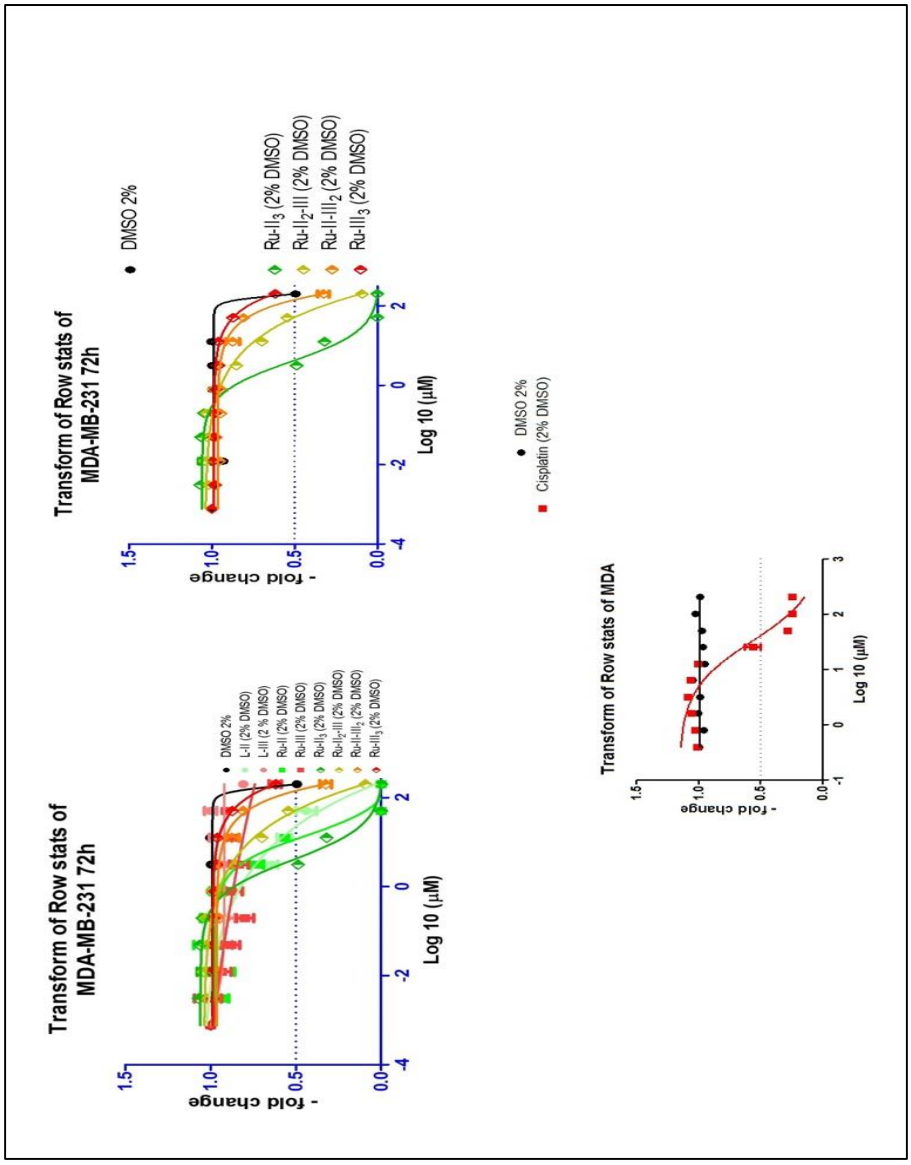
Transform of Row stats of MDA-MB-231 72h
DMSO 2%
Ru-II$_3$ (2% DMSO)
Ru-II$_2$-III (2% DMSO)
Ru-II-III$_2$ (2% DMSO)
Ru-III$_3$ (2% DMSO)
- fold change
Log 10 (µM)
Transform of Row stats of MDA-MB-231 72h
DMSO 2%
L-II (2% DMSO)
L-III (2 % DMSO)
Ru-II (2% DMSO)
Ru-III (2% DMSO)
Ru-II$_3$ (2% DMSO)
Ru-II$_2$-III (2% DMSO)
Ru-II-III$_2$ (2% DMSO)
Ru-III$_3$ (2% DMSO)
- fold change
Log 10 (µM)
DMSO 2%
Cisplatin (2% DMSO)
Transform of Row stats of MDA
- fold change
Log 10 (µM)

Appendix 19

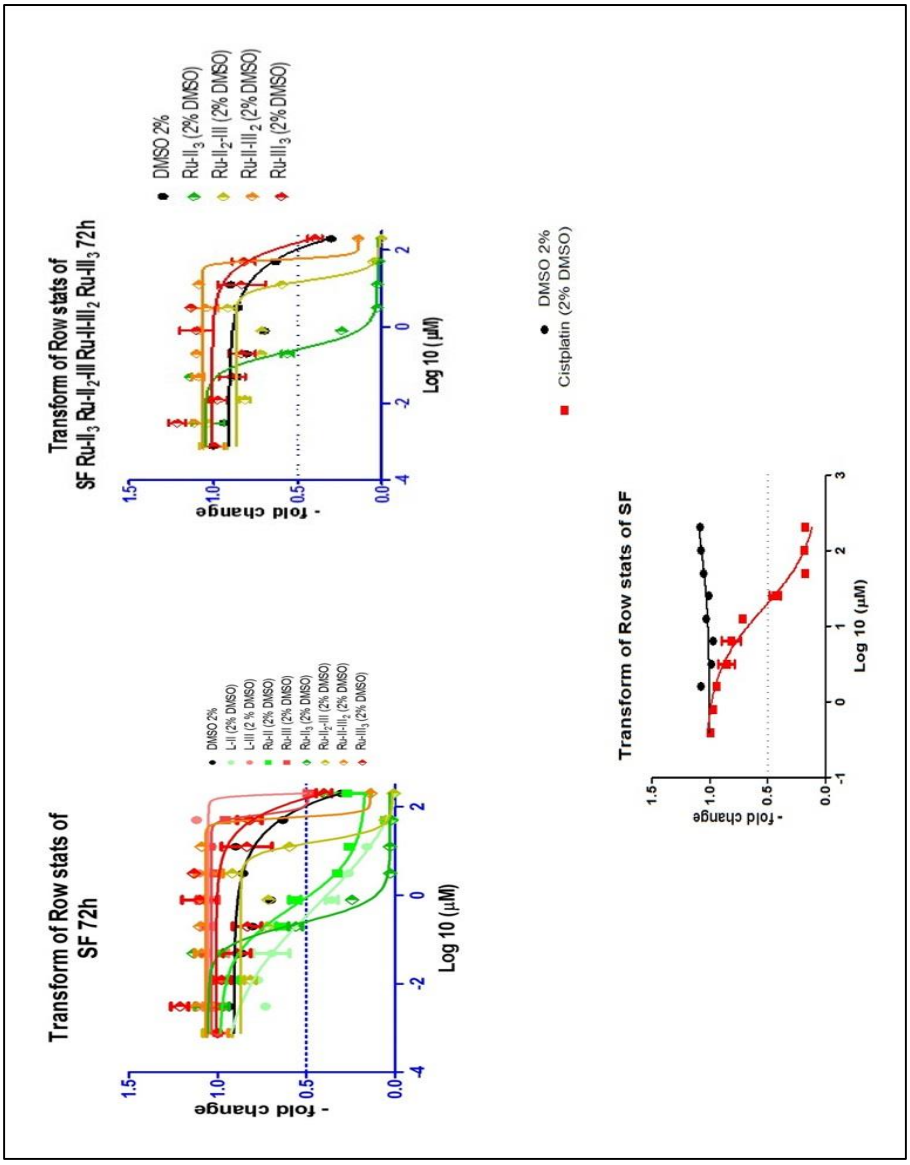
Transform of Row stats of SF Ru-II3 Ru-II2-III Ru-II-III2 Ru-III3 72h
DMSO 2%
Ru-II3 (2% DMSO)
Ru-II2-III (2% DMSO)
Ru-II-III2 (2% DMSO)
Ru-III3 (2% DMSO)
- fold change
Log 10 (µM)
Transform of Row stats of SF 72h
DMSO 2%
L-II (2% DMSO)
L-III (2 % DMSO)
Ru-II (2% DMSO)
Ru-III (2% DMSO)
Ru-II3 (2% DMSO)
Ru-II2-III (2% DMSO)
Ru-II-III2 (2% DMSO)
Ru-III3 (2% DMSO)
- fold change
Log 10 (µM)
DMSO 2%
Cisplatin (2% DMSO)
Transform of Row stats of SF
- fold change
Log 10 (µM)

Appendix 20

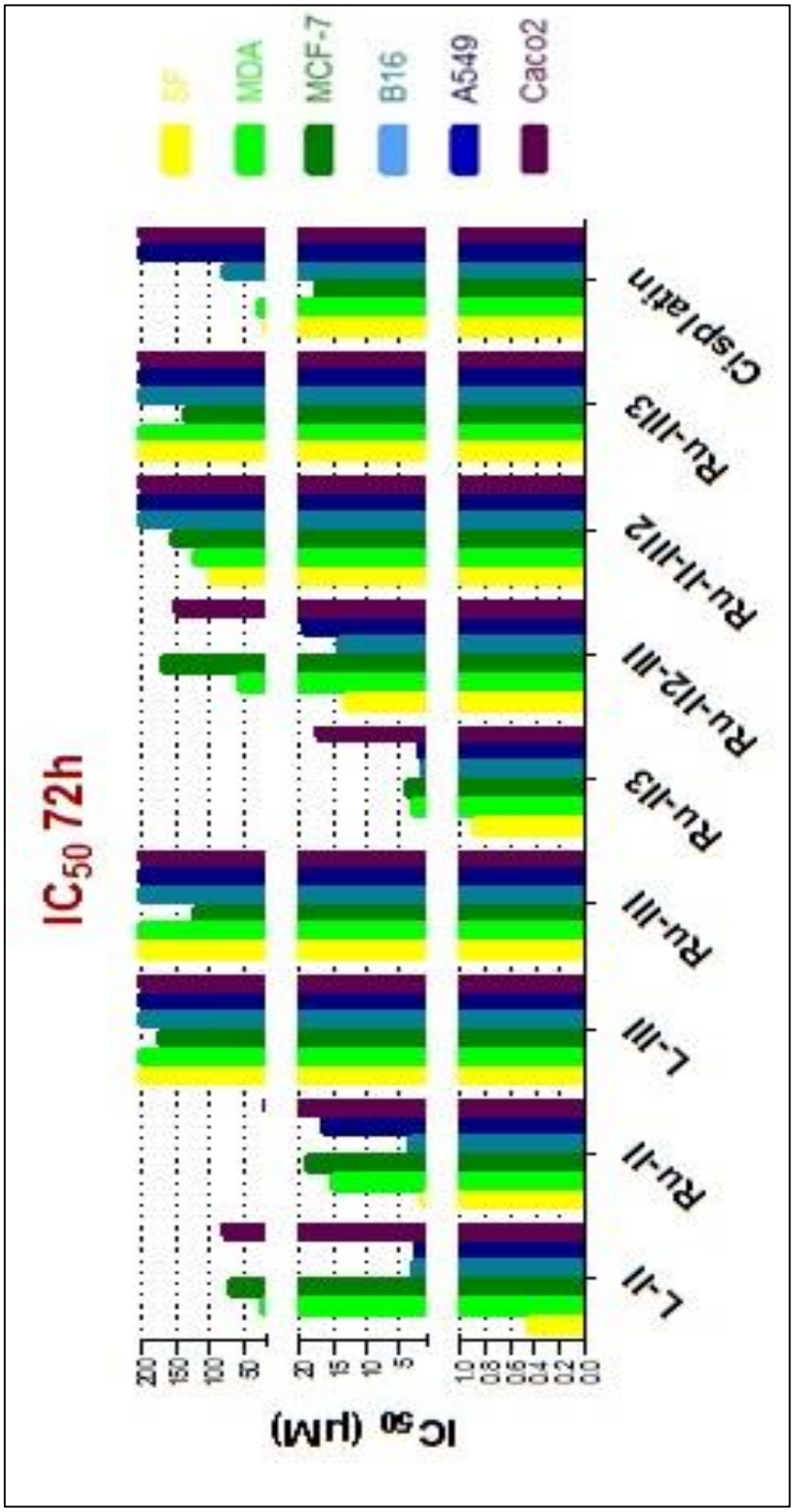
SF
MDA
MCF-7
B16
A549
Caco2
IC50 72h
IC50 (μM)
L-II
Ru-II
L-III
Ru-III
Ru-II3
Ru-II2-III
Ru-II-III2
Ru-III3
Cisplatin

Appendix 21

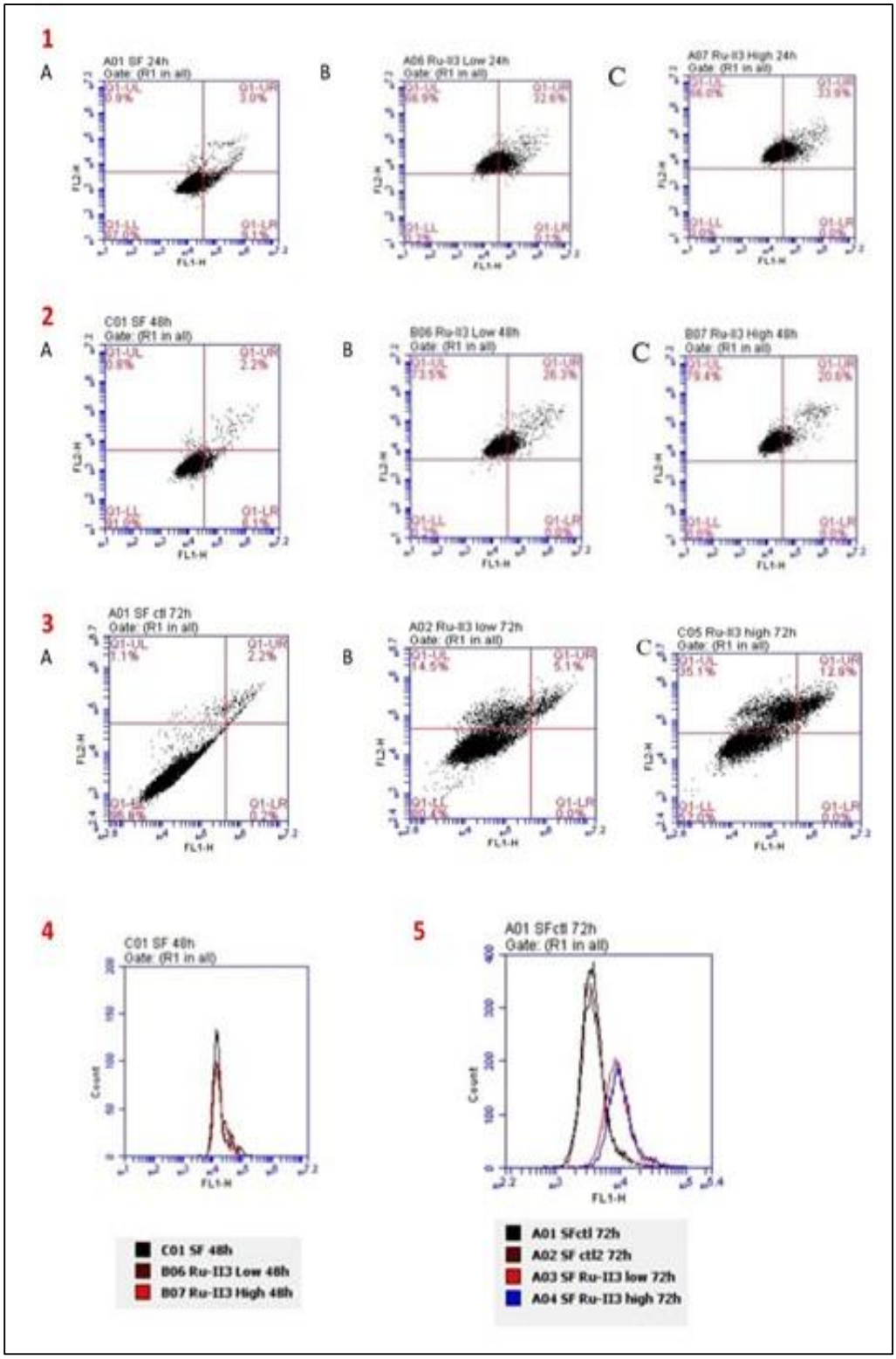
1
A
A01 SF 24h
Gate: (R1 in all)
B
A06 Ru-II3 Low 24h
Gate: (R1 in all)
C
A07 Ru-II3 High 24h
Gate: (R1 in all)
2
A
C01 SF 48h
Gate: (R1 in all)
B
B06 Ru-II3 Low 48h
Gate: (R1 in all)
C
B07 Ru-II3 High 48h
Gate: (R1 in all)
3
A
A01 SF ctl 72h
Gate: (R1 in all)
B
A02 Ru-II3 low 72h
Gate: (R1 in all)
C
C05 Ru-II3 high 72h
Gate: (R1 in all)
FL1-H
FL3-H
4
C01 SF 48h
Gate: (R1 in all)
Count
C01 SF 48h
B06 Ru-II3 Low 48h
B07 Ru-II3 High 48h
5
A01 SFctl 72h
Gate: (R1 in all)
A01 SFctl 72h
A02 SF ctl2 72h
A03 SF Ru-II3 low 72h
A04 SF Ru-II3 high 72h

Appendix 22

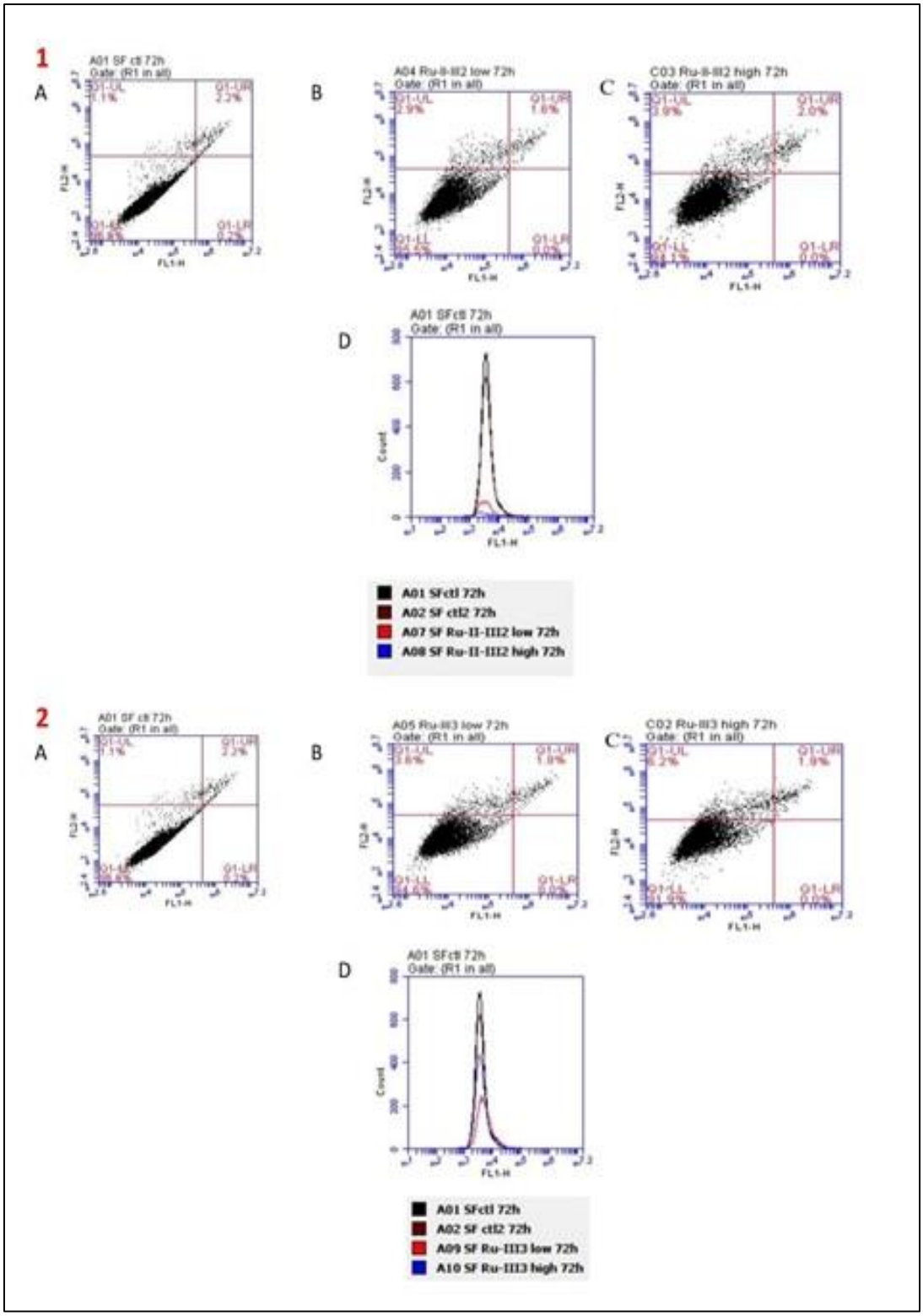
1
A
A01 SF ctl 72h
Gate: (R1 in all)
B
A04 Ru-II-III2 low 72h
Gate: (R1 in all)
C
C03 Ru-II-III2 high 72h
Gate: (R1 in all)
D
A01 SFctl 72h
Gate: (R1 in all)
A01 SFctl 72h
A02 SF ctl2 72h
A07 SF Ru-II-III2 low 72h
A08 SF Ru-II-III2 high 72h
2
A
A01 SF ctl 72h
Gate: (R1 in all)
B
A05 Ru-III3 low 72h
Gate: (R1 in all)
C
C02 Ru-III3 high 72h
Gate: (R1 in all)
D
A01 SFctl 72h
Gate: (R1 in all)
A01 SFctl 72h
A02 SF ctl2 72h
A09 SF Ru-III3 low 72h
A10 SF Ru-III3 high 72h

Appendix 23

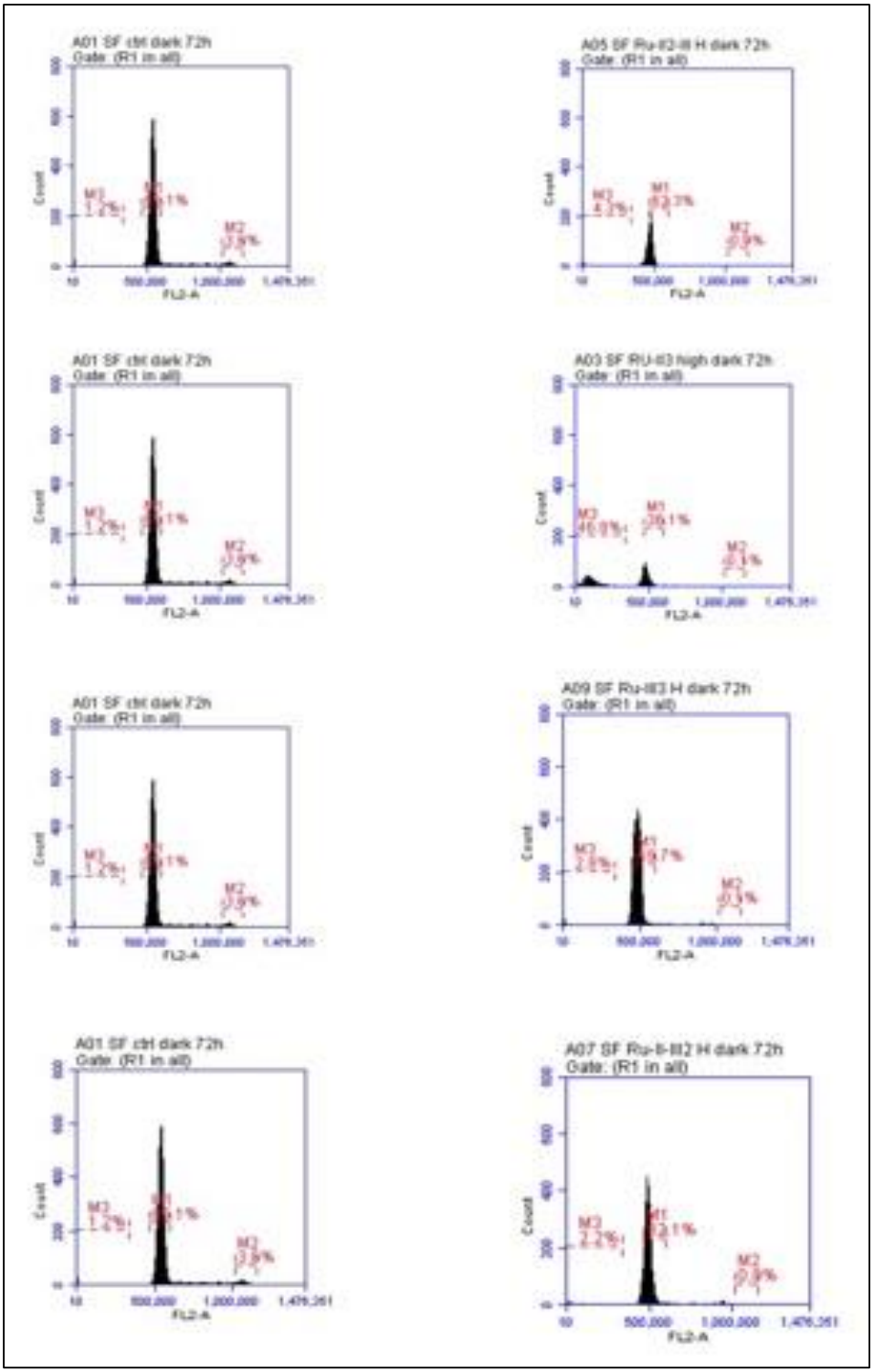
A01 SF ctrl dark 72h
Gate: (R1 in all)
A05 SF Ru-II2-III H dark 72h
Gate: (R1 in all)
A01 SF ctrl dark 72h
Gate: (R1 in all)
A03 SF RU-II3 high dark 72h
Gate: (R1 in all)
A01 SF ctrl dark 72h
Gate: (R1 in all)
A09 SF Ru-III3 H dark 72h
Gate: (R1 in all)
A01 SF ctrl dark 72h
Gate: (R1 in all)
A07 SF Ru-II-III2 H dark 72h
Gate: (R1 in all)
Count
FL2-A

Appendix 24

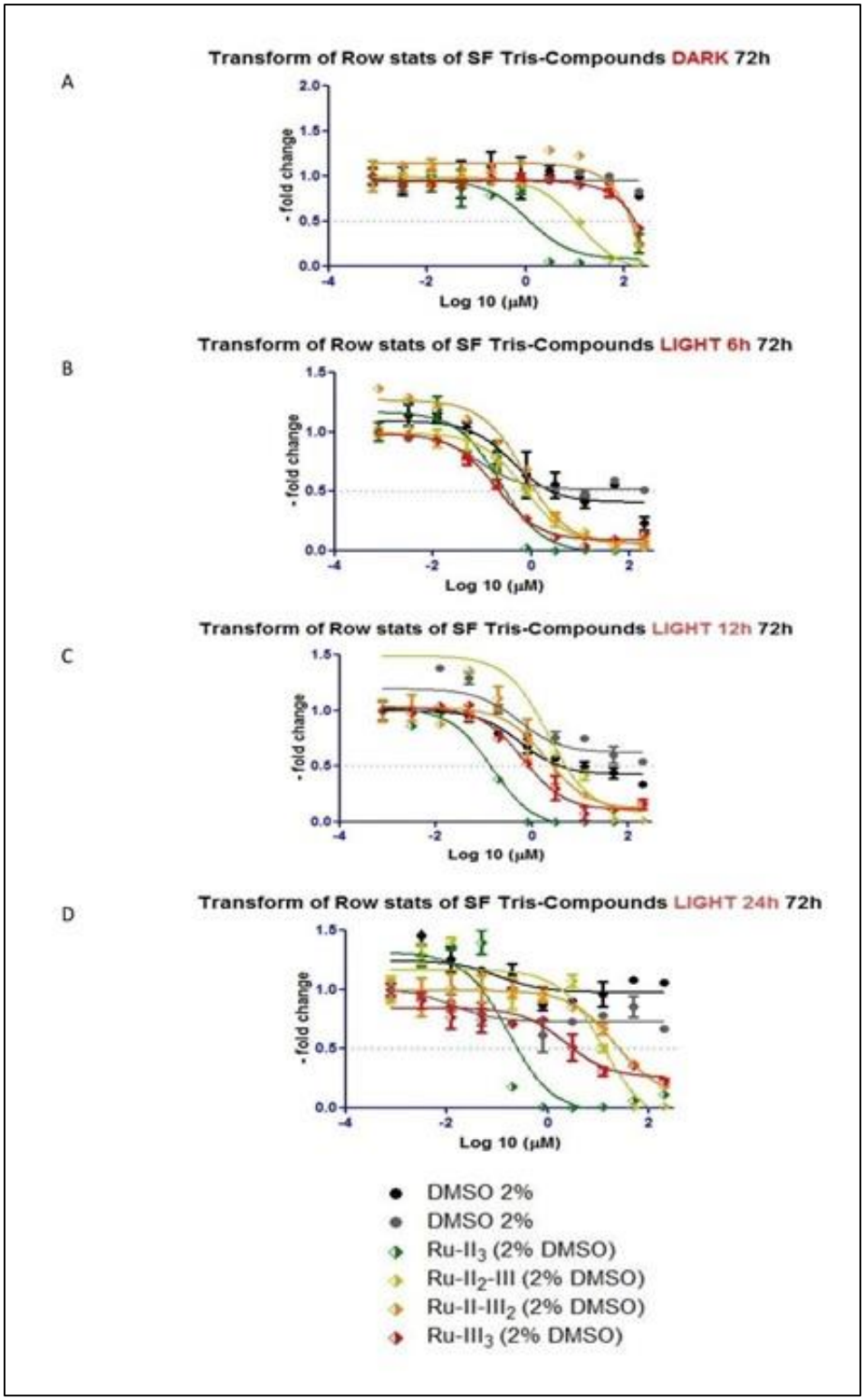
A
Transform of Row stats of SF Tris-Compounds DARK 72h
- fold change
Log 10 (μM)
B
Transform of Row stats of SF Tris-Compounds LIGHT 6h 72h
- fold change
Log 10 (μM)
C
Transform of Row stats of SF Tris-Compounds LIGHT 12h 72h
- fold change
Log 10 (μM)
D
Transform of Row stats of SF Tris-Compounds LIGHT 24h 72h
- fold change
Log 10 (μM)
DMSO 2%
DMSO 2%
Ru-II3 (2% DMSO)
Ru-II2-III (2% DMSO)
Ru-II-III2 (2% DMSO)
Ru-III3 (2% DMSO)

Appendix 25

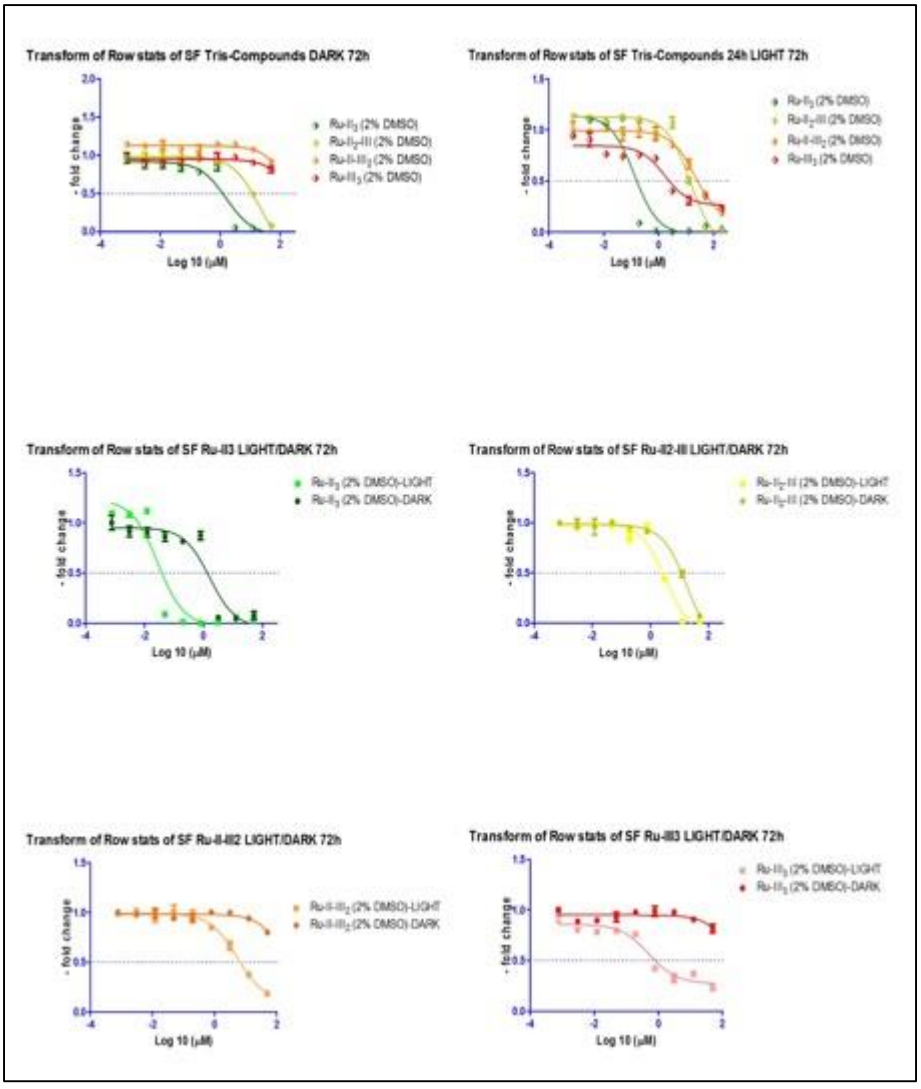
Transform of Row stats of SF Tris-Compounds DARK 72h
Transform of Row stats of SF Tris-Compounds 24h LIGHT 72h
Transform of Row stats of SF Ru-II3 LIGHT/DARK 72h
Transform of Row stats of SF Ru-II2-III LIGHT/DARK 72h
Transform of Row stats of SF Ru-II-III2 LIGHT/DARK 72h
Transform of Row stats of SF Ru-III3 LIGHT/DARK 72h
- fold change
Log 10 (μM)

Appendix 26

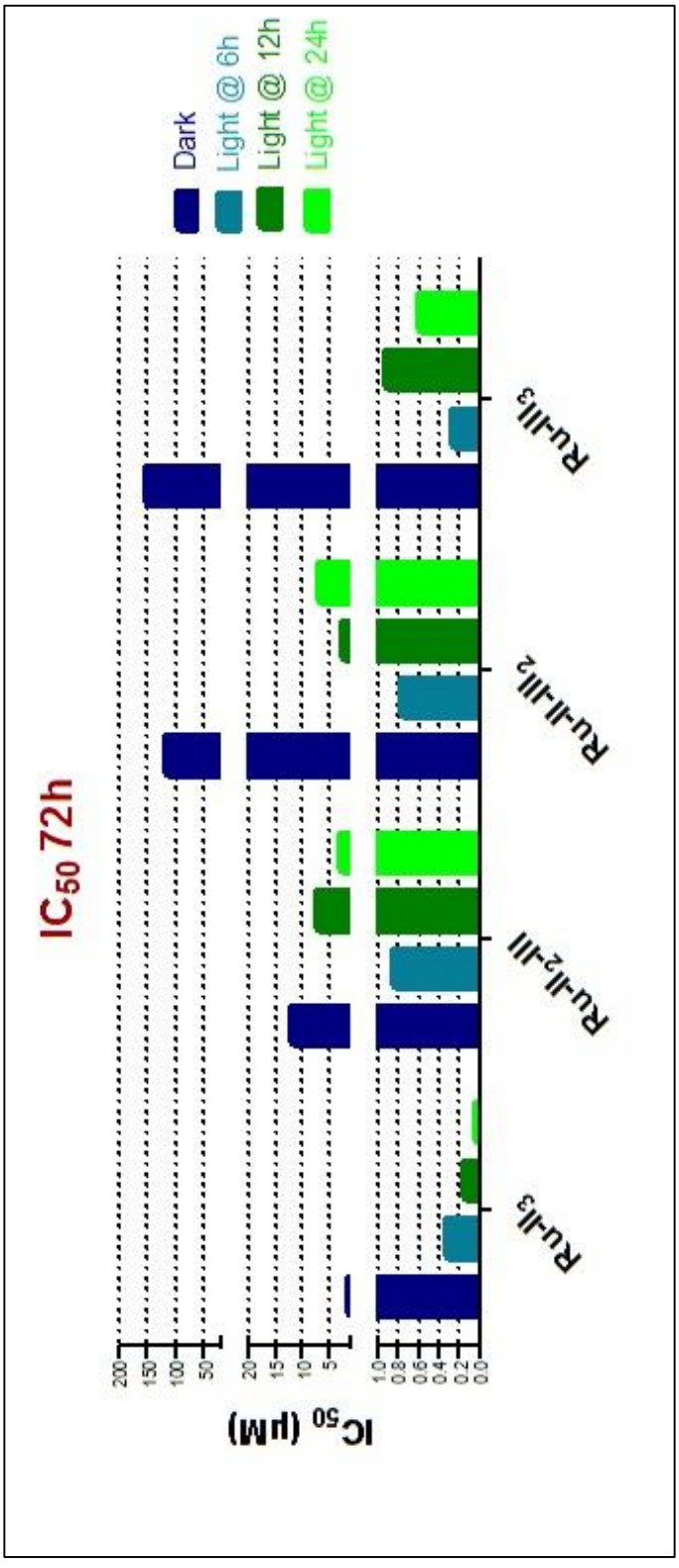
Dark
Light @ 6h
Light @ 12h
Light @ 24h
IC50 72h
IC50 (μM)
200
150
100
50
20
15
10
5
1.0
0.8
0.6
0.4
0.2
0.0
Ru-II3
Ru-II-III2
Ru-II2-III
Ru-II3

Appendix 27

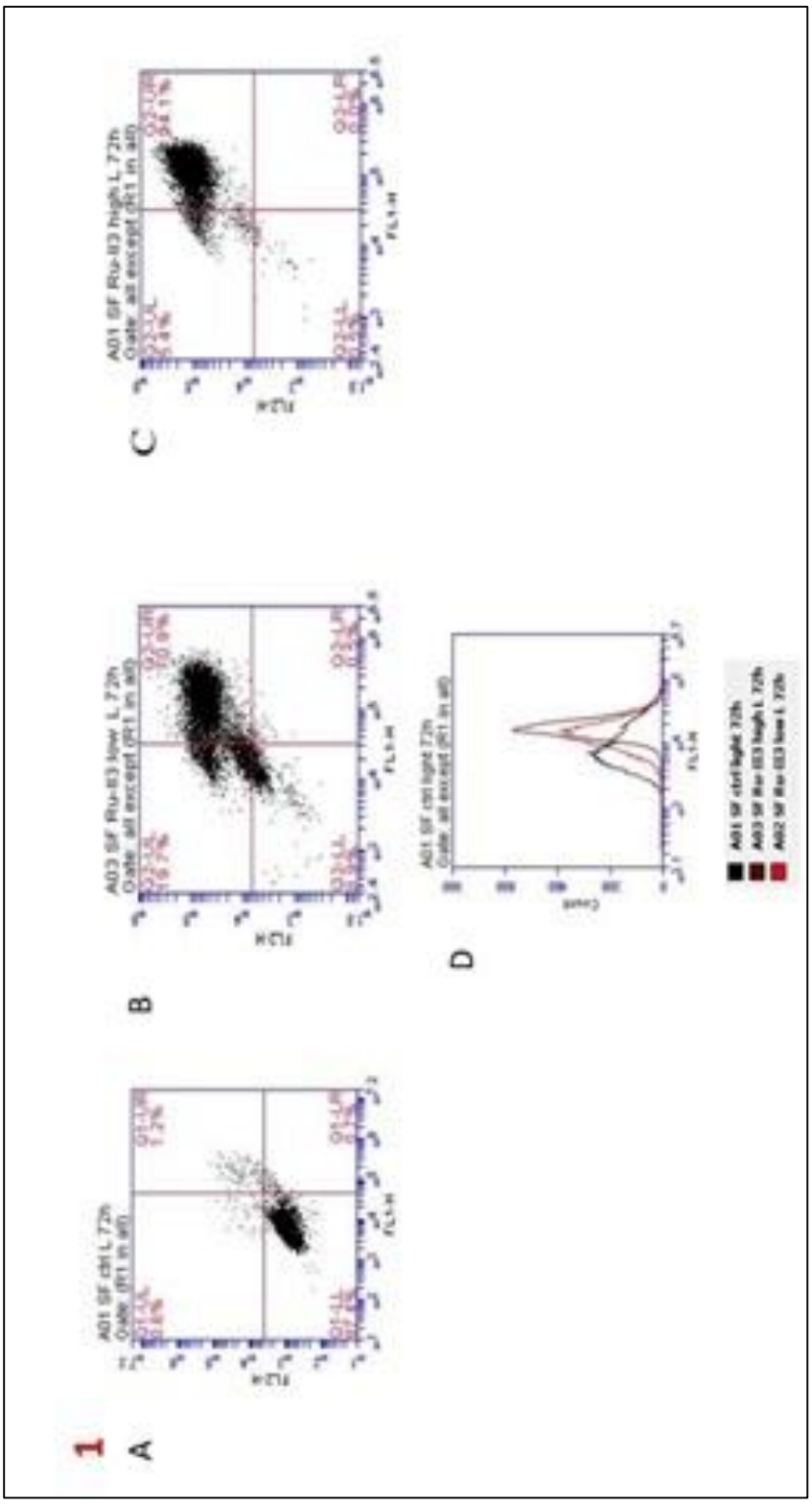
1
A
A01 SF ctrl L 72h
Gate: (R1 in all)
B
A03 SF Ru-83 low L 72h
Gate: all except (R1 in all)
C
A01 SF Ru-83 high L 72h
Gate: all except (R1 in all)
D
A01 SF ctrl light 72h
Gate: all except (R1 in all)
A01 SF ctrl light 72h
A03 SF Ru-83 high L 72h
A02 SF Ru-83 low L 72h

Appendix 28

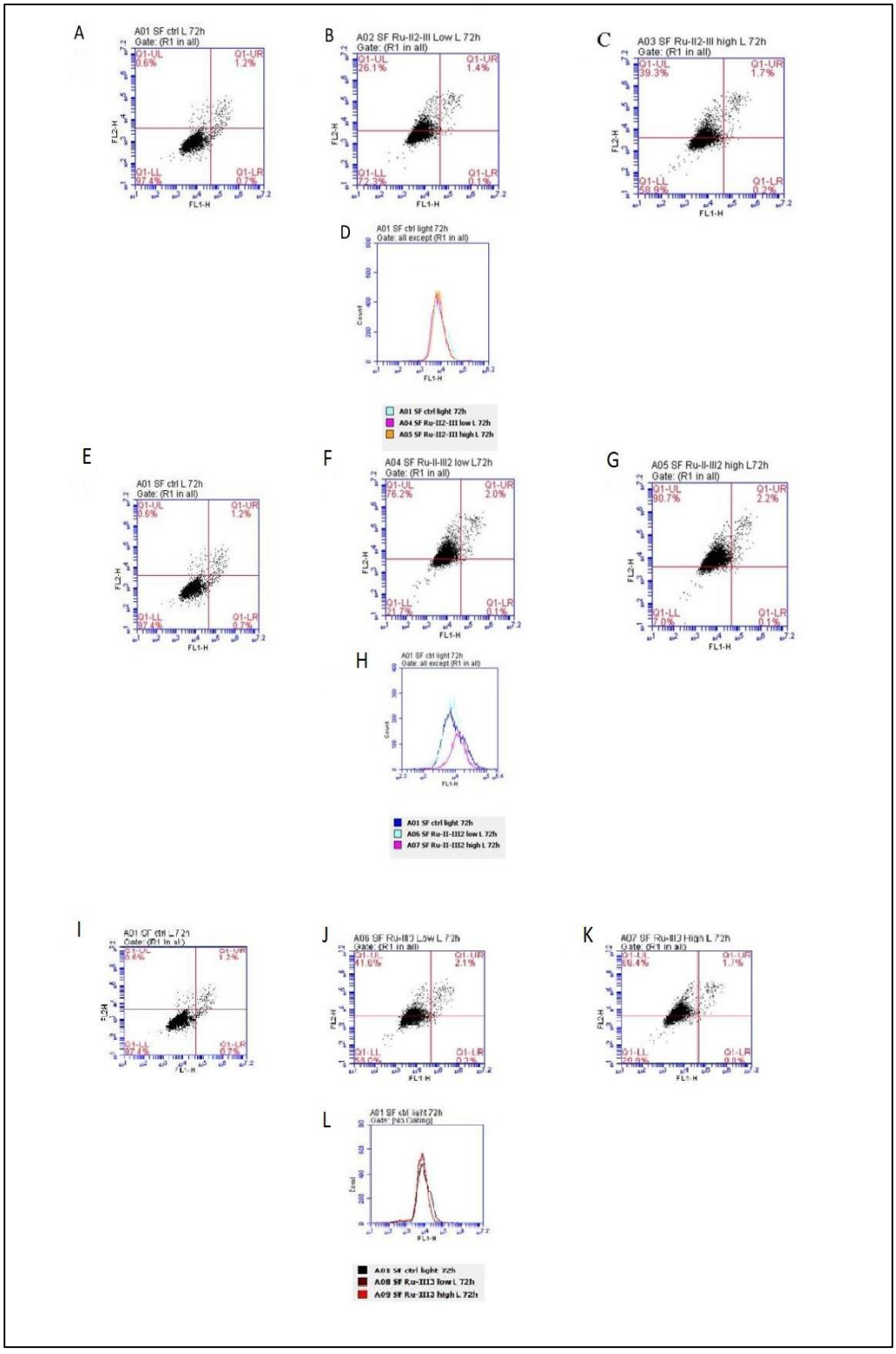
A
A01 SF ctrl L 72h
Gate: (R1 in all)
Q1-UL 0.6%
Q1-UR 1.2%
Q1-LL 97.4%
Q1-LR 0.7%
FL2-H
FL1-H
B
A02 SF Ru-II2-III Low L 72h
Gate: (R1 in all)
Q1-UL 26.1%
Q1-UR 1.4%
Q1-LL 72.2%
Q1-LR 0.1%
C
A03 SF Ru-II2-III high L 72h
Gate: (R1 in all)
Q1-UL 39.3%
Q1-UR 1.7%
Q1-LL 58.9%
Q1-LR 0.2%
D
A01 SF ctrl light 72h
Gate: all except (R1 in all)
Count
A01 SF ctrl light 72h
A04 SF Ru-II2-III low L 72h
A05 SF Ru-II2-III high L 72h
E
A01 SF ctrl L 72h
Gate: (R1 in all)
Q1-UL 0.6%
Q1-UR 1.2%
Q1-LL 97.4%
Q1-LR 0.7%
F
A04 SF Ru-II-III2 low L72h
Gate: (R1 in all)
Q1-UL 76.2%
Q1-UR 2.0%
Q1-LL 21.7%
Q1-LR 0.1%
G
A05 SF Ru-II-III2 high L72h
Gate: (R1 in all)
Q1-UL 90.7%
Q1-UR 2.2%
Q1-LL 7.0%
Q1-LR 0.1%
H
A01 SF ctrl light 72h
Gate: all except (R1 in all)
Count
A01 SF ctrl light 72h
A06 SF Ru-II-III2 low L 72h
A07 SF Ru-II-III2 high L 72h
I
J
A06 SF Ru-III3 Low L 72h
Gate: (R1 in all)
Q1-UL 41.6%
Q1-UR 2.1%
Q1-LL 56.0%
Q1-LR 0.3%
K
A07 SF Ru-III3 High L 72h
Gate: (R1 in all)
Q1-UL 98.4%
Q1-UR 1.7%
Q1-LL 0.0%
Q1-LR 0.0%
L
A01 SF ctrl light 72h
Gate: [No Gating]
Count
A01 SF ctrl light 72h
A08 SF Ru-III3 low L 72h
A09 SF Ru-III3 high L 72h

Appendix 29

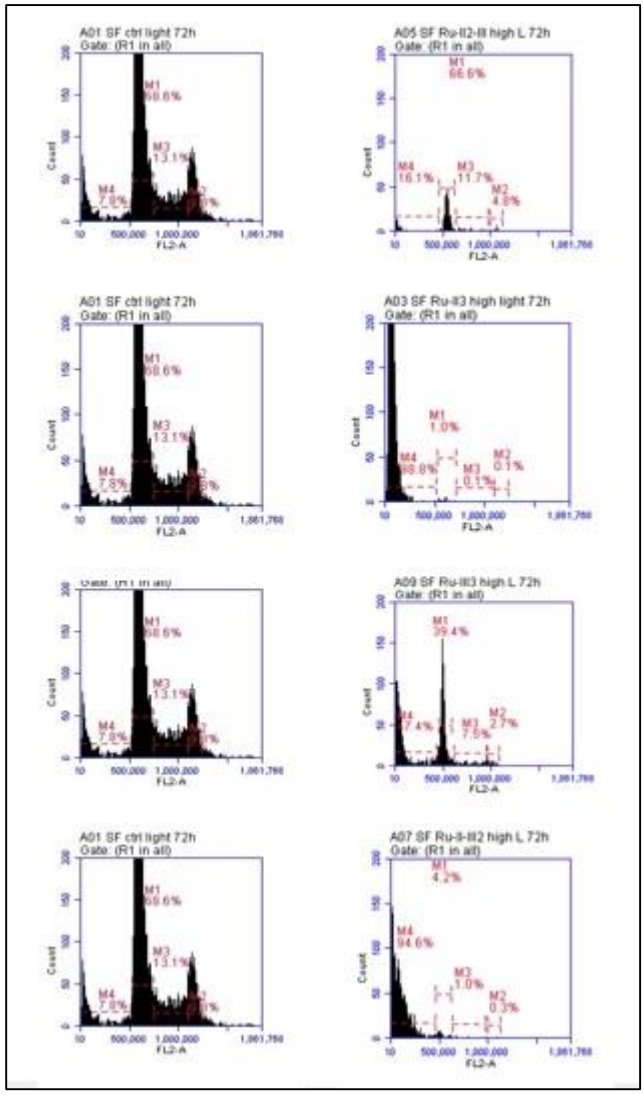
A01 SF ctrl light 72h
Gate: (R1 in all)
M1
68.6%
M3
13.1%
M4
7.8%
Count
FL2-A
A05 SF Ru-II2-III high L 72h
Gate: (R1 in all)
M1
66.6%
M4
16.1%
M3
11.7%
M2
4.8%
Count
FL2-A
A01 SF ctrl light 72h
Gate: (R1 in all)
M1
68.6%
M3
13.1%
M4
7.8%
Count
FL2-A
A03 SF Ru-II3 high light 72h
Gate: (R1 in all)
M1
1.0%
M4
89.8%
M3
0.1%
M2
0.1%
Count
FL2-A
M1
68.6%
M3
13.1%
M4
7.8%
Count
FL2-A
A09 SF Ru-III3 high L 72h
Gate: (R1 in all)
M1
39.4%
M4
47.4%
M3
7.9%
M2
2.7%
Count
FL2-A
A01 SF ctrl light 72h
Gate: (R1 in all)
M1
68.6%
M3
13.1%
M4
7.8%
Count
FL2-A
A07 SF Ru-II-III2 high L 72h
Gate: (R1 in all)
M1
4.2%
M4
94.6%
M3
1.0%
M2
0.3%
Count
FL2-A